Probing Heterogeneous Dynamics One Molecule at a Time: Polystyrene near the Glass Transition

Alyssa Sarah Jane Hennings Manz

Submitted in partial fulfillment of the
requirements for the degree of
Doctor of Philosophy
in the Graduate School of Arts and Sciences

COLUMBIA UNIVERSITY

2019

Abstract

Probing Heterogeneous Dynamics One Molecule at a Time: Polystyrene near the Glass Transition

Alyssa Sarah Jane Hennings Manz

Polymeric systems near their glass transition are known to exhibit heterogeneous dynamics that evolve both over space and time, yet many of the underlying principles of these dynamics are still poorly understood. In this thesis, experimental single molecule studies aimed at uncovering the dynamics of polystyrene near its glass transition temperature are described. In a first approach, the influence of temperature on the timescales associated with dynamic heterogeneity – also referred to as exchange times – are identified by following the dynamics of a fluorescent perylene diimide probe embedded in a high-molecular weight polystyrene host. No clear influence on the lifetime of dynamics is found in the temperature regime T_g to T_g + 10 K. In a second study, heterogeneous dynamics are investigated in the context of molecular weight and fragility. In a similar experimental approach to that of the first study, two fluorescent dyes are utilized to report on the rotational dynamics of low- to high-molecular weight polystyrene hosts. In accordance with previous reports, the stretching exponent, β, is found to be correlated with the system's molecular weight, even on a single molecule level. However, no clear correlation with the system's exchange time was found. In a final study, several single molecule approaches aimed at uncovering the dynamics in confined polystyrene films are described. As no evidence for previously-described mobile surface molecules has been found, this final chapter is meant to provide a basis for future single molecule studies in confined systems.

Contents

List of Figures

List of Tables

Acknowledgements

When I began my PhD studies, I could not have imagined all the growth, changes, and obstacles I would encounter. I am extremely grateful for all the people that have stood by me during this time and who have offered their support and wisdom over these past five years.

First and foremost, I would like to say my deepest thank you to my advisor, Prof. Laura Kaufman. Her guidance, innovation, and vast knowledge have been pivotal to both the advancement of this work, as also my own personal growth and success. Over these past five years, her door was (literally) always open to answer any questions and give advice, both professionally and personally. At the same time, she permitted me to pursue my own scientific problems, while always giving the right amount of advice. I am extremely thankful to Laura for taking me into her group early on and for being such a thoughtful professor I can look up to. Laura truly cares not only about her students, but also about the wellbeing of this department.

I would also like to thank the rest of my committee: Prof. David Reichman, Prof. Wei Min, Prof. Keewook Paeng, and Prof. Christopher Durning. One of the first courses I took during my graduate career was a *Statistical Thermodynamics* class with David, and while I initially felt very intimidated by the subject material, his patience and clear explanations – attributes that would appear often during future interactions – made this a fascinating class. Outside of the lab and academics, I would also like to thank him for his commitment to this department. Both David and Laura have put in a tremendous effort to listen to all the voices in Havemeyer, Chandler, and NWC, and I am excited about the future of Columbia Chemistry, in large due to their hard work outside of research. Meanwhile, I also had the opportunity to TA with Wei in my second year, and I learned a lot during our discussions, in and outside of the classroom. His expertise in the optical and spectroscopic field often permitted additional insight into the problems I was working on. I am

also delighted to have Keewook on my thesis committee. Although initially unplanned, he agreed to step in last minute, and I couldn't imagine a better researcher to discuss the work of my past five years with. Our paths first crossed while he was still a postdoc in our lab, and although our overlapping time was cut short, he has remained an amazing mentor during my PhD and taught me some of the most important aspects of scientific research. He introduced me to single molecule microscopy, the importance of trusting one's own work, and mentored me both from nearby and afar. I hope to be able to visit his lab in South Korea again soon. Lastly, Christopher's class *Topics in Soft Materials* gave me invaluable insight into the vast area my research topic is a part of, and I am very fortunate to now introduce him to my own research.

My graduate studies wouldn't have been the same without other people to socialize with. The Columbia network I have found here has been fundamental to my success and wellbeing, and has provided me with so much insight into the life of a PhD student, in and outside of the lab. I am equally excited and sad to see all the different directions my friends are going. Prakriti Joshi has been there in the best and worst of times – both personally and professionally – and I could not have imagined my PhD career without her and her fruitful scientific and non-academic discussions. Karen Youngah Kwon and Dr. Dat Tien Hoang have been the best coworkers and friends I could imagine, and have always given me great advice, no matter the subject. Karen and I joined the program at the same time, and we have gone through a multitude of experiences together. When Dat was still part of the lab, he was my biggest help when it came to computer-related problems. Even now, he constantly gives me amazing life advice. Dr. Michelle Ziperstein still remains one of my favorite fro-yo partners, and I miss our frequent strolls through Morningside Heights. Prof. Jaesung Yaeng and Dr. Kevin Stokely were instrumental to my success and taught me some of my most important technical and scientific skills. My lab mates, Nicole Mandel (who was always

available to brainstorm my many random ideas and questions), Alexander Devanny, Rachel Avard, Han Yang, Dr. Jieling Zhu, James Kweon, Daniel Lee, Michelle Vancura, Dr. Asja Guzman, Prof. Khan-Hoa Tran-Ba, Prof. Heungman Park, Dr. Hyung Jun Kim, and Dr. Stephen Spinella have constantly given me constructive feedback on my research, and I am proud to call myself a "Kaufman Kid." I was also fortunate enough to have had help by an undergraduate student, Mika Aly, who not only provided me with scientific support, but also taught me how to be a better mentor. Additionally, I would like to thank Joe Matragrano, Dr. Jamie Brisbois, Kihong Lee, James Shee, Lisa Kahl, Dr. Michael Gaschler, Isaac Hughes, and Felisa Conrad-Burton; their friendship and advice definitely made my PhD career more enjoyable.

Outside of Columbia, I have found an amazing network of friends who I count as my adopted family. My partner, Phillip Leung, has listened to (too) many hours of group meeting preparations, seen my stress before important deadlines, and has cooked some of the best meals I could ask for while I was busy reading and writing. His family has taken me in as one of their own and has supported me so much during my PhD work. My close friends, Nipun Basrur and Tracy Pa, have been my constant companions for over six years; they have always been there, day or night, near or far, and I am so lucky to have continued our friendship from Iowa to New York. The other Grinnellian family I have found has been just as important for my success: Kamila Berkalieva was there when I most needed her and still remains a true confidant. Chinar Verma has been an amazing friend and neighbor, while Naina Chhiber, Sivan Philo, and Lindsay Schwartz have been some of the most grounding friends I could ask for. From afar, several of my friendships continue, and I would like to thank Carolin Scholz, Dr. Charlotte Feddersen, Kirsten Shriver, Dr. Nancy Hernández, Dr. med. Sophia Chen, and Giulia Deiana-Schöninger for their long-distance support and constant words of (academic) affirmation.

Lastly, but perhaps most importantly, I would like to thank my family, and in particular the woman who encouraged me to pursue my dreams and who always stood behind me, supporting any decision I made (good or bad), but who cannot be here today to see the product of these past few years. My mother, Dr. Terri J. Hennings, dedicated her PhD dissertation to me, and I am honored to now dedicate mine to her. Indeed, one of my favorite pictures of us is a young me being held by her in her own PhD robes. While I wish we could take a picture with the roles reversed, I will at least hold her in my heart; without her love and support, I doubt I would be standing here today. Of course, there is a second half to me, and I am equally grateful for the love and support I have received from my father, Gerhard Manz. I don't know how he did it, but I am so thankful for all the hours he spent listening to my doubts, and all the words of encouragement he had for me during my most stressful times. My grandmother, Jane Anderson, has been another faithful constant in my life, and I am lucky to have her by my side. I would also like to thank Prof. Linda Schulte-Sasse for all her proofreading and academic tips and tricks.

Of course, this research would not have been possible without funding. The research discussed in this thesis was funded by the National Science Foundation. Stipend support has come from the Chemistry department, the NSF Graduate Research Fellowship Program, the GSAS Lead Teaching Fellows Program, and the GSAS Academic Fellowship Program. Elizabeth Strauss and the rest of the PDL team have been an invaluable asset and constant voices of encouragement, and I will always look back fondly to my time in Mudd. The CTL graduate team – especially Dr. Christopher V. H.-H. Chen – have given me so much advice on teaching, researching, and career search, and I am extremely grateful for all their insight and encouragement.

This thesis is dedicated to my mother, Dr. Terri J. Hennings.

Without her support, love, and dedication I never would have dared to move across the Atlantic to pursue my education and experience so many life changing things.

I miss you every day, Mom.

Chapter 1. Introduction

1.1 Supercooled Liquids, Polymer Melts, and Glasses

1.1.1 Insights into the Glass Transition

Typically, when a liquid is cooled below its melting point (T_m), it will undergo a first-order phase transition and turn into a solid with long-range order. However, if a material is cooled rapidly enough, this phase transition can be avoided, and the material can initially enter a metastable state that is typically either referred to as a supercooled liquid or a polymer in the rubbery regime, which for the purpose of this thesis will be referred to as a polymer melt. When cooled even further, the

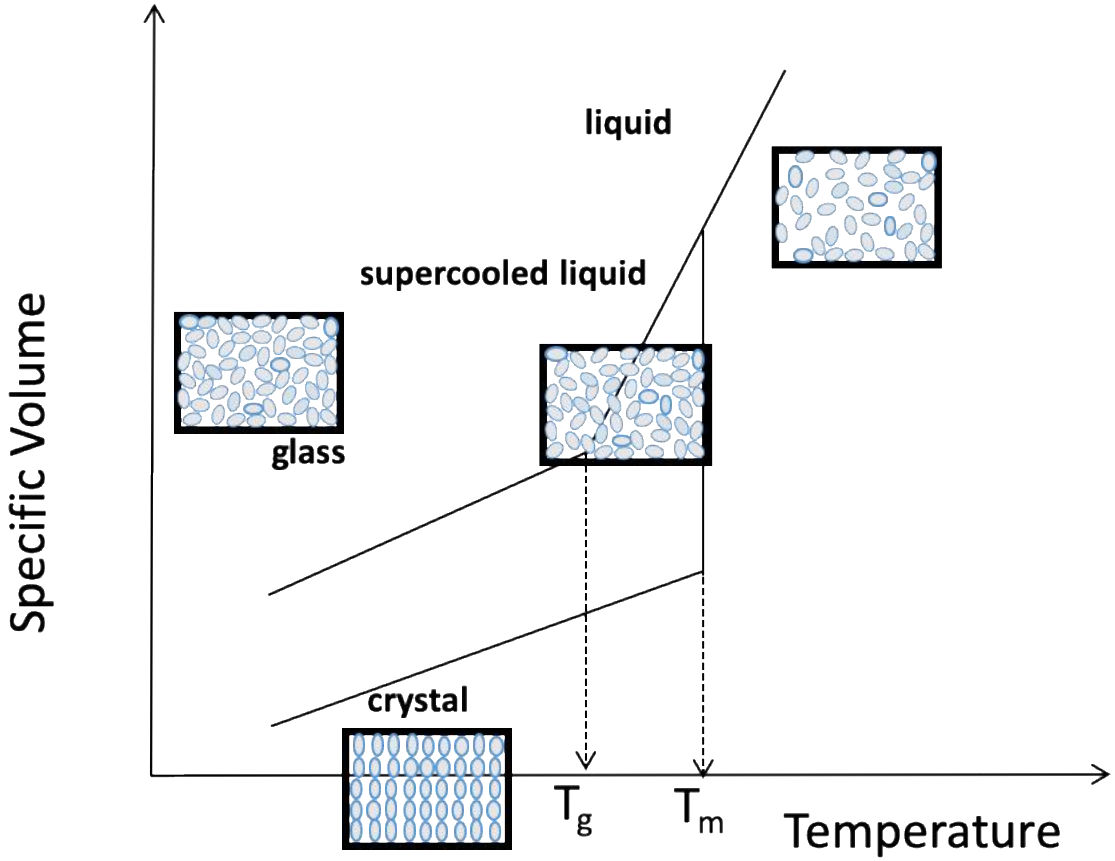

Figure 1. Schematic representation of changes in specific volume when a liquid undergoes cooling. When a typical liquid cools, it will undergo a first-order phase transition and become a crystalline solid, usually resulting in a decrease of specific volume (water being the most common exception). If a liquid is cooled rapidly enough, however, this phase transition can be avoided and the liquid can enter a supercooled state. When cooled even further, the supercooled liquid becomes a solid lacking long-range order, referred to as a glass.

supercooled liquid or polymer melt will rapidly increase in viscosity until it reaches its glass transition temperature (T_g), as depicted in Figure 1. At this point, the material has fallen out of equilibrium and enters a solid-like state referred to as a glass. In popular terms, the word glass is typically associated with silicate glasses, for example those found in windows or bottles. However, from a scientific perspective, the term glass is much broader, with the definition applying to a range of materials from metallic alloys to polymers, ionic solids, and small molecule amorphous solids. Despite the ubiquity of this class of material, understanding the processes and particularities accompanying the glass transition has been a major scientific challenge for over a century, and many questions around these phenomena still remain unanswered.[1–3] Even something as seemingly straightforward as defining the temperature associated with the glass transition can be challenging. Indeed, several definitions of T_g exist, in part because unlike the melting temperature associated with a first order phase transition, T_g depends on the cooling rate. Often, the glass transition temperature is determined through differential scanning calorimetry (DSC) measurements, with T_g defined as the temperature at which a notable decrease in heat capacity occurs.[4,5] However, even here, two definitions arise: T_g can be defined as either the onset or the midpoint of the step change in the measured heat capacity. Alternatively, the glass transition can be defined as the point when the shear viscosity of the material reaches 10^{13} poise upon cooling, usually corresponding to a characteristic molecular relaxation time of 100 seconds.[6]

An additional interesting aspect of glassy materials is the difference between their macroscopic and microscopic behavior: macroscopically, glasses behave like solids, while microscopically, they resemble a liquid and lack the long-range order typical of a crystal.[7] At the same time, the dynamics of glasses and supercooled liquids do not resemble those of typical liquids at all.[6] Molecules in glassy materials near their T_g have drastically slowed dynamics, moving up

to 10 magnitudes more slowy than molecules near T_m.[8,9] Angell first characterized the degree to which these dynamics slow down as a glassy material approaches T_g and termed it fragility, a concept that will be further discussed in Chapter 4.[3,10] In brief, the viscosity of polymer melts and supercooled liquids increases as the glass transition temperature is approached from above, corresponding to a slowing down of dynamics. From a kinetic point of view, this slowdown in dynamics results in a glass transition due to limited molecular rearrangements.[9] In other words, as a supercooled liquid is cooled below its melting temperature, the molecules will reach a point at which they are no longer capable of rearranging before the temperature is further lowered as the timescales of rearrangement begin to far exceed the rate of cooling. At this point, the molecules move so slowly that they appear "frozen" on experimental timescales and the liquid becomes a glass.[9]

Meanwhile, thermodynamic explanations of the glass transition also exist, and related theories are constantly evolving. As originally proposed by Adam and Gibbs, regions within a sample near T_g are thought to cooperatively rearrange independently of their environment, with these regions only being able to rearrange with sufficient activation energy, E_a.[11,12] This energy in turn is inversely proportional to both the system's temperature and configurational entropy, *i.e.* the number of metastable states accessible to the system: the system's relaxations slow down as the temperature decreases since fewer entropic states are available for exploration. Thus, as later suggested by Goldstein, the glass transition can be explained by molecules becoming energetically trapped. Above T_g, the system explores an energy landscape consisting of many local minima. These minima are separated by energy barriers that increase as the temperature decreases.[13,14] At T_g, the energy barriers have become large enough to trap the system in a specific minimum, resulting in the formation of an amorphous glass. This idea was further expanded by Kirkpatrick

and Wolynes in the random-first order theory (RFOT).[15] In this theory, the system consists of "droplets" forming a "mosaic," with each droplet exhibiting random local configurational entropies.[14,16] On the one hand, each mosaic patch constantly attempts to rearrange and explore various entropic states; on the other hand, neighboring patches create varying boundaries, and the system pays an energetic cost when a patch rearranges due to the altered boundary.[17] Hence, this constant compromise between entropic and energetic gains leaves the system in an unstable state. Additionally, the barrier to rearrangement grows with increasing patch size, and this size in turn grows with decreasing temperature, in accord with earlier theories such as that of Adam and Gibbs, thus finally resulting in a glass at T_g. However, unlike in the Adam-Gibbs approach, the patches present in the RFOT model depend on the boundaries set by adjacent molecules.

As the temperature-dependent rearrangements suggested by Adam and Gibbs require a certain energy to occur, relations between the observed slowing down of dynamics/increase in viscosity upon cooling and the system's activation energy have been made. Based on Angell's fragility approach, some glass formers, typically characterized as "strong," exhibit an Arrhenius-like temperature dependence of the viscosity, given by

$$\eta(T) = A \cdot e^{\frac{E_a}{k_B T}},$$

where $\eta(T)$ corresponds to the viscosity, E_a is the activation energy, and k_B is the Boltzman constant. In contrast, "fragile" glass formers deviate from this relationship and exhibit a non-Arrhenius temperature dependence of their viscosity.[6,9,18–20] This in turn can be represented by the Vogel-Fulcher-Tammann (VFT) equation,

$$\eta(T) = \eta_0 \cdot e^{\frac{B}{T - T_\infty}},$$

where η_0 is the viscosity at infinite high temperature, T_∞ corresponds to the VFT divergence temperature, and B is a material-specific parameter related to the activation energy.[21,22] A detailed

view and small molecule examples of these different temperature dependences is given in Figure 2.[3] Polymers are excluded from this figure as they typically exhibit a chain length dependence of their fragility, with larger polymers usually exhibiting a stronger deviation from Arrhenius-like behavior than their oligomers.[23] At this point it should be noted that other mathematically equivalent (as well as some non-equivalent) representations that capture the temperature dependence of viscosity as a function of temperature in glassy materials, such as the Willams-Landel-Ferry (WLF) equation, also exist; however the VFT approximation will be used for the purpose of this thesis.[24–27]

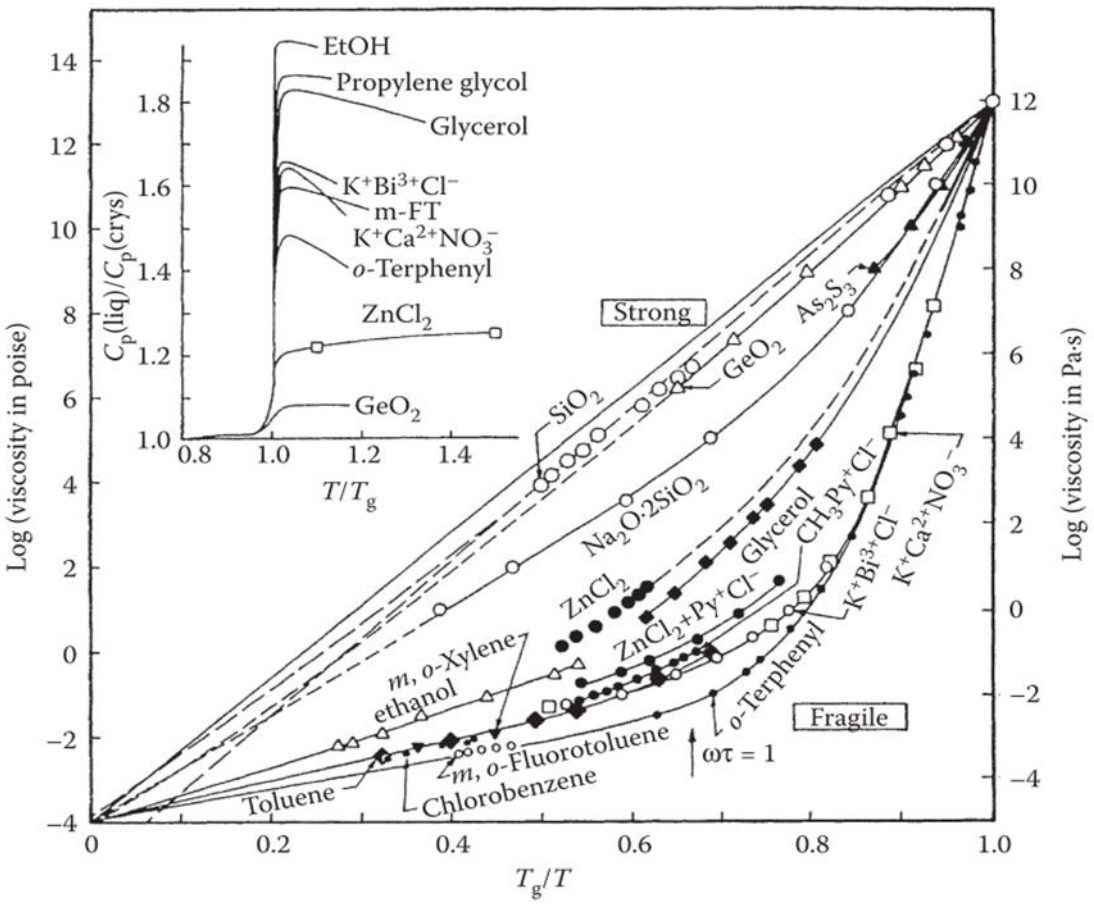

Figure 2. Viscosity as a function of temperature for strong and fragile molecular glass formers. Strong glass formers, such as SiO_2, show an Arrhenius-like temperature dependence of their viscosity, while fragile glass formers, such as o-terphenyl (OTP), show a deviation from this dependence. In addition, the inset shows the jump in heat capacity at T_g for several glassy systems. This figure is reproduced from reference 3 with permission from the publisher.

Despite the clear observation that there is a sharp increase of viscosity as T_g is approached and the multitude of theories aimed at explaining the glass transition, the underlying dynamics and causes of such a slowdown are still incompletely understood and, considering the slow timescales involved, quite difficult to study experimentally. Given the rapid change in viscosity near T_g, glasses at and below T_g may be difficult to access and characterize experimentally, yet similar measurements just a few degrees above T_g are viable. This permits measurements of the dynamics in supercooled liquids and polymers in the rubbery regime on the laboratory timescale. Much work has thus been performed at these temperatures below T_m yet above T_g, giving further insight into some of the interesting properties arising near the glass transition.

1.1.2 The Particular Dynamics near T_g

Curiously, the dynamics of molecules in glassy materials in this temperature regime not only exhibit a wide range of different temperature dependences based on their fragility (Figure 2) but also the timescales on which molecules move appear to vary as a function of time (referred to as temporal heterogeneity) and over space (spatial heterogeneity) near T_g. This phenomenon has been coined dynamic heterogeneity and is not seen in typical liquids.[28–30] A schematic of the differences between temporal, spatial, and spatio-temporal (dynamic) heterogeneity is presented in Figure 3, where τ corresponds to the molecular relaxation timescale.[31] In systems with spatial heterogeneity, relaxations differ from one region to another but are not affected by time. In contrast, in systems with temporal heterogeneity, all molecules relax on the same timescales, but these relaxations change over time. In systems with dynamic heterogeneity, the timescales differ both between regions and also change over time.

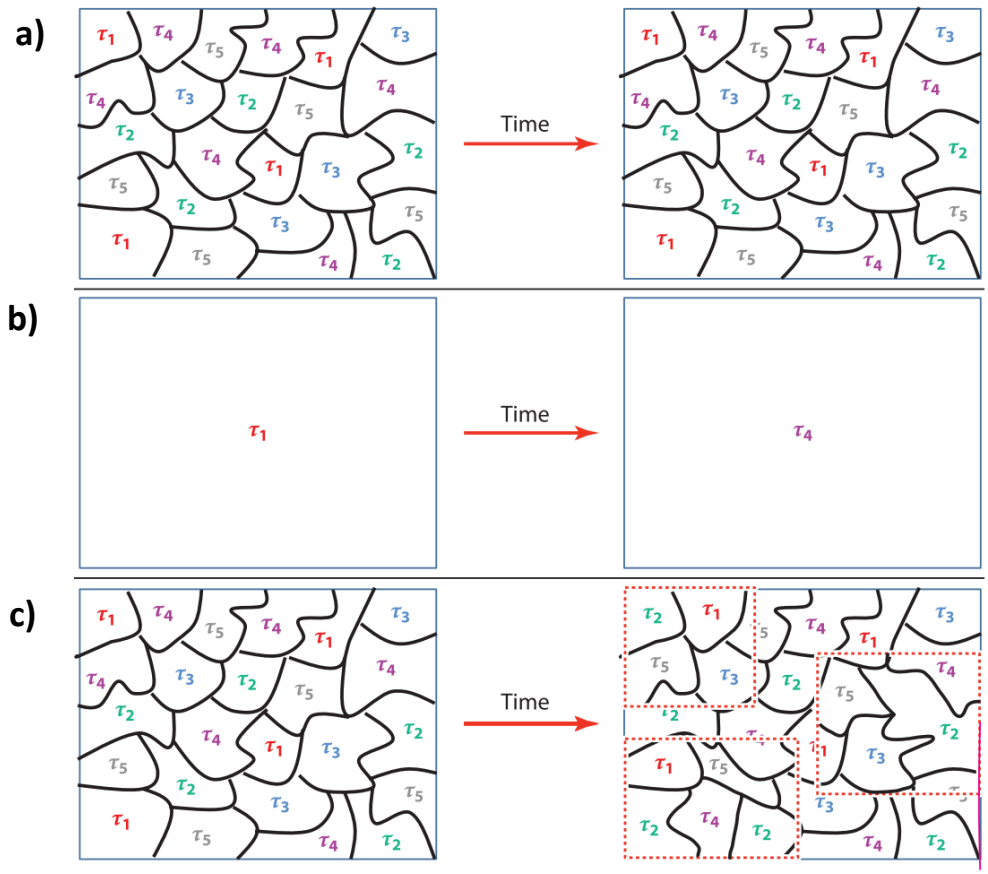

Figure 3. A system with (a) spatial heterogeneity, (b) temporal heterogeneity, and (c) spatio-temporal (dynamic) heterogeneity.
In a system with spatial heterogeneity, relaxation timescales, τ, do not change over time, but do differ from one region to another. In a system with temporal heterogeneity, all regions experience the same τ, but this value changes over time. In a system with spatio-termporal heterogeneity, τ changes both over time, and also between regions. Reproduced from reference 31 with permission from publisher.

These observed heterogeneities have been suggested to be related to the cooperatively rearranging regions (CRRs) originally proposed by Adam and Gibbs, with the system's relaxation time determined by the configurational entropy.[11,12,32,33] Interestingly, the observed heterogeneity in dynamics does not appear to cause, be caused by, or exist alongside any structural heterogeneities in the system.[28,29,34,35] Questions regarding the size of the CRRs and the lifetime of dynamic heterogeneities, the time it takes for slow regions to become fast, and the temperature dependence of these heterogeneous dynamics – to name a few – have been the focus of a multitude

of experimental and theoretical studies.[29,30,36–47] Many experimental techniques exist to gain additional understanding of these dynamics and begin answering these questions, with approaches typically relying on perturbing a system and monitoring its relaxations or monitoring fluctuations in molecular dynamics.

In all cases of these glassy systems, the measured molecular relaxations display a non-exponential decay and can be described by the Kohlrausch-Williams-Watts (KWW) equation,

$$\phi(t) = e^{-\left(\frac{t}{\tau}\right)^{\beta}},$$

where τ is the characteristic relaxation time and the degree to which β deviates below 1 characterizes the degree of heterogeneous behavior and the existence of multiple relaxation timescales present in the liquid, which can stem from differences in space and/or time. While the phenomenon of dynamic heterogeneity has been well-established, many past experiments have relied on ensemble and sub-ensemble approaches, such as dielectric spectroscopy, photobleaching techniques, and NMR.[48–50] These techniques have undoubtedly led to great progress in the field,

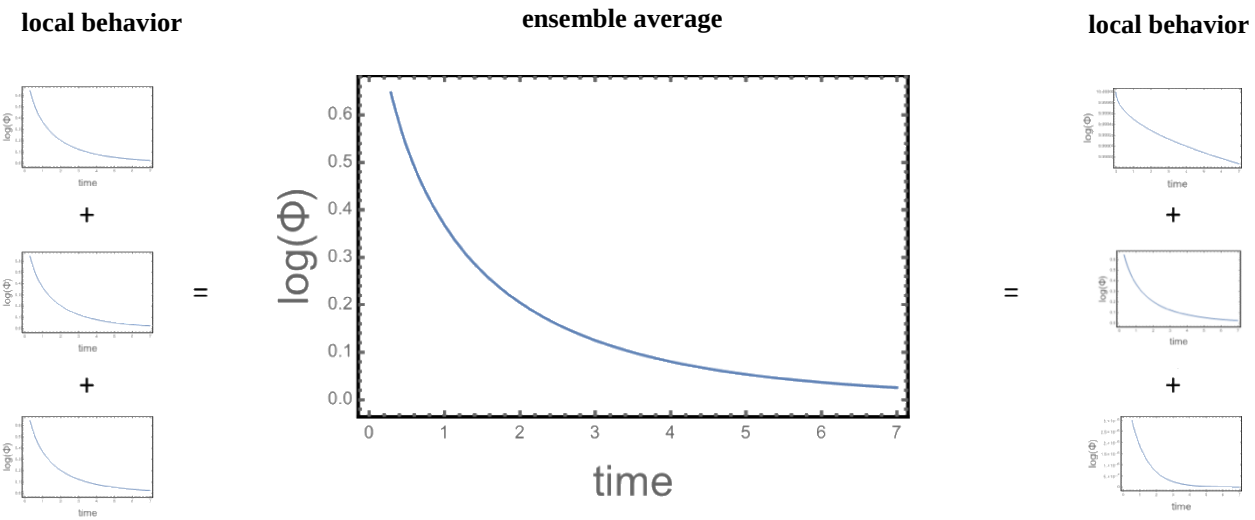

Figure 4. Temporal (left) and dynamic (right) heterogeneous single molecule explanations for an averaged (middle) stretched-exponential relaxation function.

yet they average over large numbers of molecules and thus cannot distinguish spatial and temporal heterogeneity or characterize the full breadth of dynamics present in supercooled liquids. Experimentally, this is expressed by a single averaged stretched exponential relaxation function, which obscures the dynamics of individual molecules.

Averaged stretched exponentials can arise from multiple scenarios, with two extreme cases shown in Figure 4: in the purely temporal heterogeneity case, the relaxations of all molecules would give rise to the same stretched exponential, which corresponds to an averaged relaxation function identical to the individual ones. In contrast, at the single molecule level, dynamic heterogeneity would give rise to a variety of differing relaxation functions, incorporating temporal and spatial heterogeneity, potentially ranging from purely to highly stretched exponential decays. The averaged function may be the same in the temporal, spatial, or dynamic heterogeneity cases, and differentiating between these scenarios is not possible due to the information lost during averaging. It should thus come as no surprise that previous ensemble studies have not fully resolved many questions about glassy systems and approaches allowing differentiation between individual molecules – and thus dynamics – have grown in popularity over the past years.

1.2 Single Molecule Studies near the Glass Transition

The emergence of optical single molecule techniques in the late 1980s initially began with measurements in crystals restricted to cryogenic temperatures.[51–54] Advances in single molecule approaches have expanded the experimental possibilities and now permit the dynamic study of systems near their glass transition temperature. These approaches circumvent many of the issues that result from ensemble averaging. Over the past decade, fluorescence microscopy approaches in particular have given additional insight into glassy phenomena that previous techniques may have obscured.[21,55–65] Typically, in these studies probes are dispersed very dilutely in a host – in

this case the supercooled liquid or polymer in the rubbery regime – and the dye's fluorescence is monitored over a given period of time. The probe is expected to accurately report on the dynamics of its host and is present at very low concentrations, limiting concerns the probe perturbs the system and permitting optical identification of individual probe molecules. The first experiment aimed at uncovering the dynamics of a supercooled liquids via a single molecule approach occurred almost two decades ago and relied on interrogating heterogeneous dynamics by measuring the probe's rotation through its linear dichroism (LD).[66] Indeed, the rotational relaxation timescale of the probe can be easily linked to the host's viscosity, and thus dynamics, through the Debye-Stokes-Einstein equation:

$$\tau_c = \frac{4\pi\eta r_s^3}{3k_B T},$$

with τ_c corresponding to the rotational relaxation, η the viscosity of the host, r_s the hydrodynamic radius of the probe, and k_b the Boltzmann constant.[66,67] Since the probe reports on the rotations of the host it should also report on any changes in rotations over time and/or within space (*i.e.* temporal and spatial heterogeneity). A detailed view of this is given in Figure 5: a probe (black oval) is embedded in a dynamically heterogeneous system, where different colors represent regions

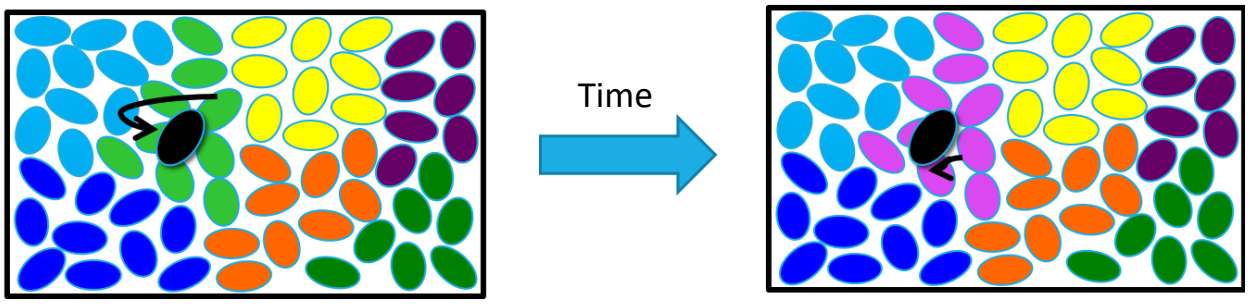

Figure 5. Probe rotations in a dynamically heterogeneous host over time.
Different relaxation timescales are shown by varying colors, while the probe's relaxation (black oval) is represented by a black arrow.

with different relaxation timescales. As time progresses, a region changes from a fast timescale (green) to a slower timescale (pink), and the probe embedded in this region changes its rotational motion, as represented by the size of the probe's arrow.

However, since these rotations are indirectly reporting on the host's dynamics, careful considerations must be made prior to choosing a probe.[60,68–70] For one, interactions between the probe and the host, as well as large probe size, can limit information gained due to averaging over several regions in space and/or time.[34,71,72] Factors such as hydrogen bonding can severely slow down the probe in comparison to the host, resulting in longer timescales reported than found in probe-free ensemble studies.[73] Additionally, fluorescent probes used for single molecule studies must also have a high quantum efficiency and be sufficiently photostable. Errors arising from low quantum efficiency and resultant poor signal-to-noise ratios can greatly limit the advantages gained from single molecule approaches. Similarly, if a fluorophore photobleaches too quickly, single molecule experiments may not be able to fully cover the timescales of interest and show finite trajectory length effects, as in part discussed in Appendix A.[74,75] This in turn can lead to large errors in reported relaxation times and stretching exponents, even resulting in incorrectly classifying a heterogeneous system as homogeneous and vice-versa.[76] Fortunately, much previous work has been done in this group to identify optimal fluorescent probes for single molecule measurements.[69,77,78]

1.3 Polymeric Glass Formers

1.3.1 Background and Previous Work

Avoidance of a first-order phase transition upon rapid cooling, dynamic heterogeneity without structural heterogeneity, and extreme viscous slowdown near the glass transition temperature are common to all glassy materials. However, a particularly interesting class of glass

formers are polymeric glass formers. Like all glassy materials, they are amorphous solids below T_g, and these glassy polymers appear quite brittle when cooled. Above T_g however, they have a high viscoelasticity and are often termed rubbery polymers or polymer melts. Glassy polymers are the basis of many modern technologies as they can be produced at low cost and have attractive material properties. These polymers can be found in technologies ranging from optical devices and solar cells to food and tissue preservatives.[79,80] Additionally, many industrial processing methods involve rapid cooling, thus further increasing the abundance of glassy rather than crystalline polymers.[81] This class of material is also particularly interesting to study, as polymers are typically good glass formers, owing to the difficulty of crystallizing large molecules and polymers' tendency to display high fragilities.[23,82,83] In fact polymeric glass formers can exhibit fragilities twice as high as their molecular counterparts. Unlike small molecule glass formers, polymer dynamics can be slowed down due to chain connectivity and rigidity, decreased cooperative chain motion, and interchain entanglements. These factors translate into strongly increasing viscosity upon cooling, and thus high fragility.[8,20,23,83] Much attention has hence been devoted to the relaxation dynamics found in polymers near their glass transition temperature.[84,85]

Polystyrene in particular is a commonly-studied polymer melt: while its glass transition temperature is molecular-weight dependent, its T_g saturates at ~100^{o}C at moderate to high molecular weights and is thus sufficiently high to allow polystyrene's incorporation into many devices. At the same time, this glass transition temperature is low enough to be easily accessible in laboratory settings. Both the monomer and polymer are inexpensive, resulting in polystyrene's frequent usage in consumer products, such as food packaging, plastic toys, and automobile parts.[86,87] Like many other polymers, atactic polystyrene (*i.e.* polystyrene with random stereochemistry) is highly viscous above its T_g and readily undergoes the glass transition;

additionally, high molecular-weight polystyrene exhibits a relatively high fragility, thus resulting in this polymer being a frequent focus of polymeric glass studies.[40,88,89]

In early experimental work, Ehlich and Sillescu studied the diffusion of sub-ensembles of variously sized tracer molecules by forced Rayleigh scattering below and above the host's T_g in multiple polymer melts, including high molecular weight polystyrene, to follow the transport of small molecules in polymeric systems. In a later study, Ediger and co-workers used a sub-ensemble fluorescence recovery after photobleaching (FRAP) approach to study both the translational and rotational motion of various probes in polystyrene above its glass transition temperature, with both studies finding evidence for spatial heterogeneity in this glassy polymer.[30,90] Additionally, early single molecule studies on this polymer by Flier *et al*. have given insight into the temporal and dynamic heterogeneity of polystyrene, though use of a very large single molecule probe in these studies likely prohibits full elaboration of dynamics despite the single molecule approach.[58,91] Work in our group has continued the search for an ideal single molecule probe, *i.e.* a highly fluorescent molecule that reports the full breadth of dynamic heterogeneity of the host, for measurements in polystyrene. Recent work by Paeng *et al.* focused on the investigation of two perylene dicarboximide dyes as potential probes and found one to mirror and report the heterogeneous dynamics of the host polystyrene quite successfully.[78] Indeed, much of the work presented in this thesis is based on studies using this probe.

1.3.2 Exchange Time and Dynamic Heterogeneity

Monitoring probe rotations and translations in glassy systems has provided much insight into the dynamics near T_g. However, additional information can be gained by following subsets of molecules and analyzing the time they spend in a given dynamic environment. This time scale, often referred to as either the lifetime of dynamic heterogeneity or the exchange time, gives further

insight into the particular environments individual molecules may experience in a supercooled liquid or polymer melt over time. This time scale is of particular interest in polymers: it can have a large impact on the transport and mechanical properties of these glass formers as many technologies rely on small molecule diffusion through heterogeneous environments.[40,92] While some studies report time scales of exchange to be on the order of the relaxation time of the host, most studies have suggested the exchange time to be multiple orders of magnitudes longer.[38,40,46,64,78,93] The reported differences could, in part, arise from the subsets of molecules studied.[94] Early studies investigating the exchange time in both polymeric and small molecule glass formers focused on multi-dimensional NMR techniques.[38,46,95] Soon, theoretical and optical approaches followed, and differences in subsets analyzed and resulting time scales of exchange began to emerge.[40,96–98]

A recent study in our group by Paeng *et al.* relied on a single molecule approach that followed both slow and fast subsets of probe molecules in polystyrene near T_g and found different time scales of exchange for these two subsets: the slow subset of molecules exhibited a characteristic exchange time ~4 times longer than the fast subset, as evidenced by the time it took this subset to report an average rotational time.[78] Indeed, a photobleaching approach by Ediger *et al.* solely followed slow molecules in polystyrene and reported exchange time scales similar to those found in the single molecule experiment for a slow subset of molecules.[40] It is thus possible that studies reporting on exchange time scales matching the overall relaxation time only monitored fast subsets of molecules. Interestingly, although the single molecule study did not focus on a temperature dependence of these exchange time, no evidence for such a dependence was found, contrary to prior sub-ensemble results by Ediger and co-workers.[40,96] However, most technologies

relying on glassy polymers operate over a range of temperatures, and further work must thus be done to characterize these lifetimes of heterogeneous environments.

1.3.3 Fragility and Polymer Chain Length

Temperature plays an important role in the properties of polymers, yet additional factors can also influence the characteristics of these glassy systems. Many polymers – including polystyrene – not only exhibit a much stronger temperature dependence of their structural relaxation and viscosity than their molecular counterparts but also appear to have molecular-weight dependent fragilities.[83,88,99] Fragility, *m*, is defined as

$$m = \left. \frac{\partial \log \tau}{\partial [\frac{T_g}{T}]} \right|_{T=T_g}$$

with τ a characteristic relaxation time and with a larger *m* value corresponding to a more fragile liquid. Typically, $m < 100$ for molecular glass formers, but this value can easily go as high as 150-200 for polymeric systems and often scales with molecular weight.[8,20] Interestingly, even the oligomers (*i.e.* low-molecular weight counterparts) of polymers with extremely high fragilities usually exhibit viscosity dependences typical of molecular glass formers.[83,100] Similarly, polymers with flexible backbones, *e.g.* polybutadiene and polyisobutylene, typically exhibit much lower fragilities and a weaker molecular weight dependence of both *m* or T_g than more rigid polymers, such as polystyrene and poly(methyl methacrylate).[83,101]

The exact mechanism of these molecular weight-dependences is not completely clear, yet Dalle-Ferrier *et al*. have suggested it may be correlated, at least in part, with the relative size of the polymers compared to the length scale of cooperatively rearranging regions (CRRs).[83] Previous studies have suggested that the size of these regions is on the range of 2-5 nm.[9,38,99,102] Meanwhile,

the radius of gyration of high-molecular weight polystyrene can reach ~15 nm, far exceeding the length scales typically associated with regions of distinct relaxation dynamics in glassy systems.[83] Furthermore, the authors of reference 83 suggest that this difference between the sizes of CRRs and polymer radii could result in conformational states becoming inaccessible to the polymer, leading to a decrease in the configurational entropy, S_c, accessible to the system. As proposed by Adam and Gibbs, the timescales of molecular relaxations depend inversely on both temperature and S_c. Hence, an increase in molecular weight would lead to lower S_c and result in a steeper temperature variation of dynamics, *i.e.* fragility. Similarly, studies have suggested an increase in activation energy upon cooling in fragile liquids; while competing explanations for this phenomenon exist, the proposed energy increase is consistent with the drastic slow-down of dynamics in fragile liquids as the system's E_a depends on both τ and η.[103] Interestingly, the relations proposed by Dalle-Ferrier and others could also explain the difference in molecular weight-dependences seen between polymers: while rigid polymers experience an increase in inaccessible configurations with increasing molecular weight, flexible polymers have a lower barrier to accessing a variety of configurations (thus resulting in a lesser decrease in S_c accessible by the system), consistent with smaller changes in T_g and fragility observed in these polymers.

As polystyrene's fragility and glass transition temperature are so strongly dependent on its molecular weight, the dynamics and related heterogeneities may also change with chain length. However, while studies exist relating factors such as fragility and the stretching exponent or the system's activation energy, most research has either focused on the relationship between a polymer's fragility and its structure or solely studied the dynamics of one (typically high) molecular weight.[20,22,30,40,104–106] A clear relationship between molecular weight, fragility, and the heterogeneous dynamics found in glassy polymers near T_g is thus still lacking.

1.3.4 Polymer Confinement

As previously evidenced, a polymer's molecular weight can strongly influence its glass transition temperature; however, chain length is not the only factor affecting T_g. While the glassy regime of bulk polymers has been and continues to be widely studied, additional interesting phenomena arise once polymers are spatially confined. As amorphous polymers are confined to nanoscale lengths and thicknesses, a change in T_g relative to their bulk value has been observed.[107,108] Similar observations have been seen in polymers confined to other nanoscale geometries, such as in nanospheres and nanocomposistes.[109–113] Interestingly, no clear consensus on either the magnitude or the direction of this shift exists. However a majority of studies – in particular in polystyrene, the focus of this thesis – suggest a lowering of T_g with decreasing size, with the magnitude depending on factors such as experimental methods, cooling rate, and sample preparation.[111,114–124] From a technological point of view, this is especially interesting: advanced materials rely on the long-term use of polymers in confined geometries, such as nanopores and narrow channels, and the lack of a clear understanding of the particularities of polymer thin films can drastically limit industrial applications.[79] Transport mechanisms, for example, may change on the nanoscale, yet many technologies rely on small molecule diffusion – and thus relaxations – through heterogeneous environments in confined polymers.

Polymer thin films, a specific type of confinement typically defined as films < 100 nm thick, are commonly used in microelectronics, membranes in separation technologies, and organic photovoltaic cells.[125] One widely accepted model is that such films are composed of layers with differing dynamics. In particular, both experiments and simulations suggest that polymer films exhibit a bulk layer with typical glassy dynamics and a surface layer consisting of particularly fast molecules.[119,123,126] In fact, these enhanced dynamics are critical in the production of ultrastable

glasses through physical vapor deposition (PVD).[127,128] During typical glass preparation, *i.e.* rapid cooling, most energetically stable states are not immediately accessible to the system and accessing these states occurs only on very long timescales (a process typically referred to as aging).[129] In contrast, PVD relies on depositing thin layers of glassy materials. Due to enhanced surface dynamics, low potential energy states can be reached much faster: Swallen and co-workers report timescales of hours, rather than the typical years, for two organic glasses to reach a stable state when prepared via PVD.[128]

Previous work by Paeng *et al.* has suggested that the dynamics found in the surface layer of polystyrene are enhanced by a factor of several decades as compared to the bulk.[130] In this work, a photobleaching approach was used to analyze the dynamics of free-standing films, down to a thickness of 14 nm, and a temperature-dependent surface layer of up to 7 nm with enhanced dynamics was found. While this study found no molecular-weight dependence on the thickness of the mobilized surface layer, Fakhraii and co-workers later performed cooling-rate dependent T_g studies on supported thin films and did find a lesser T_g reduction with increased molecular weight.[131] However, the existence of a mobile surface layer was not disputed: this cooling-rate dependent and other studies by the Fakhraai group suggest a mobile layer with dynamics enhanced by several decades as compared to the bulk.[127,132] Other studies suggest a three-layer model in which molecules near a substrate experience even slower dynamics than the bulk, dictated by polymer-substrate interactions.[133,134] In fact, both the two- and three-layer models can in part explain the differences in T_g observed in thin films across studies: while a slow substrate layer could result in either a lowering of the glass transition temperature or no change due to competing surface and substrate dynamics, it would only be observed in studies involving the use of substrate-bound films. In contrast, no substrate is present in free-standing film approaches, and thus most

likely only the fast surface layer would impact the glass transition temperature, resulting in the commonly-observed T_g depression.[135] One possible explanation for the presence of this fast surface layer is decreased cooperative motion between polymers due to a free interface, thus permitting accelerated dynamics of surface molecules.[125] Indeed, from a thermodynamic standpoint, the RFOT model previously discussed would predict a specific temperature-dependent $\tau_{surface}$ that is dependent on, yet also different from, the bulk relaxation as the entropic landscape differs near the free-surface.[127]

Recent studies have shifted away from focusing on the observed change in T_g and toward understanding the dynamics associated with the change in surface dynamics. Nonetheless, a clear single-molecule understanding of the distinct dynamics present in the layers of these thin films is lacking, in part due to the same restrictions found in many measurements aimed at accessing the dynamics of bulk films, such as poor probe choice or limited spatial and temporal resolution.[21,58,91,110,113,136–139]

1.4 Motivation and Thesis Outline

Many of the questions around glassy materials posed in Chapter 1.1.2 still remain unanswered, in particular in polymeric materials such as polystyrene. Several models aiming at explaining the glass transition and relating the particular dynamics found above T_g to macroscopic properties exist, yet consensus between the various theories has not yet been reached.[12,140] The work presented in this thesis is aimed at providing additional answers via a single molecule approach to some of these unsettled questions, with a particular focus on polystyrene near its glass transition temperature. Going beyond a theoretical perspective, many of these questions also have important practical implications. Small molecule transport in rubbery polymers can be tuned by gaining a better understanding of the heterogeneous environments and their exchange times, while

the stability of many glass formers can be further enhanced through a better understanding of the enhanced surface dynamics prominent in confined systems. The following chapters thus present new insight – in part contradicting previous (sub)ensemble studies – into the heterogeneous dynamics of polystyrene near its glass transition temperature.

In particular, in-depth descriptions of materials and methods for both experimental and theoretical studies can be found in Chapter 2. The focus of Chapter 3 is on answering questions around the temperature dependence and lifetime of heterogeneous dynamics of high-molecular weight polystyrene near its T_g. Multiple studies with contradicting results exist, yet an experimental single molecule understanding was previously lacking. In Chapter 4, the focus is shifted toward gaining additional insight into aspects of heterogeneous dynamics associated with a change in molecular weight (and thus fragility) of polystyrene through the use of two probes. While a shift in glass transition temperature with a change in molecular weight has been widely accepted since the mid 20^{th} century, a single-molecule analysis of the associated dynamics had previously not existed. Lastly, in Chapter 5, various attempts to characterize the surface dynamics of thin films on a single molecule level are described. While no clear evidence of distinct dynamics of a mobile layer has yet been identified with single molecule approaches, several attempts aimed at simultaneously observing surface and bulk molecules are described. This chapter should ideally be viewed as the basis for future single-molecule studies in confined systems.

As the focus of this thesis is an experimental single-molecule approach to understanding heterogeneous dynamics in polystyrene near its glass transition temperature, theoretical and spectroscopic material that further validate the presented findings can be found in the Appendix. In particular, Appendix A highlights the importance of investigating all parameters gained from

single molecule approaches in order to discriminate between heterogeneous and homogeneous systems, while Appendices B and C present supporting experimental data.

Chapter 2. Materials and Methods

2.1 Optical Setup

For all experiments discussed in this thesis, the rotations of probe molecules in polystyrene near T_g were studied using a homebuilt microscope in a wide-field configuration. The light from a continuous wave diode Nd:Vanadate laser (532 nm) was first focused through a quarter (Thorlabs, WPQ05M-532) and then a half wave plate (Karl Lambrecht, MWPQ2–12). It was subsequently coupled into a multimode fiber, which was shaken at constant frequency and amplitude by a speaker to eliminate speckles and produce a randomly polarized and homogeneously illuminated field of view (diameter ≈ 100 μm), assuring excitation of probes regardless of their orientations in the sample. The light was then focused at the back of the objective lens (Zeiss, LD Plan-Neofluar, air 63×, NA= 0.75) and through a 0.5 mm thick cryostat window to illuminate the sample. The sample was placed on top of a sample stage, coupled to both a heating system and a liquid nitrogen cooling system, and separated ~0.25 mm from the cryostat window. Fluorescence was collected in the epi-direction, through the same objective lens, and then passed through a dichroic mirror, a

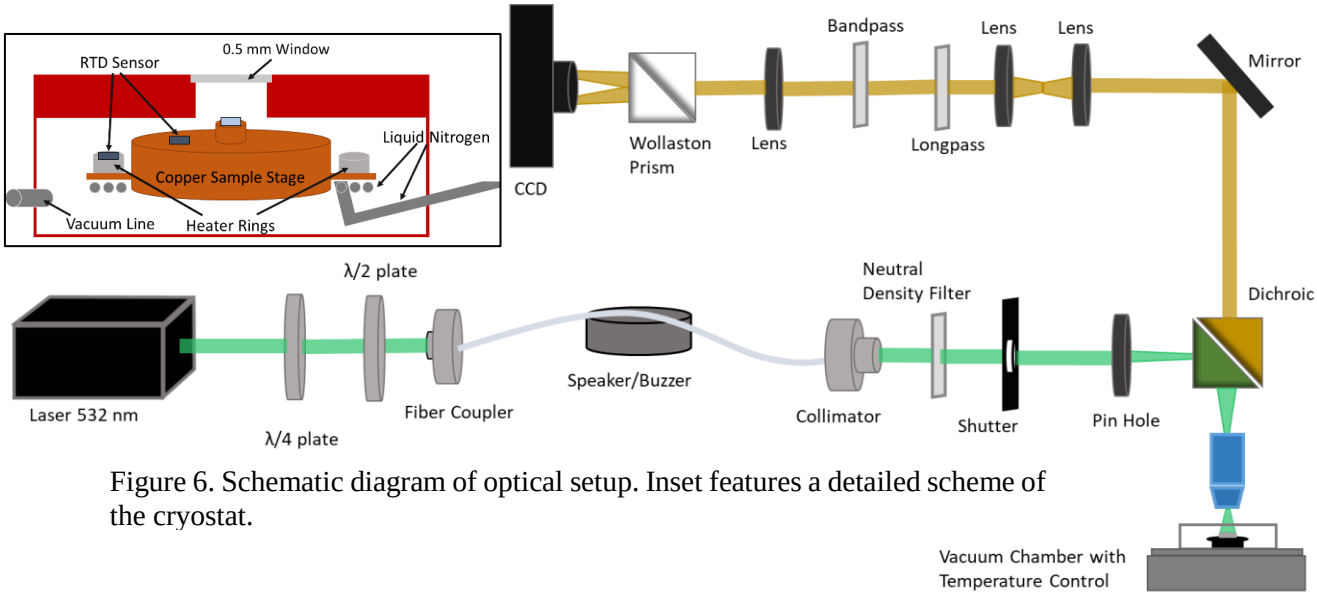

Figure 6. Schematic diagram of optical setup. Inset features a detailed scheme of the cryostat.

long-pass (Semrock, LP03-532RU-25), and a band-pass filter (Semrock, FF01-582/75). A Wollaston prism was used to split the image into orthogonal polarizations, which were imaged onto an electron multiplying charge-coupled device camera (EMCCD; Andor iXon DV887). A detailed schematic of this setup is presented in Figure 6. Excitation power was always 10-20 mW at the back of the objective lens, corresponding to a power density of 100-200 W/cm^2 at the sample.

To best capture rotational dynamics of a majority of molecules, frame rates were typically chosen to be ≈ 20 frames per median relaxation time (τ_{fit}) for the longest set of movies. In the temperature dependent studies, this corresponds to 7 s (373.0 K), 0.2 s (378.1 K), 0.06732 s (379.6 K), and 0.00801 s (383.6 K), and the longest movies consisted of 20,000 frames. For movies collected at the highest temperature in this study, only a portion of the CCD chip was used to maximize frame rate. All movies with a frame rate > 5 Hz were collected continuously while slower frame rate movies were collected with a 0.2 s exposure time, with illumination shuttered between frames to limit photobleaching.

For molecular weight dependent studies, all data was collected at frame rates that produced $\tau_{fit,med} \approx 4$s. Thus, a frame rate of 0.2 s – corresponding to 20 frames per $\tau_{fit,med}$ – was chosen, and this frame rate was used for all molecular weights and probe combinations, with no modification of exposure time. Again, all long movies were 20,000 frames long. Lastly, for thickness-dependent studies, both the time between frames and exposure times were varied. The time between frames ranged from 0.1 s to 20 s, while exposure time ranged from 0.1 s to 1.5 s, and the longest set of movies did not exceed 8,000 frames.

For temperature and molecular weight dependent studies, several long movies were collected on the same sample, such that data was collected from at least 1000 molecules at each temperature. Fewer and shorter movies were collected for thickness-dependent studies, in part to

avoid photobleaching at longer exposure times. All movies were recorded in 14-bit using LabView. To account for a small degree of sample heating, set temperatures were corrected from measured temperatures in both the temperature- and molecular weight-dependent studies. Power dependence measurements of tbPDI in o-terphenyl, as reported by Mackowiak *et al*., were used for these corrections: in both o-terphenyl and polystyrene, sample heating is expected to result solely from substrate heating as the hosts do not absorb at 532 nm.[94] Hence, the temperature increase as a function of excitation power is expected to be host independent. No temperature correction was performed for the thin-film studies.

2.2 Sample Preparation

2.2.1 Temperature Dependent Studies

Polystyrene (M_w =168 kg/mol, PDI = 1.05) was obtained from Polymer Source, re-precipitated in hexane three times, and then dissolved in toluene. The 3.4 wt % polystyrene in toluene solution was photobleached in a home-built, high power light emitting diode (LED) based setup for at least 48 h to achieve a non-fluorescent host. Silicon wafers were cut into ≈ 6.5 × 6.5 mm pieces and cleaned with piranha solution (H_2SO_4:H_2O_2 = 1:1). The fluorescent dye N,N′-dipentyl-3,4,9,10-perylenedicarboximide (pPDI, Figure 7) was obtained from Sigma-Aldrich and diluted to $5x10^{-9}$ M. 4 µl was then added to 400 µl of the polystyrene solution, resulting in a solution of ≈ $5x10^{-11}$ M.

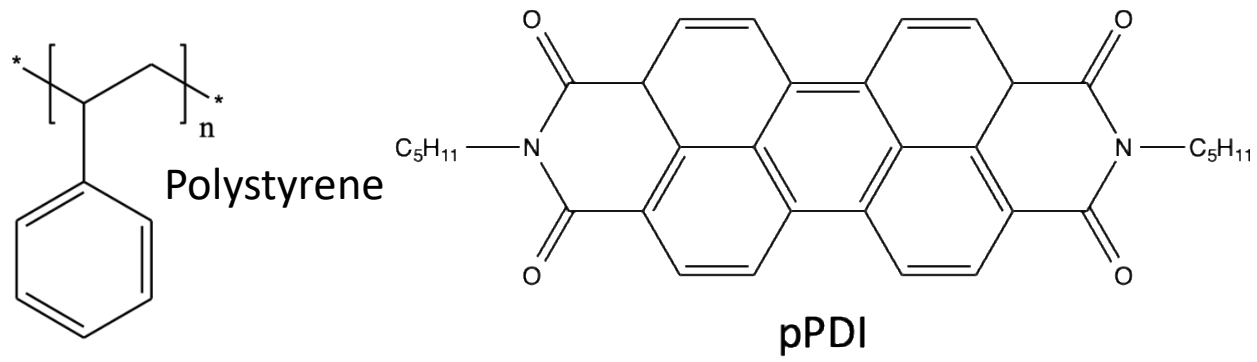

Figure 7. Structures of the host polystyrene and the fluorescent probe *N,N′*-dipentyl-3,4,9,10-perylenedicarboximide (pPDI).

The solution was subsequently spin-coat at 2000 rpm onto a cleaned silicon wafer, which resulted in a film of ≈ 200 nm thickness as measured by ellipsometry. At this thickness, films were sufficiently thick such that bulk dynamics dominate. Molecules in near vicinity of the supported and free surfaces are unlikely to be detected in our study due to a combination of their relative rarity in the sample, potential quenching near the silicon surface, and the dynamic range of the measurement, which is 1-2 orders of magnitude in detected relaxation times for a given frame rate, as chosen for each temperature interrogated.[77,141–144] After spin-coating, the final fluorophore concentration was ≈ 2 x10^{-9} M, sufficiently dilute to avoid multiple probe molecules within a diffraction limited spot yet concentrated enough to provide on average 200 analyzable fluorophores per field of view. The sample was placed in a vacuum cryostat (Janis ST-500) integrated with a home-built wide-field microscope. The cryostat provides temperature control, facilitates removal of toluene from the sample, and limits oxygen-induced photobleaching of the fluorescent probes. Vacuum grease (Braycote 601EF) was applied to the sample stage of the cryostat to ensure thermal contact between the sample and the stage. Once the sample was placed in the cryostat, the pressure was lowered to ≈ 1.8 mTorr and the temperature was raised a minimum of 10 K above the glass transition temperature (383-385 K) and held there for at least 1h to assist

in removal of residual solvent and ensure stable pressure.[141] Given that the temperatures probed were so close to the glass transition temperature, the sample was then lowered to the measurement temperature and held there for an additional 2-3 hours to ensure the system was at equilibrium and not an aging glass.

2.2.2 Molecular Weight Dependent Studies

Polystyrene samples of 0.6 kg mol^{-1} (PDI = 1.05), 6.4 kg mol^{-1} (PDI = 1.2), 27.5 kg mol^{-1} (PDI = 1.3), 168.0 kg mol^{-1} (PDI = 1.05), and 1364.0 kg mol^{-1} (PDI = 1.3) were obtained from Polymer Source. All samples except the lowest molecular weight polystyrene were re-precipitated in hexane a minimum of two times and then dissolved in toluene to yield solutions of 8.0 wt% (6.4 kg mol^{-1}), 6.8 wt% (27.5 kg mol^{-1}), 3.4 wt% (168.0 kg mol^{-1}), and 3.1 wt% (1364 kg mol^{-1}) polystyrene. These solutions were then photobleached in a home-built, high power light emitting diode (LED) based setup for at least 48 h to achieve a non-fluorescent host. Due to its comparatively low glass transition temperature, the 0.6 kg mol^{-1} polystyrene sample was not re-precipitated in hexane, but rather dissolved in toluene, resulting in a 10.0 wt% solution, which was photobleached for a minimum of one week. The first fluorescent dye, N,N′-dipentyl-3,4,9,10-perylenedicarboximide (pPDI), was obtained from Sigma-Aldrich and diluted to $5x10^{-9}$ M in toluene. The second dye, BODIPY268 (Figure 8), was synthesized as previously described by Paeng *et al.*, and diluted in toluene to $5x10^{-9}$ M.[77] Absorption and emission spectra of this dye at both room temperature and at ~370K are given in Appendix B.1. The dye solutions were then further individually diluted with the polystyrene solutions, and the resulting solutions were subsequently spin-coat at 2000-3000 rpm onto a silicon wafer (≈ 6.5 × 6.5 mm, cleaned with piranha solution (H_2SO_4:H_2O_2 = 1:1)), resulting in films of at least 200 nm thickness as measured by ellipsometry. Each sample was then placed in a vacuum cryostat (Janis ST-500) integrated with

a home-built wide-field microscope and held at ≈ 1.8 mTorr. For the higher molecular weight samples, Braycote 601EF vacuum grease was applied to the sample stage of the cryostat to ensure thermal contact between the sample and the stage. For the lowest molecular weight, the vacuum grease used was specifically for low temperatures and high pressure (Apiezon N) and was chosen to ensure proper thermal contact. Once the sample was placed in the cryostat, the temperature was raised a minimum of 10 K above the glass transition temperature, as reported from Polymer Source, and held there for at least 1h to assist in removal of residual solvent and ensure stable pressure.[78] In all higher molecular weight cases, this corresponded to a temperature above the boiling point of the solvent (110-111 ^{o}C). In contrast, to remove residual solvent in the lowest molecular weight samples, these samples were held under vacuum for a minimum of 16 h. The final fluorophore concentrations of all samples were sufficiently dilute to avoid multiple probe molecules within a diffraction limited spot yet concentrated enough to provide on average 200 analyzable fluorophores per field of view.

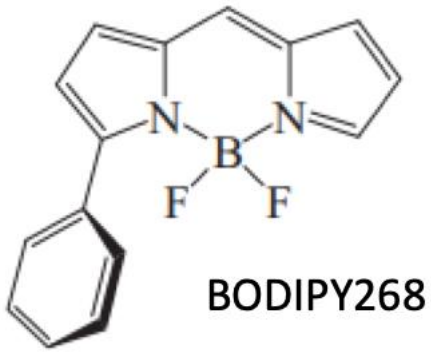

Figure 8. Structure of BODIPY 268.

2.2.3 Thin Film Studies

To avoid any molecular-weight dependence, the same sized polystyrene as in the temperature-dependent studies was used. As previously, polystyrene with M_w =168 kg/mol and a PDI = 1.05 was obtained from Polymer Source, re-precipitated in hexane three times, and then dissolved in toluene. Several factors, including polymer concentration and volatility of solvent, affect film thickness.[145] Thus, to achieve a variety of film thicknesses, several polystyrene solutions with varying concentrations were prepared: 1.0 wt%, 2.0 wt%, 3.1 wt%, and 3.6 wt%. All polystyrene in toluene solutions were photobleached as previously for at least 48 h to achieve a non-fluorescent host. Silicon wafers were cut into ≈ 6.5 × 6.5 mm pieces and cleaned with piranha solution (H_2SO_4:H_2O_2 = 1:1). For the thinnest films (~25 nm), quartz wafers backed with ~160 nm aluminum were used to limit interference between reflected and emitted light. The quartz wafer was initially cut into ≈ 6.5 × 6.5 mm pieces and cleaned with piranha solution (H_2SO_4:H_2O_2 = 1:1). The aluminum was subsequently deposited through thermal evaporation by Jaeeun Yu (Nuckolls Group, Columbia University) onto the backside of the quartz substrate. All substrates were cleaned with acetone prior to sample deposition.

The first dye, pPDI, was prepared as in the previous studies, resulting in solutions in toluene of ~$5*10^{-9}$ M. Additional larger PDI-based nanostructures were provided by Sam Peurifoy (Nuckolls group, Columbia University) and first described in reference 146. These nanostructures are shown in Figure 9 and differ by the number of PDI segments attached to the core. In the following, these nanostructures will be referred to as NS1 (3 PDI attached), NS2 (6 PDI attached) and NS3 (9 PDI attached). Anisotropy measurements of all nanostructures are shown in Appendix C and compared to those of pPDI. These nanostructures were diluted in toluene, however to higher concentrations than previously (~$1*10^{-7}$ M) to compensate for lower emission intensities. All dye

solutions were, as previously, further diluted in the polystyrene solutions, resulting in final dye concentrations of ~10^{-10}-10^{-11} M.

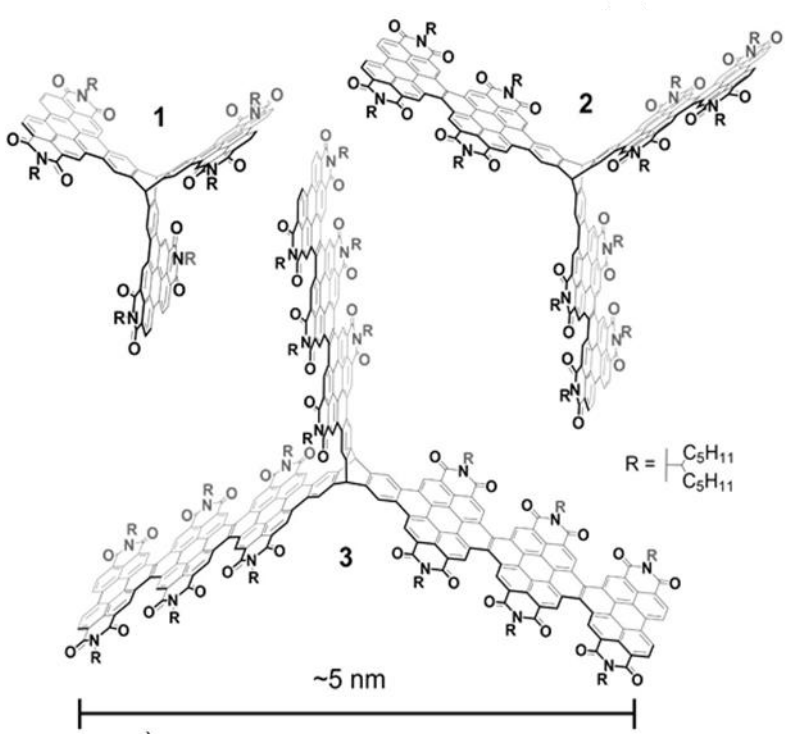

Figure 9. Structures of nanostructures used in thickness-dependent studies.
In the following, structure 1 will be referred to as NS1, 2 as NS2, and 3 as NS3. This figure is reproduced from reference 146 with permission from the publisher.

As both the polystyrene concentration and the rate of spin coating determine film thickness, samples were spin coat at rates ranging from 2000 to 8000 rpm. The samples were then placed in the previously described Janis ST-500 cryostat and heated to 10 K above the bulk T_g for at least 30 minutes. Thermal contact was ensured by placing Braycote vacuum grease between the sample stage and the substrate, and the pressure was held at a constant ~1.8 mTorr. Prior to imaging, the temperature was lowered and kept at imaging temperature for a minimum of 3 hours to ensure the bulk of the sample reached equilibrium. The final fluorophore concentrations provided on average 100-200 analyzable fluorophores per field of view. The film thickness was confirmed post-imaging through ellipsometry.

2.3 Data Analysis

All analysis of single molecule rotation was performed using IDL software (ITT Visual Information Solutions), as adapted from Hoang *et al.* and Mackowiak *et al*.[60,147] Due to the slow rotations and thus long duration of data acquisition at the lowest temperature, movies at 373.0 K were de-drifted prior to analysis. The de-drifting approach relies on a method of residual overlays: a movie is initially split up into a given number of segments, in this case 200, and then summed to ensure each molecule is fairly distinct. The shift, *i.e.* drift, of the movie is then estimated by comparing the previously summed segments and finding the best overlap. The output is a new movie that is corrected for any horizontal and vertical drift. For data collected at all temperatures, molecular weights, and sample thicknesses, molecules were chosen from a band passed set of 500 summed images, found in the temporal middle of the longest movies, using the "feature" algorithm as described by Crocker and Grier.[148] The summed movie image was then subsequently filtered with a Gaussian intensity distribution, after which individual features of a minimum intensity were picked and paired up (one left channel, one right channel) based off of the channel separation on the CCD chip. Only the features chosen were analyzed, and all subsequent analysis was performed on the raw and unfiltered images.

Polarized fluorescence intensities (I_s, I_p) of the selected molecules were extracted from the two orthogonal polarization images of each molecule collected on the CCD at each time point. These intensities were calculated in both channels by integrating the intensities of the channels within ~2 pixels of the identified pixel center. Single molecule linear dichroism (LD) was then calculated via

$$LD(t) = (I_s - I_p)/(I_s + I_p),$$

of which an autocorrelation function, *C(t)*, was constructed using the deviation of the LD signal from a mean, $a(t) = LD(t) - < LD(t) >$,

$$C(t) = [\sum_{t'} a(t') \cdot a(t' + t)]/[\sum_{t'} a(t') \cdot a(t')].$$

Least-squares fitting was used to fit each autocorrelation function (ACF) to a stretched exponential function,

$$C(t) = C(0) \cdot \exp[-(t/\tau_{fit})^{\beta}],$$

with β corresponding to the stretching exponent.

For the analysis of full-length movies taken with pPDI in which molecules were not tracked as a function of trajectory length, as well as for all movies taken with the nanostructures, the correlation function was fit until it decayed to 0.1. *C(t)* values were constrained to $0.2 < \beta < 2.0$ and $0.3 < C(0) < 2.0$, and the average rotational correlation time, τ_c, was calculated from the fit values of τ_{fit} and β via

$$\tau_c = (\tau_{fit}/\beta) \cdot \Gamma(1/\beta),$$

where Γ is the gamma function. Following analysis of the full-length movies in the temperature- and molecular weight-dependent studies, movies were cut to a specified number of frames to allow analysis of single molecule dynamics as a function of trajectory length. For some analyses in the temperature-dependent studies, the same molecules that were analyzed in the longest movies were also selected in the cut movies for data analysis. In other analyses in the temperature- and molecular weight-dependent studies, all analyzable molecules were retained regardless of whether they were analyzed in the full length movies. For analyses in which specific molecules as a function of trajectory length were tracked, initial feature finding was performed from the shortest trajectory length data. For such analysis, the constraints for β and *C(0)* were lifted, and the only constraint applied was (number of frames)/$\tau_{fit} \geq 2$.

Due to a low signal to noise ratio present in movies taken with the probe BODIPY268, the *C(0)* constraint was lifted for all trajectories, with the previously discussed constraints remaining. All pPDI movies that were not followed had all constraints applied. Full widths at half maximum (FWHM) are given by $2\sqrt{2\ln 2}\,\sigma$ and were found by fitting obtained data to Gaussian distributions,

$$y = \frac{1}{\sqrt{2\pi\sigma^2}} \exp^{-\frac{(x-x_c)^2}{2\sigma^2}},$$

where x_c indicates the center of the peak and σ^2 is the variance.

Lastly, to more accurately compare single molecule results to those typically gained from ensemble approaches, quasi-ensemble autocorrelations (ACF_{QE}) were obtained by averaging single molecule autocorrelation decays, and $\tau_{fit,QE}$, β_{QE}, and $\tau_{c,QE}$ were obtained by fitting the ACF_{QE} to a stretched exponential. These ACF_{QE}s were constructed by using a weighted average, based on the number of molecules, of the single molecule autocorrelation decays for a particular set of movies.

2.4 Inverse Laplace Transform (ILT) Analysis

ILT analysis was performed in the molecular-weight dependent studies. An in-depth discussion on constructing ILT-distributions is given in Reference 70. In brief, the ILT of a stretched exponential function can be expressed by

$$\exp[-(t/\tau_{fit})^{\beta}] = \int_{-\infty}^{\infty} P(\log\tau;\tau_{fit},\beta)\cdot\exp(-t/\tau_{fit})\,d\log\tau,$$

which assumes that a stretched exponential form results from a superposition of exponential relaxations with different relaxation times. The distribution of the normalized probability density function, P(log τ; τfit, β), can be numerically obtained for any τ_{fit} and β values and reflects the

distribution of exponential relaxations that constitute the stretched exponential function. In a first step, the expected exponential relaxation distribution of an AFC_{QE} was obtained from the longest trajectory length measured and the ILT analysis was performed, giving rise to a distribution subsequently labeled the ILT distribution. A set of reference distributions for $\tau_{fit} = 1$ and β ranging from 0.20 to 0.99 in 0.01 steps were previously built, and the reference distributions were used to approximate the distribution for any τfit and β values obtained experimentally. These reference distributions were built using an iterative process of correcting generated $P(\log\tau; \tau_{fit}, \beta)$ distributions: stretched exponential functions constructed by the corrected distributions were fit until the reconstructed stretched exponential functions produced fitted β values that were within 0.3% error relative to the original β values. Thus, in a second step, ILT-built distributions were constructed from this set of reference ILT distributions, and τ_{fit} and β values obtained from the experimental single molecule ACFs were the basis of these ILT-built distributions. For two molecular weights – 6.405 k and 168 k – the fitted set of τ_{fit} and β was obtained from the data set of single molecule ACFs via the two probes, fitted β_{QE} values of the corresponding ACF_{QE} were chosen, and the reference distribution was chosen from the corresponding reference ILT distribution and shifted in time by the fitted τ_{fit} value. This approach was applied to all single molecule ACFs of the two molecular weights chosen, and the distributions of a particular probe-molecular weight combination were added and normalized by the area under the distribution to produce the final ILT-built distributions.

2.5 Simulations

Simulations of homogeneous rotational diffusion were carried out so that effects of finite trajectory length on measured τ_{fit} and β values (independent of dynamic heterogeneity) could be assessed for all temperature-dependent measurements in Chapter 3. The heterogeneous parallel and its implications are discussed in Appendix A as this was not the focus of the present study. Reference 75 was used as a basis for the following methods.

The rotation of a single molecule (SM) probe is modeled as a diffusive process in which probes are set to have a rotational diffusion constant D_r, as dictated by the local environment. This was performed at each simulation step by rotating a unit vector in R^3 through an angle δ chosen from a Rayleigh distribution of width $\sqrt{2}Dr$. The rank-l rotational autocorrelation function (ACF) is then given by

$$C_l(t) = \left\langle P_l(\hat{\phi}(t_0) \cdot \hat{\phi}(t_0 + t)) \right\rangle_{t_0},$$

where $P_l(x)$ is the rank-l Legendre polynomial, and the average is performed over the entire trajectory. For the isotropic probes undergoing homogeneous rotational diffusion through small angular displacements and within a certain environment given by D_r, all ranks exhibit exponential relaxation,

$$C_l(t) = e^{-l(l+1)D_r t} \equiv e^{-t/\tau_l},$$

where $\tau_l \equiv (l(l+1)D_r)^{-1}$ is the relaxation timescale of the local environment.[149]

It is to be noted that SM probes may experience relaxations that are non-exponential not only because they are typically anisotropic but also because most SM experiments monitoring rotation measure linear dichroism, having components from all even rank rotational correlation functions. In practice however, the second-rank term strongly dominates any linear dichroism measurements and any effects due to anisotropy are negligible. As such, in simulations for Chapter

3, $\tau_r \equiv \tau_2$ was computed and discussed. The diffusion constant was chosen such that $\tau_r = 100$ steps, and every trajectory length simulated consisted of 500 molecules. Each trajectory was then cut to the appropriate number of steps, prior to fitting for trajectory length analysis. For each simulated probe, an autocorrelation was computed and fit to a stretched exponential, and all subsequent data analysis was performed as for experimental data. In-depth instructions for running both homogeneous and heterogeneous rotational simulations are given in Appendix A.2.

Chapter 3. Lifetime of Dynamic Heterogeneity in Polystyrene across Temperature

The following chapter is adapted from Manz *et al*.[150]

In this chapter, results of single molecule experiments in supercooled polystyrene of a single high-molecular weight at temperatures ranging from T_g to 10 K above the glass transition temperature are presented. Polymeric systems close to their glass transition temperature are known to exhibit heterogeneous dynamics that evolve both over space and time, yet the influence of temperature on the associated timescales still remains unclear. Through the use of widefield (WF) single molecule microscopy, these dynamics are identified by following rotational dynamics of a perylene diimide probe embedded in a high-molecular weight polystyrene host. Several analysis approaches are utilized to assess the influence of temperature on the lifetime of these dynamic heterogeneities of polystyrene, with a particular focus given to the breadth of the rotational relaxation time of the probe and how this breadth evolves over time. Measurements are also presented in a fashion similar to previous ensemble and sub-ensemble approaches to fully emphasize the necessity of ideal probes in single molecule approaches.[96]

3.1 Motivation for Temperature Dependent Single Molecule Studies

The fundamental properties of polymeric systems near their glass transition temperatures (T_g) have been an area of study for decades. In part due to the ubiquity of thin polymeric films in emerging technologies, including in organic optoelectronics, coatings, and battery cells, there has been heightened focus on the properties and surface molecular dynamics of such films.[137,138,141] However, even aspects of the properties of bulk polymeric films are poorly understood owing to the incomplete understanding of the glass transition and molecular motion as it occurs in systems at temperatures between their melting point and glass transition.[151]

Both polymeric melts and small molecule supercooled liquids display non-exponential fluctuations and relaxations, which have been characterized using a variety of techniques. Such non-exponential behaviors have been associated with dynamic heterogeneity, in which dynamics in such systems vary both as a function of position (spatial heterogeneity) and over time (temporal heterogeneity) even in the absence of identifiable structural heterogeneity.[66,147] The causal relationship between the emergence of dynamic heterogeneity and the extreme slowdown of dynamics in liquids as they approach the glass transition is not entirely clear. However, the observation that dynamic heterogeneity in the absence of structural heterogeneity occurs always and only alongside an approaching glass transition encourages continued study and characterization of the spatial and temporal character of dynamic heterogeneity over a range of temperatures. Simulations and a few experiments have suggested relevant length scales of heterogeneity are just a few nanometers, making them very difficult to directly access experimentally.[38,97,102,152,153] Timescales associated with dynamic heterogeneity are much more accessible in typical experiments, and thus persistence of dynamic heterogeneity has been studied quite extensively, typically characterized through an exchange time (τ_{ex}) or a dynamic

heterogeneity lifetime (τ_{hetero}). While various definitions exist, we will distinguish exchange time and dynamic heterogeneity lifetime as follows: τ_{ex} describes the time a particular molecule displays dynamics characterized by a well-defined timescale before transitioning to a different well-defined timescale, while τ_{hetero} refers to the time over which a molecule or set of molecules exhibits particular dynamics that are distinct from those of other sub-ensembles in the system. Substantial differences in exchange time and of dynamic heterogeneity lifetime have been reported across systems and techniques, with some differences attributed to the fact that measurements have been performed at different temperatures relative to T_g, and these quantities may vary with temperature, though no consensus currently exists on their temperature dependence.[40,55,61,66,95,96,154–160]

Over the past decade, single molecule experiments have been used to characterize aspects of dynamic heterogeneity in polymeric melts.[55,144,161–166] Prior to this study, single molecule measurements of rotational motion of probe molecules in polystyrene was used to characterize the range of exchange times present in this system. This study, only performed at the single temperature of ≈ 378 K (T_g + 5K; 1.01T_g), revealed that exchange between environments with distinct dynamics occurs over a broad range of times scales, including those as short as 70 τ_α, with τ_α the alpha-relaxation time in polystyrene, which corresponds to the segmental dynamics of the host polymer. This study revealed several characteristic timescales associated with dynamic exchange, including ≈ 2300 τ_α as the time in which the average molecule explored most environments in the system and ≈ 35000 τ_α as the extrapolated time at which every molecule would have explored all environments in the system. To obtain closer analogy to measurements that have characterized lifetime of dynamic heterogeneity in glassy systems through sub-ensemble approaches, we also stratified molecules into fast and slow sub-ensembles and found that initially fast molecules randomize on a timescale of ≈ 60 τ_α and slow ones on a timescale of ≈ 250 τ_α.

These timescales are somewhat longer than those measured previously in polystyrene at some temperatures; however, a prior experiment has shown strong temperature dependence of the lifetime of dynamic heterogeneity in PS in the range of T_g - T_g + 10K.[40] Here, we aim to resolve outstanding questions regarding the temperature dependence of the lifetime of dynamic heterogeneity in polystyrene near T_g through single molecule measurements and a variety of data analysis approaches.

3.2 Results

3.2.1 Evaluation of pPDI as an Adequate Probe

In advance of using pPDI as a probe with which to interrogate the temperature dependence of the lifetime of dynamic heterogeneity in polystyrene, we first confirmed that pPDI acts as an ideal single molecule probe for polystyrene. To demonstrate a single molecule probe is an ideal probe for a given host requires demonstrating that the probe dynamics are slaved to those of the

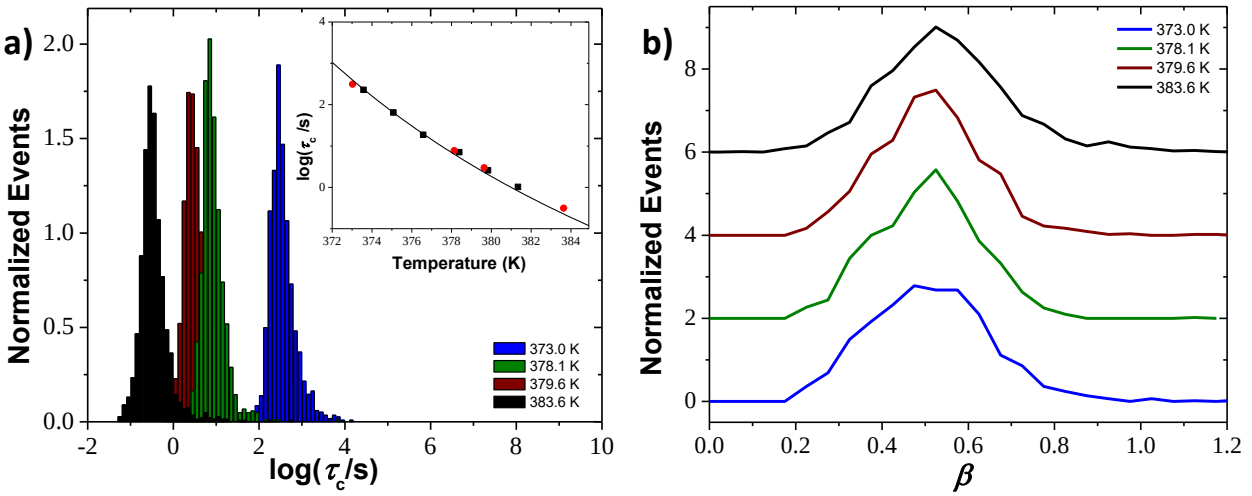

Figure 10. Distributions of KWW parameters of pPDI in PS over the temperature range T_g – T_g + 10K. (a) Normalized distributions of τ_c at the longest trajectory studied over the temperature range T_g - T_g +10K (T_g – 1.03 T_g), with the inset showing median τ_c values at each temperature probed (red circles). The data is compared to previously published values (black squares) by Paeng et al, with the line drawn being the VFT fit to the temperature dependence as reported by Roland and coworkers from dielectric spectroscopy measurements and shifted by 0.85 decades.[167,168] (b) Vertically offset normalized distributions of β values at each temperature.

host and that the probes report the full extent of heterogeneity in the system, as characterized in bulk probe-free experiments. Both results were shown previously for pPDI in polystyrene, though here we cover a broader temperature range than in the previous work.[167] Briefly, each single molecule linear dichroism auto-correlation constructed from trajectories of given length was fit to the Kohlrausch-Williams-Watt equation, $C(t)= C(0) \exp[-(t/\tau_{fit})^{\beta}]$, and τ_{fit}, β, and τ_c were obtained from each single molecule trajectory.

Distributions of τ_c at temperatures between 373.0 and 383.6 K for trajectories of ≈ 900 τ_{fit} in length at each temperature are shown in Figure 10a. Distributions are approximately log-normal and show no notable shape difference as a function of temperature, consistent with previous reports. Median τ_c values are shown in Figure 10a, inset, and fit to a Vogel-Fulcher-Tannmann (VFT) curve, consistent with previous single molecule and bulk measurements in polystyrene, which demonstrates probe molecules follow the dynamics of the host.[167,168] While the temperature dependence of the probe rotation tracks that of the host segmental dynamics, the probe rotational correlation time is ≈ 0.85 decades or ≈ 7 times slower than the host segmental dynamics (τ_c/τ_α = 7.07). Given the fact that the probe rotates slower than the host segmental dynamics, it is possible

Temperature (K)	373.0	378.1	379.6	383.6	Combined
number of molecules	1164	1054	1095	1443	4756
median τ_c (s)	312.24	7.70	2.98	0.32	1.00
median τ_{fit} (s)	146.56	3.66	1.39	0.17	1.00
median β	0.51	0.51	0.51	0.54	0.51
median trajectory length ($\tau_{fit,med}$)	912	872	932	935	913
median frame rate (frames/τ_{fit})	20.93	18.27	20.72	20.6	20.13
FWHM (τ_c distribution)	0.50	0.45	0.49	0.51	0.49
FWHM (τ_{fit} distribution)	0.54	0.44	0.48	0.44	0.48
FWHM (β distribution)	0.33	0.32	0.29	0.31	0.30

Table 1. Characteristics of data obtained from longest trajectory pPDI measurements in polystyrene.

the probe averages over some dynamic heterogeneity in the system. To ensure pPDI accesses and can report the full breadth of dynamic heterogeneity as reflected by bulk probe-free experiments, the median stretching exponent was examined. Distributions of stretching exponents, β, obtained from the same data from which τ_c values were obtained are plot in Figure 10b and given in Table 1. Median β values are ≈ 0.5 and do not vary as a function of temperature, consistent with previous bulk measurements.[169] While there are various literature values of probe-free or small probe ensemble or sub-ensemble measurements of β in moderate molecular weight polystyrene near T_g, most are similar to the median values obtained in this study.[40,168–170] The data in Figure 10 verifies that pPDI reflects the dynamic heterogeneity of the host. Moreover, it adds additional evidence that for trajectories of a given length, single molecule reports return distributions of τ_c and β values that do not vary as a function of temperature near T_g, with the current study providing the largest temperature range probed with an ideal probe to date.[77,167]

3.2.2 Evolution of Relaxation Times in Terms of Trajectory Length

In previous work, pPDI dynamics in PS were evaluated as a function of trajectory length, which is equivalent to observation time, to identify times scales associated with temporal heterogeneity in the system at T_g + 5K. Here we present the first ideal probe measurements of lifetime of dynamic heterogeneity across temperatures. First, data was collected for trajectory lengths of ≈ 900 τ_{fit} at each of four temperatures, with the data shown in Figure 10 obtained from these long trajectories. At all temperatures, single molecule trajectories were then truncated to a variety of lengths from ≈ 20 – 500 τ_{fit}, autocorrelations were re-constructed and re-fit, and τ_{fit} and β distributions were obtained. The distributions associated with measurements of the lowest and highest temperatures interrogated, 373.0 K and 383.6 K, are shown in Figure 11(a-d) as a function

of trajectory length. At both temperatures, as well as at the other two temperatures at which data was collected, with increasing observation time the τ_{fit} and β distributions get narrower, and the median β value shifts from near 1.0 to near 0.5, indicative of molecules sampling different dynamic environments as the observation window increases, with numerical details given in Table 2. To further quantify how these distributions change as a function of trajectory length and temperature, distribution width (FWHM) and, in the case of β, median value, were assessed for all temperatures

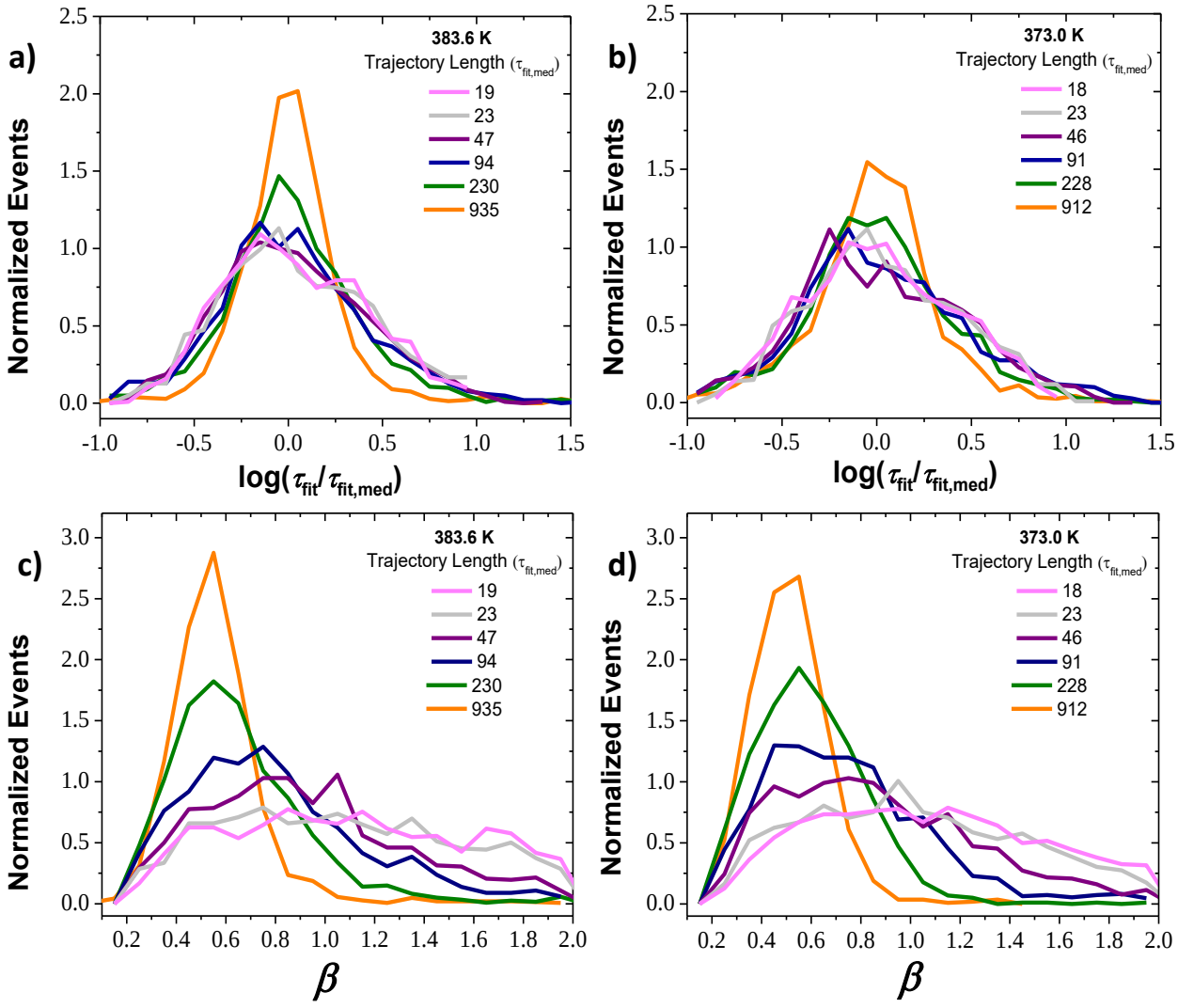

Figure 11. Rotational relaxation measurements as a function of trajectory length for the lowest and highest temperatures probed.
Normalized τ_{fit} distribution at all trajectory lengths at (a) 373.0 K and (b) 383.6 K and β distributions at (c) 373.0 K and (d) 383.6 K.

and investigated as a function of trajectory length (Figure 12a,b). This reveals that at all temperatures studied, τ_{fit} and β distributions evolve in a very similar manner. The smooth evolution of β_{med} from ≈ 1 at the shortest trajectory evaluated (≈20τ_{fit}) to that associated with a bulk

Temperature (K)	trajectory length (τ_{fit})	number of molecules	median β	τ_{fit} distribution FWHM
373.0	18	1105	1.04	1.17
	23	1092	0.97	1.04
	46	1059	0.82	1.08
	91	1101	0.70	0.91
	228	1019	0.58	0.73
	456	1298	0.53	0.54
	912	1164	0.51	0.54
378.1	18	1101	1.01	0.94
	20	1174	0.98	0.95
	41	1034	0.83	0.86
	87	1174	0.71	0.78
	205	1090	0.59	0.67
	461	993	0.54	0.57
	872	1054	0.51	0.44
379.6	19	1216	1.05	1.03
	23	1344	0.98	1.03
	47	1343	0.79	0.95
	93	1501	0.69	0.81
	233	1652	0.58	0.66
	466	1129	0.55	0.56
	932	1095	0.51	0.48
383.6	19	1007	1.07	1.08
	23	1016	1.04	1.00
	47	1020	0.87	0.91
	94	1011	0.76	0.77
	230	1212	0.60	0.65
	460	1301	0.56	0.53
	935	1443	0.54	0.44

Table 2. Characteristics of data obtained from trajectory length-dependent pPDI measurements in polystyrene

measurement at the longest trajectories evaluated (≈ 900τ_{fit}) confirms that dynamic exchange occurs over that range of timescales for all temperatures interrogated.

3.2.3 Lifetime of Dynamic Heterogeneity

To characterize the lifetime of dynamic heterogeneity in polystyrene more precisely, for data collected at each temperature, molecules analyzed were grouped into five sub-ensembles based on their initial τ_{fit} values. For each movie, molecules were characterized at the ≈ 18 τ_{fit} trajectory length, and the same molecules were analyzed at trajectories of ≈ 23, 45, 90, 225, and 900 τ_{fit}. The τ_{fit} values for each molecule at the 18 τ_{fit} trajectory were used to determine sub-ensembles, and three sub-ensembles (the fastest fifth of molecules, slowest fifth of molecules, and the fifth of molecules in the center of the τ_{fit} distribution) were analyzed for their dynamical evolution as a function of trajectory length, or observation time. We note that this analysis is distinct from that described above and depicted in Figure 12, as here particular molecules are tracked as a function of observation time while in the previous analysis all molecules were included. This analysis,

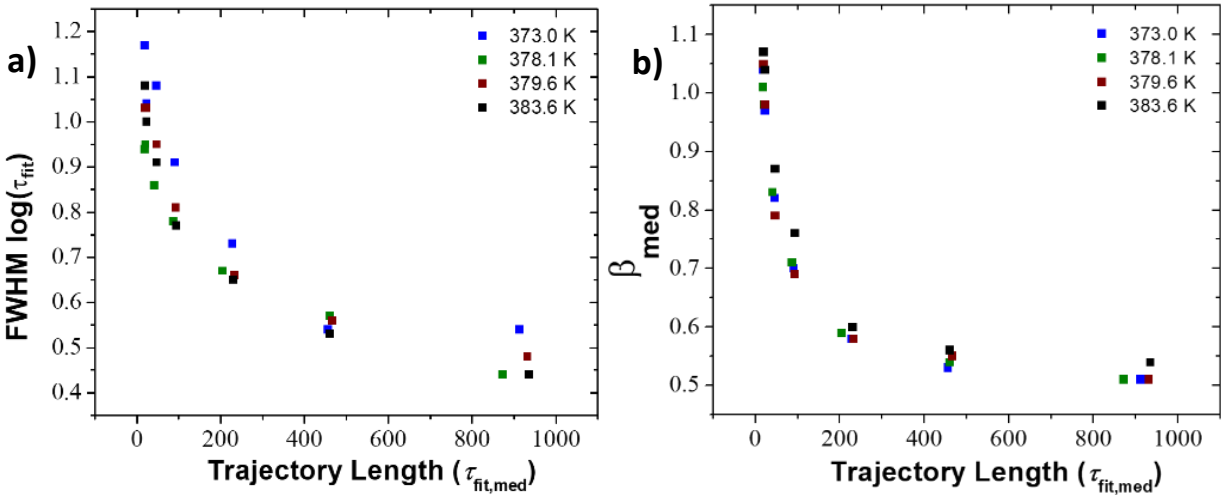

Figure 12. The evolution of the FWHM of log(τfit) and median β with trajectory length. Trajectory lengths are the same as from the distributions shown in Figure 11, as well as equivalent data at the other temperatures studied. Detailed characteristics of the data sets and distributions are given in Table 2.

therefore, clarifies how long molecules that are, for example, slow upon initial (short) observation window, and remain among the slowest in the distribution as a function of observation time. Figure 13a reveals that all temperatures studied show the same trend: initially, the fastest and slowest molecules are clearly separated, with τ_{fit} values differing by approximately a factor of 10. As observation time increases, the initially fastest and slowest molecules converge. We note that in all cases the central sub-ensemble, representing average molecules, slows to a certain extent as observation time increases. This points to the limited dynamic range of measurements as short as 18 τ_{fit}, which cannot fully capture the dynamics of the slowest sub-set of molecules.

To assess whether statistical effects associated with analysis of short trajectories play a role in the measured spread between the fastest and slowest sub-ensembles, particularly for short trajectories, simulations of probes exhibiting homogeneous dynamics (with τ_{fit} = 100s) were analyzed in the same manner as experimental results. These simulations, based on rotational

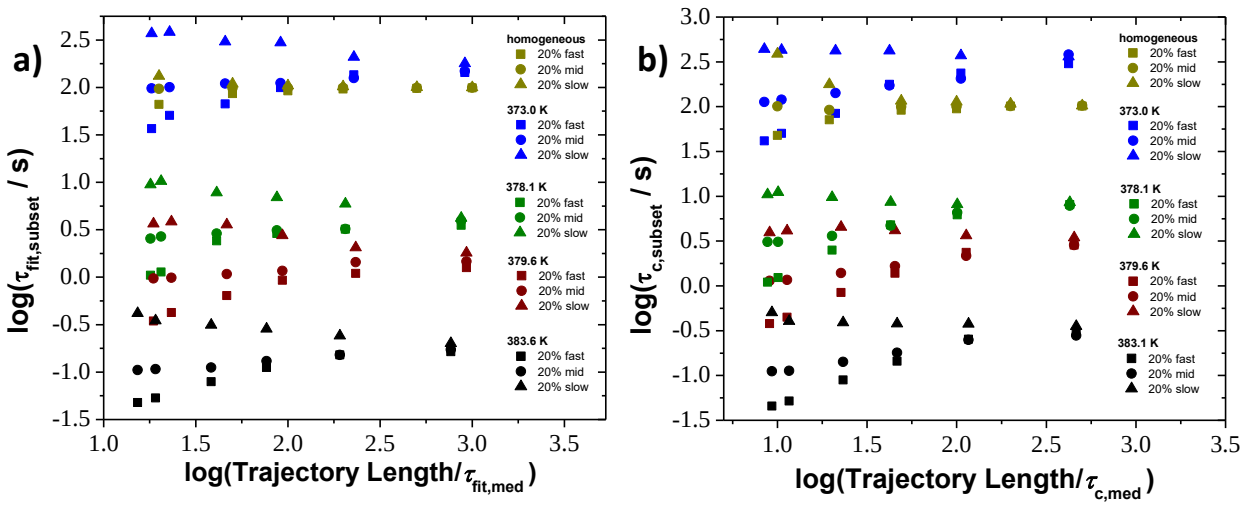

Figure 13. Tracking of subset of fast and slow molecules, in terms of τ_{fit} and τ_c, over several temperatures
(a) Median τ_{fit} and (b) median τ_c values as a function of trajectory length for the 20% initially fastest (squares), initially slowest (triangles), and initially average (circles) molecule sub-ensembles at each temperature studied, as well as for a homogeneous simulation.

diffusions dominated by rank two linear dichroisms, show limited spread in τ_{fit} dynamics but a large spread, comparable to that seen experimentally, in τ_c dynamics (Figure 13b). This large spread in the simulated τ_c data arises from the strong effect of short trajectories on measured β values and points to the importance of evaluating experimental τ_{fit} rather than τ_c data for such analysis.[65,76,171] An in-depth study on associated trajectory effects is presented in Appendix A. Comparing the simulated and experimental τ_{fit} data confirms that the spread seen in the experimental results is not due to statistical effects associated with analysis of short trajectories. Instead, the convergence in dynamics of the initially fastest and slowest molecules requires that the probes experience distinct dynamics, through dynamical evolution of the local environment over time and/or through the probe physically moving from a region of given dynamics to a region of distinct dynamics. Importantly, the time over which the sub-ensembles converge occurs at approximately the same trajectory length, or observation time, in terms of τ_{fit} for all temperatures (Figure 13a). This time to convergence can be considered the lifetime of dynamic heterogeneity,

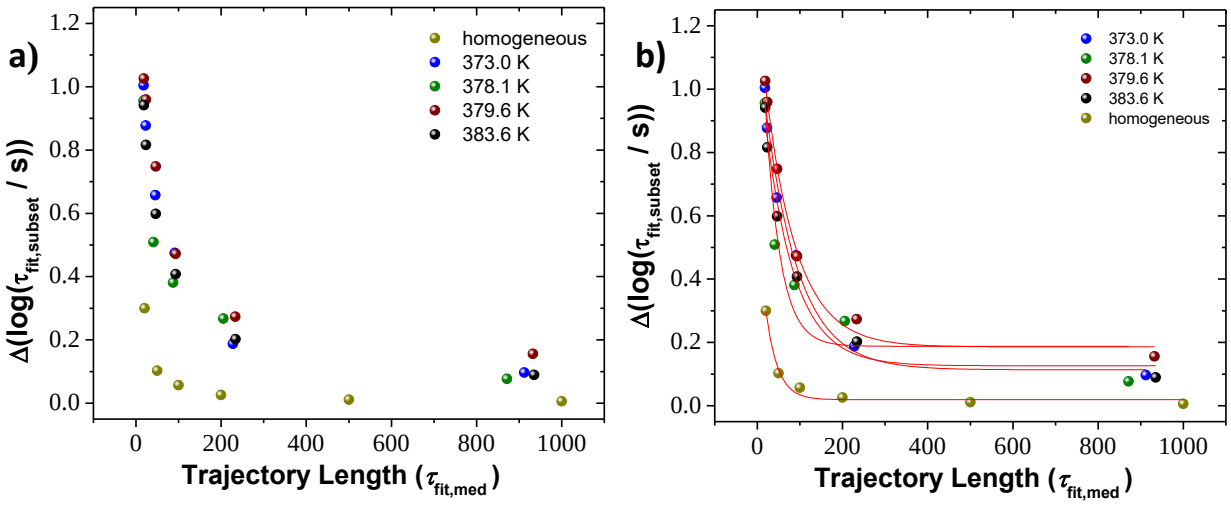

Figure 14. (a) Difference in median log(τ_{fit})of the fastest and slowest subsets of molecules, and (b) fit to exponential functions to extract timescales of convergence.

τ_{hetero}, as it marks the time required for initially distinct dynamic sub-ensembles to become indistinguishable.

To quantitatively characterize the timescale over which the sub-ensembles converge as a function of observation time, the difference in median $\log(\tau_{fit})$ of the fastest and slowest subsets of molecules was analyzed (Figure 14a). At first, a large difference between molecules is observed, with $\Delta(\log(\tau_{fit})) \approx 1$ for all temperatures, indicating the molecules' rotational correlation times span approximately one decade at short times, consistent with the data presented in Figure 11 and Table 2. As observation time increases, $\Delta(\log(\tau_{fit}))$ values decrease and reach ≈ 0 at the longest trajectory lengths. This demonstrates that molecules that started out both particularly fast and particularly slow have sufficiently sampled the range of dynamic environments in the system to report the same average relaxation time at long observation times. To quantify lifetime of dynamic heterogeneity, the evolution of the $\Delta(\log(\tau_{fit}))$ values were fit to exponential decays (Figure 14b). At all temperatures, the characteristic time required for molecules in the slow and fast sub-ensembles to converge was between 40 and 80 τ_{fit} (140 – 280 τ_{α}), with no trend as a function of temperature. To quantitatively compare the evolution of the full distribution (Figure 11) to that associated with molecules from particular sub-ensembles (Figure 13a,b), we looked at the difference between the median fastest and slowest portions of the distribution without following individual molecules. This difference converges more slowly than do the rotational correlation times of tracked molecules (Figure 15). Indeed, the $\Delta(\log(\tau fit,subset))$ of the 20% slowest and 20% fastest molecules at all trajectory lengths, where individual molecules were not followed, differs greatly from the $\Delta(\log(\tau fit,subset))$ of tracked molecules at 383.6 K, also shown in Figure 14, and shown by open symbols in Figure 15. This indicates that there is no tendency for molecules in a particular

dynamic sub-ensemble at the beginning of the experiment to stay in that dynamic sub-ensemble, and indeed the fastest molecules may become among the slowest and vice-versa over time.

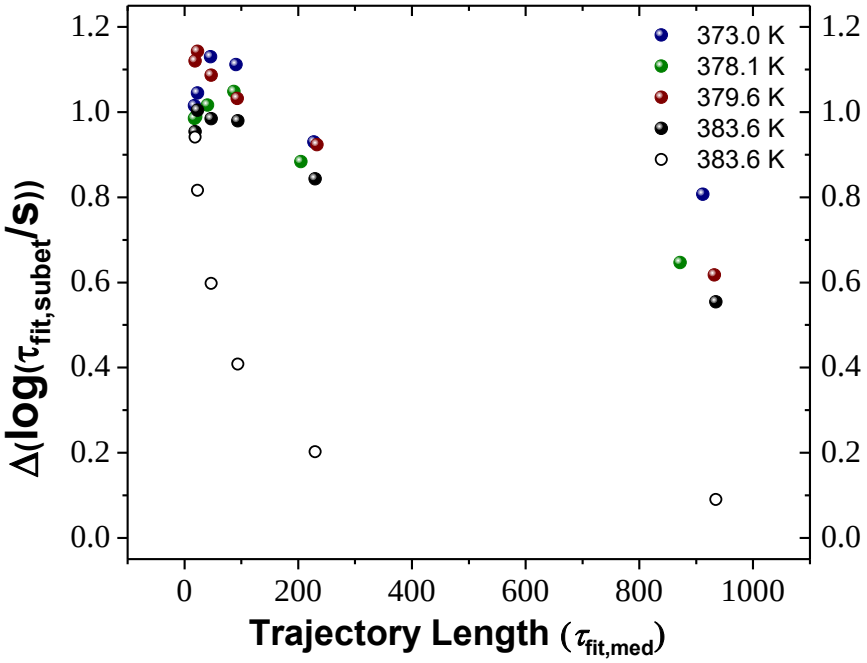

Figure 15. Δ(log(τfit,subset)) of the 20% slowest and 20% fastest molecules at all trajectory lengths without following individual molecules.
The open symbols correspond to Δ[log(τfit,subset)] of followed molecules at 383.6 K, also shown in Figure 14.

3.3 Discussion

Using single molecule fluorescence microscopy, rotational dynamics in polystyrene at temperatures from T_g to T_g + 10 K was studied. Lifetime of dynamic heterogeneity showed no trend as a function of temperature when considering either (1) how the full distributions of rotational relaxation times and stretching exponents evolved as a function of observation time (Fig. 8) or (2) how molecules initially in particular dynamic sub-ensembles evolved towards the average (Fig. 9, 10). From the latter analysis, designed to mimic aspects of earlier sub-ensemble NMR and

photobleaching experiments[40,46,96], average lifetime of dynamic heterogeneity was found to be ≈ 60 τ_{fit} (≈ 210 τ_α), with fast and slow initial sub-ensembles fully randomizing on this timescale at all temperatures probed.

The dynamic heterogeneity and its temperature independence relative to τ_α is in partial contradiction to several previous studies that have shown a temperature dependence for exchange time.[40,96] Differences in host matrix, temperatures probed, dynamic range of the experiments, sub-ensemble considered, and dynamic heterogeneity lifetime definitions may explain at least a subset of differences that have been observed. For example, simulations have shown that dynamic heterogeneity lifetime is system dependent, with more fragile systems exhibiting both longer lived dynamic heterogeneities at a given temperature and stronger temperature dependence of dynamic heterogeneity lifetime.[39,172] Indeed, in a recent study, the lifetime of dynamic heterogeneity, τ_{hetero}, for an array of model supercooled systems was obtained from relaxation of a three time correlation function and was found to vary as $\tau_{hetero} \sim \tau_\alpha^{0.9}$ - $\tau_\alpha^{1.9}$.[39] Our measurement yields a result in this range, with $\tau_{hetero} \sim \tau_\alpha$, with τ_{hetero} defined by the convergence of the fast and slow sub-ensembles through fits to the data presented in Figure 14.

Experimentally, the temperature dependence of the lifetime of dynamic heterogeneity was addressed by Ediger and co-workers in supercooled o-terphenyl (OTP) following two earlier reports, each of which characterized the quantity at a single temperature.[46,49,96] Initially, Cicerone and Ediger used a photo-bleaching technique to probe a sub-ensemble of slow probe molecules in OTP at T_g + 1 K while Böhmer and co-workers used multi-dimensional NMR to interrogate slow sub-ensembles of neat OTP at T_g + 10 K.[46,49] These studies, together with a follow-up study by Ediger and co-workers, suggested that dynamic heterogeneity lifetime was strongly temperature dependent in this system, with τ_{hetero} increasing relative to τ_α as temperature decreased.[96] A later

study using the same techniques in polystyrene yielded similar results: here, photobleaching measurements revealed that dynamic heterogeneity varied from ≈ 11 τ_α at T_g + 2 K to 65 τ_α at T_g for the smallest probe employed.[40] In this study, a deep photobleach was used to preferentially bleach molecules that were rotating quickly relative to the average molecule, leaving behind a slow sub-ensemble that was interrogated after variable waiting time. While the analysis performed in Figure 13 and Figure 14 in some ways approximates this approach, a more directly analogous analysis can be achieved starting with single molecule trajectories. Here, a fast and slow subset of molecules are followed, but in contrast to the analysis shown in Figure 13 and Figure 14, dynamics are not averaged over increasing observation windows but instead are assessed for a given amount of time (100 τ_{fit}) as a function of increasing waiting time between two such windows (Figure 16). Unlike the other approaches used here as well as a window-sliding approach used previously[60,94,142], this approach provides a history independent accounting of dynamic heterogeneity lifetime. Again, no temperature dependence of the extracted dynamic heterogeneity lifetimes times is seen, consistent with all other approaches we used to characterize dynamic heterogeneity lifetime. To quantify dynamic heterogeneity lifetime using this approach, the data in Figure 16 was fit to exponential decays and a characteristic timescale was extracted. For the slow subset of molecules, we find dynamic heterogeneity lifetimes of 30 – 40 τ_{fit} (105 – 140 τ_α) with no trend as a function of temperature. The fast subset evolves more quickly, such that nearly all relaxation time randomization occurs within the first waiting time window, preventing extraction of dynamic heterogeneity lifetimes for this fast subset of molecules. We note that while the temperature dependence is clearly distinct in our measurements relative to previous measurements, the absolute values of the lifetime of dynamic heterogeneity in polystyrene are

more similar to those reported previously once single molecule data analysis proceeds in a manner more closely approximating the earlier experimental approach.

The lack of temperature dependence of dynamic heterogeneity lifetime is not the only difference in this experiment compared to that of Ediger and co-workers.[40] Notably, the slow sub-ensemble in the current experiment is 3.5 – 4.5 times slower than the median at each temperature while the slow sub-ensemble in Ref. 40 was a factor of 1.1 – 2.0 (with some temperature and probe variation) slower than average, suggesting that our sub-ensemble is distinct from that studied by Ediger *et al.*, which could account for differences between our and their findings on the temperature dependence of τ_{hetero} relative to τ_{α}.

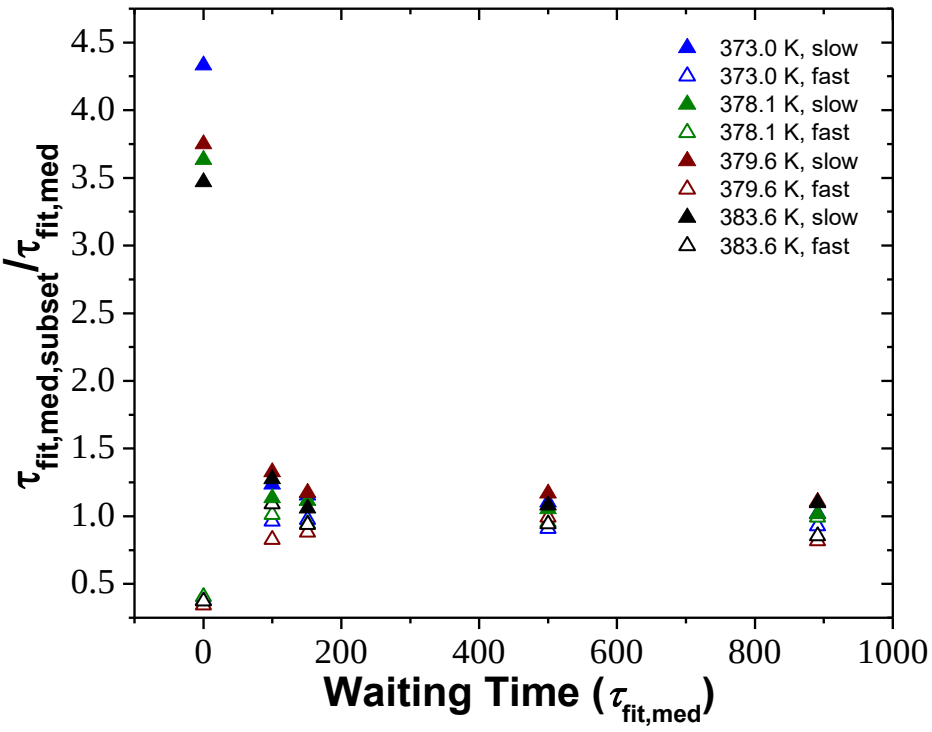

Figure 16. Waiting time analysis for all temperatures probed.
Median τ_{fit} for fast (open symbols) and slow (closed) subsets relative to the median τ_{fit} for all molecules as a function of waiting time between 100 τ_{fit} trajectory length assessed windows. Sub-ensembles were determined from the initial 100 τ_{fit} window (waiting time = 0) and subsequent $\tau_{fit,med,subset}$ values were obtained from the same molecules interrogated during a second 100 τ_{fit} window a waiting time later.

Our findings of temperature independence of τ_{hetero} ($\tau_{hetero} \sim \tau_\alpha$) is consistent with the fact that for long trajectory lengths we find no difference in median single molecule β value or distribution of β, τ_{fit} or τ_c values, each of which suggests there is no difference in degree of dynamic heterogeneity in polystyrene over the temperature range investigated. The behavior of the stretching exponent β for a system over a given temperature range appears to be a strong predictor of the temperature dependence of lifetime of dynamic heterogeneity, with those systems with limited β change over temperature also showing limited or no change in dynamic heterogeneity lifetime relative to structural relaxation time with temperature.[6,36,39,172] The scaling of τ_{hetero} with τ_α in polystyrene over the approximately three orders of magnitude variation in alpha-relaxation explored here leaves open the possibility that the segmental relaxation of the polymer and the randomization of distinct dynamic environments within the melt are governed by a single process. This finding also suggests limited growth in domains of slow dynamics and locally preferred structures in polystyrene with cooling over the range of relaxation timescales interrogated[39]; this behavior may prove to be a distinction between polymeric melts, which tend to have relatively weak β dependence on temperature[173], and small molecule supercooled liquids, though experimental approaches to directly identifying such structures in polymeric and molecular systems are currently lacking.

3.4 Conclusion

We investigated the temperature dependence of dynamic heterogeneity lifetime in polystyrene near its glass transition temperature using a single molecule approach in which the rotations of an ideal probe, pPDI, reported the dynamics and dynamic heterogeneity of the host polystyrene over the temperature range of T_g – T_g +10 K. Applying various data analysis approaches, no temperature dependence of lifetime of dynamic heterogeneity relative to τ_α in the studied temperature range was detected. By following sub-ensembles of fast and slow molecules as their dynamics evolve towards that of the average molecule as a function of observation time, we identified a characteristic lifetime of dynamic heterogeneity between 140 and 280 τ_α with no apparent trend as a function of temperature.

Chapter 4. Influence of Molecular Weight and Fragility on the Dynamics in Polystyrene

This chapter is adapted from Manz *et al. Manuscript submitted to JCP.*

Many macroscopic properties of polymers depend on their molecular weight, with one notable example being glass transition temperature: polymers with higher molecular weights typically have higher glass transition temperatures than their lower molecular weight polymeric and oligomeric counterparts. Polymeric systems close to their glass transition temperatures also exhibit interesting properties showing both high (and molecular weight dependent) fragility and strong evidence of dynamic heterogeneity. While studies have detailed the correlations between molecular weight and fragility, studies clearly detailing correlations between molecular weight and degree of heterogeneous dynamics are lacking. In this chapter, we describe single molecule rotational measurements used to investigate the impact of molecular weight on polystyrene's degree of heterogeneity near its glass transition temperature. To this end, two types of fluorescent probes are embedded in films composed of polystyrene ranging from 0.6 – 1364.0 kg mol^{-1}. We find correlation between polystyrene molecular weight, fragility, and degree of dynamic heterogeneity as reported by single molecule stretching exponents but do not find clear correlation between these quantities and timescales associated with dynamic exchange.

4.1 Motivation for Molecular Weight Dependent Studies

It is well known that chain length, and thus molecular weight, of polymers influences many of their macroscopic characteristics. In fact, Fox and Flory reported on molecular weight dependent properties including the viscoelastic behavior and glass transition temperature (T_g) of polystyrene as early as the mid-20th century.[87,174–176] A multitude of additional studies on the influence of molecular weight on polymers in the rubbery regime – *i.e.* between their melting point and glass transition temperature – have followed. For polystyrene in particular, it has been noted that fragility increases as molecular weight increases, at least in some molecular weight regimes.[88,99,168] Fragility, *m*, is a parameter that describes the degree to which the temperature dependence of the viscosity or structural relaxation time near the glass transition temperature of a system is non-Arrhenius.[3] Fragility is thus a well-accepted measure of anomalous behavior in glass-forming systems, with high fragility a mark of highly anomalous behavior.[19,22,83]

Empirical correlations between fragility and other quantities that characterize anomalous behavior in glassy systems have been identified, with one such quantity the stretching exponent.[104,105] Stretching exponents characterize the degree to which fluctuations and relaxations present in glass formers near the glass transition temperature are non-exponential. These complex fluctuations and relaxations are typically characterized with the Kohlrausch-Williams-Watts (KWW) equation, [$C(t) = C(0)*\exp[-(t/\tau_{fit})^{\beta}]$], with β the stretching exponent, whose deviation below 1 signifies divergence from the exponential decay associated with liquids far above T_g. Non-exponential behaviors in glassy materials have been associated with dynamic heterogeneity, in which dynamics vary both as a function of position (spatial heterogeneity) and time (temporal heterogeneity), even in the absence of identifiable structural heterogeneity.[28,35,177] The reported anti-correlation between fragility and stretching exponent undergirds the idea that both quantities

encode information about dynamic heterogeneity and the related issue of degree of cooperative dynamics in glassy systems.[8,11,104,105]

Recently, we used single molecule measurements to study polystyrene of a given molecular weight (168 kg mol^{-1}), showing that neither stretching exponent nor time scales associated with temporal heterogeneity vary over temperature from 1.00 – 1.02 T_g.[178] Here, we use a similar approach to characterize polystyrene over a range of molecular weights (0.6 – 1364.0 kg mol^{-1}) that alter its fragility from m ≈ 75 - 120, while simultaneously shifting its glass transition temperature by more than 100 K. These experiments clarify whether 1) reported correlations between fragility and stretching exponent hold when stretching exponents are obtained from single molecule measurements and 2) timescales of dynamic exchange, which have also been associated with degree of dynamic heterogeneity, vary as a function of polystyrene molecular weight.[40,46,61,95]

4.2 Results and Discussion

4.2.1 Investigating Molecular Weight Dependent Dynamics with pPDI

Previous studies have shown that the glass transition temperatures of polystyrene and other polymers vary with molecular weight and plateau at long chain length.[87,88,179,180] Dalle-Ferrier *et al.* have suggested that for rigid polymers such as polystyrene this saturation will occur between 30 and 100 kg mol^{-1}, consistent with measurements of Ding *et al.*[83,100] Here, we study the dynamics of polystyrene ranging from 0.6 – 1364 kg mol^{-1}, with a particular focus on lower molecular weights, to capture changes that can be detected by single molecule rotational measurements that may exist as a function of molecular weight, glass transition temperature, and fragility. In two previous reports, we showed that the fluorescent probe pPDI demonstrates dynamics slaved to moderate molecular weight (168 kg mol^{-1}) polystyrene and reports that polystyrene displays significant dynamic heterogeneity over temperatures from 1.00 – 1.02 T_g (373.0 – 383.6 K),

yielding both median single molecule (β_{med}) and quasi-ensemble (β_{QE}) stretching exponents of ≈ 0.5, similar to those reported by bulk probe-free experiments.[78,168,170,178]

In the current study, first we experimentally identified temperatures that yielded the desired rotational dynamics in polystyrene of each molecular weight, with a target of τ_{fit} = 4 s. Rotations on this timescale can be captured straightforwardly with the CCD set to a frame rate of 5 Hz and with dynamic range of at least 1 decade to each side of the median relaxation time. The temperatures identified in this manner track measured values of T_g as a function of molecular weight as reported from Hintermeyer *et al.*[180] We also note that these temperatures track measured values of fragility as a function of polystyrene molecular weight (Figure 17a).[100] All data was initially collected at long trajectory lengths (or observation times), corresponding to ≈ 900 τ_{fit}, a length previously recognized to allow the probes to explore all dynamic environments as reflected in a median β value that does not evolve further with longer observation time.[78,178]

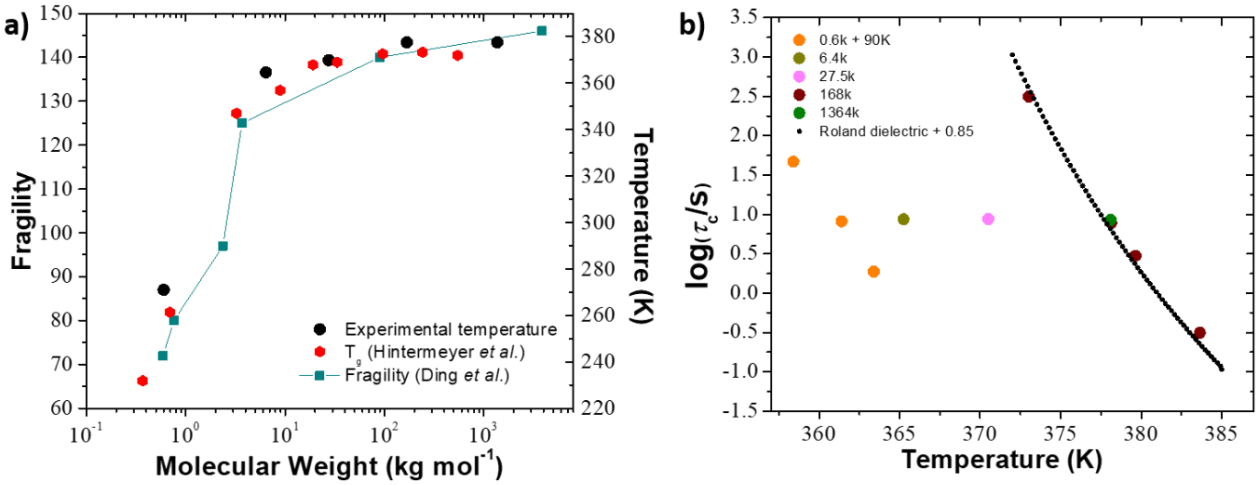

Figure 17. (a) Fragility (green squares, left axis) adapted from Ding *et al.*[100] compared to temperatures at which dynamics were captured in the current report (black circles, right axis), as well as T_g values from Hintermeyer *et al.*[180] (red circles, right axis), each as a function of polystyrene molecular weight. (b) Measured median τ_c values of pPDI as a function of temperature and polystyrene molecular weight. Measurements in 0.6 kg mol^{-1} polystyrene are plotted 90 K higher than the actual measured temperature. Data collected in 168 kg mol^{-1} polystyrene is compared to the VFT fit of the temperature dependence reported by Roland and co-workers from dielectric spectroscopy measurements and shifted by 0.85 decades.[168]

Additional experiments were then undertaken to confirm that pPDI in both high and low molecular weight polystyrene yielded expected temperature dependences (Figure 17b). As we reported previously, in 168 kg mol^{-1} polystyrene, the temperature dependence of probe rotational correlation times follows that reported by Roland, *et al.*[168] In the 0.6 kg mol^{-1} polystyrene, a less pronounced temperature dependence is apparent, consistent with the expected lower fragility of this lower molecular weight polystyrene. Fragility, m, can be defined as $m = \frac{d\log(\tau_\alpha)}{d(T_g/T)}\Big|_{T_g}$, and fragility values reported here were calculated from the tangent of the best fits to calculated τ_α versus temperature plots at T_g. This yields fragilities of ~75 for the lowest molecular weight (0.6 kg mol^{-1}) and ~120 for the higher (168 kg mol^{-1}) molecular weight polystyrene. This matches trends found in the literature, reinforcing that pPDI is an appropriate probe for characterizing polystyrene across molecular weights even for systems where T_g varies by more than 100K.[83,100,169,180]

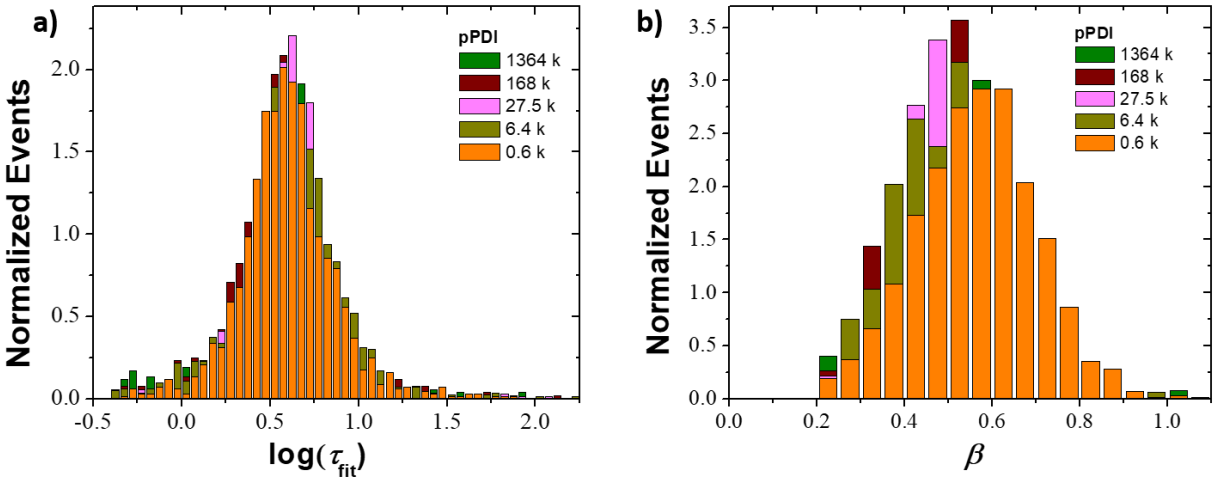

Figure 18. (a) τ_{fit} and (b) β distributions of pPDI in all molecular weights of polystyrene for the longest trajectory length measurements.
While no change in τ_{fit} distribution is observed, the β distribution shifts to higher values for the lowest molecular weight polystyrene. Detailed characteristics are given in Table 3.

From the same measurements that yield the τ_c values shown in Figure 17b, the full distribution of time scales reported by the single molecules is also available. Figure 18a shows the distributions of τ_{fit} values for all pPDI probes measured in polystyrene across molecular weights, each at the temperature that led to median $\tau_{fit} \approx 4$ s. No difference in the breadth of relaxation times across molecular weights probed is apparent as reflected by τ_{fit} values. The distribution of β values does, however, shift to higher values for the lowest molecular weight polystyrene (Figure 18b), suggesting that the lowest molecular weight polystyrene is less dynamically heterogeneous than the others.

Molecular Weights (g mol^{-1})	600	6405	27500	168000	1364000
temperature (K)	271.4	365.3	370.5	378.1	378.1
number of molecules	1362	1657	1467	1047	1046
median τ_c (s)	7.0	8.7	8.7	7.7	8.3
median τ_{fit} (s)	3.9	4.0	4.0	3.7	4.1
median β	0.57	0.51	0.50	0.51	0.51
β_{QE}	0.55	0.50	0.48	0.49	0.49
median trajectory (τ_{fit},med)	841	839	923	901	842
median frame rate (frames/τ_{fit})	19.3	19.9	20.2	18.3	20.4
fwhm (τ_c distribution)	0.50	0.51	0.49	0.49	0.43
fwhm (τ_{fit} distribution)	0.47	0.50	0.46	0.43	0.45
fwhm (β distribution)	0.31	0.32	0.29	0.32	0.30

Table 3. Characteristics of data obtained from the longest trajectory pPDI measurements in polystyrene and presented graphically in Figure 18.

To further examine dynamic heterogeneity, and in particular timescales associated with dynamic exchange as a function of molecular weight in polystyrene, τ_{fit} and β distributions were evaluated as a function of trajectory length, with the premise that observing individual molecules for short times reveals time-local dynamics experienced by the molecule while observing molecules for long times allows them to experience and report changes in dynamics.[77,150] For the full set of single molecules investigated, it is thus expected that the widths of the τ_{fit} and β

distributions will decrease and median β values will decrease with increased observation time or trajectory length. This approach was used previously to characterize exchange time, τ_{ex}, as a function of temperature in 168 kg mol^{-1} polystyrene using pPDI as a probe and revealed no difference in overall degree of dynamic heterogeneity (as reported by β) or exchange time relative to structural relaxation time (τ_{ex}/τ_{α}) as a function of temperature.[178] For this analysis, the single molecule trajectories associated with the data shown in Figure 18 were cut to shorter lengths ranging from ≈ 30 – 500 τ_{fit} and re-fit to obtain new KWW parameters and distributions that were then analyzed as a function of trajectory length (Figure 19). While some variation in τ_{fit} distribution width as a function of trajectory length for different molecular weight polystyrene is apparent (Figure 19a), no clear trend as a function of molecular weight is observed. Additionally, no differences are seen in the width of the β distributions vs. trajectory length as a function of molecular weight (Figure 19a, inset). This is expected given that this quantity has been shown to be dominated by finite trajectory length effects rather than host dynamic heterogeneity.[74,75] Evolution of the median β value as a function of trajectory length was also investigated (Figure 19b). At short trajectory lengths, the evolution of the median β value is very similar for all molecular weights. However, starting at trajectories of ≈ 200 τ_{fit} in length, the lowest molecular weight polystyrene shows consistently higher median β values than the other molecular weights, consistent with the distinctly right shifted β distribution seen in Figure 18b, with the plateau median β value of ≈ 0.57, suggesting a lesser degree of dynamic heterogeneity compared to the higher molecular weight polystyrenes, where the β values plateau to ≈ 0.50. The evolution of the

β value to a plateau occurs on similar timescales for all molecular weights, suggesting the timescale of dynamic exchange does not vary with molecular weight or fragility in this system.[178]

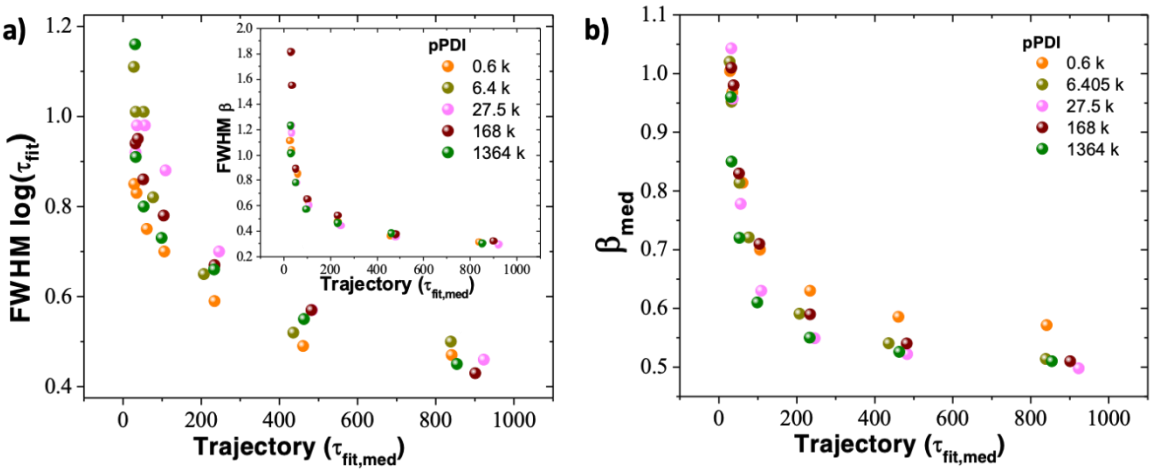

Figure 19. The evolution of (a) the FWHM of $\log(\tau_{fit})$ and (inset) β and (b) median β with trajectory length of the pPDI in polystyrene data also shown in Figure 18.

Given the differences in measured and reported fragility over the polystyrene molecular weight range investigated here and the very large change in glass transition temperature over this range, the relatively modest differences seen in measured single molecule β values and timescales associated with dynamic exchange across the systems studied is somewhat surprising. In particular, the β value for low molecular weight polystyrene plateaued at ≈ 0.57 whereas all higher molecular weight hosts plateaued at β ≈ 0.50 even while previous measurements had shown differences in fragility across most of the molecular weight range explored. Additionally, while β ≈ 0.50 is in the range of previous reports, it is higher than some reported values of probe-free or small probe ensemble or sub-ensemble measurements of β in moderate to high molecular weight polystyrene near T_g.[40,168–170,181,182] For example, Ediger and coworkers reported a β as low as 0.35 using a fluorescence recovery after photobleaching approach with the probe tetracene in 50 kg mol^{-1} polystyrene (expected fragility > 100) and Plazek *et al.* reported β ≈ 0.35 for polystyrene

with a fragility of 139 in probe-free experiments.[181,182] Taken together, these findings hinted that the pPDI probe may actually not report the full breadth of heterogeneity present in moderate to high molecular weight polystyrene, instead averaging over some dynamic heterogeneity in the system. This is plausible given that the probe rotational correlation time is ≈ 7 times slower than the high-molecular weight host segmental dynamics (τ_c/τ_α = 7.07), and any difference in probe relative to host dynamics can result in probe averaging over dynamic environments in the host.[34]

4.2.2 Further Investigation via the Fluorescent Probe BODIPY268

Previously, a small BODIPY probe (BODIPY268) was used to characterize the molecular glass former *o*-terphenyl, with a τ_c value nearly identical to that of the host, eliminating potential time averaging by the probe.[77] While BODIPY268 does not have the total photon yield of pPDI, limiting the signal to noise and/or trajectory length of measurements, it is approximately half the molecular weight of pPDI while exhibiting similar absorption and emission properties. It is thus a candidate to clarify whether pPDI reports of median β as a function of polystyrene molecular weight were impacted by potential averaging over dynamic heterogeneity in high fragility polystyrene. Because BODIPY268 has less favorable photophysics than pPDI, measurements are challenging, and measurements were taken only in the 6.4 and 168.0 kg mol^{-1} polystyrene samples, each at a single temperature. Again, temperature was adjusted to target a mean τ_{fit} value of 4 s. For BODIPY268 measurements, this resulted in measurements at 364.3 and 374.8 K. To estimate τ_c/τ_α for BODIPY268 in polystyrene, using the VFT fit from Roland *et al*. the τ_c value of pPDI in 168 kg mol^{-1} polystyrene at 374.8 K was found and compared to that obtained via BODIPY268 measurements at the same temperature. This procedure suggested a τ_c/τ_α value of ≈ 1 for BODIPY268 in polystyrene. We note that single molecule measurements of BODIPY268 in the lowest molecular weight polystyrene (0.6 kg mol^{-1}) were not successful, possibly due to the

combination of low probe signal and comparatively high host background, the latter of which most likely results from the lack of recrystallization of this low molecular weight polystyrene (for additional details, see Materials and Methods).

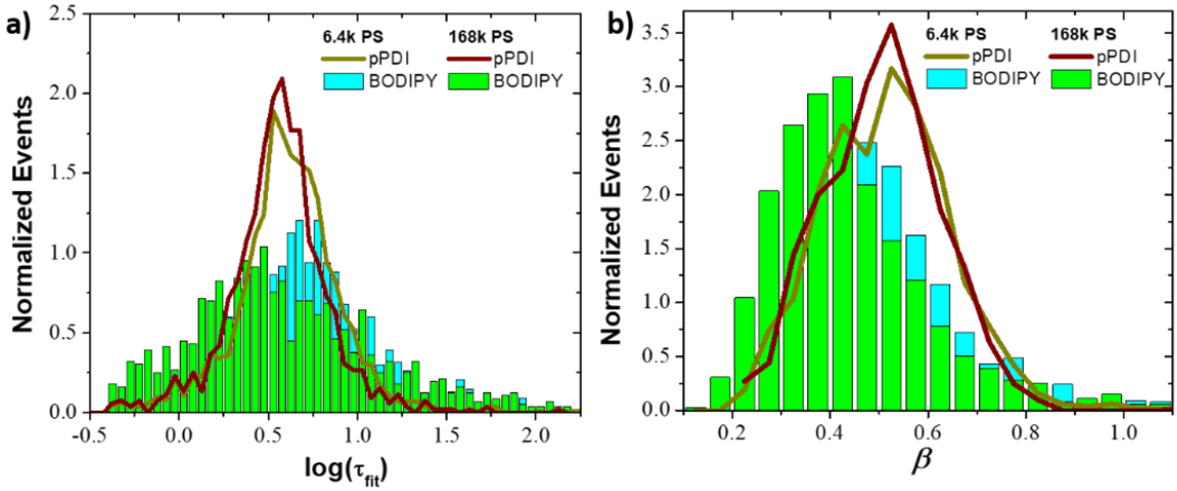

Figure 20. Characteristic measurements via BODIPY 268.
(a) FWHM of $\log(\tau_{fit})$ of polystyrene of two molecular weights using BODIPY268 (columns) overlaid by distributions for pPDI (lines) in polystyrene of the same molecular weights and similar trajectory lengths, with the pPDI data also shown in Figure 18a. (b) β distributions of the same systems shown in (a). Detailed characteristics of the BODIPY268 data are given in Table 4.

It is apparent from Figure 20 that the τ_{fit} and β distributions reported by BODIPY268 differ from those reported by pPDI for these (nearly) isochronic (same relaxation time) probe measurements. Notably, the median β values for the two molecular weights measured are lower than those obtained from pPDI, with a value of $\beta \approx 0.45$ for the 6.4 kg mol^{-1} and $\beta \approx 0.40$ for the 168 kg mol^{-1}, suggestive of the fact that pPDI – despite capturing significant heterogeneity in moderate and high molecular weight polystyrene – may not capture its full dynamic heterogeneity. Given that BODIPY268 measurements are both noisier and yield shorter trajectories than pPDI in polystyrene, we checked consistency between single molecule reports and ensemble reports of heterogeneity for both probes. In this approach, described in more detail in Reference 77, each

individual single molecule autocorrelation is transformed through an inverse Laplace transform to yield the set of timescales experienced by each single molecule over the course of the experiment. Such distributions are aggregated over all molecules as described in Materials and Methods. Assuming the single molecule traces offer robust reports of the dynamic environments probes experience, this approach should reproduce the distribution obtained from the inverse Laplace transform of the quasi-ensemble stretched exponential. For both pPDI and BODIPY268, the single molecule results match that obtained from the quasi-ensemble stretched exponential (Figure 21), suggesting that the limitations associated with the BODIPY268 probe (in particular, relatively low signal to noise) do not preclude robust reporting of the local environments in polystyrene through single molecule measurements.

Molecular Weights (g mol^{-1})	6405	168000
temperature (K)	364.3	374.8
number of molecules	1699	1406
median τ_c (s)	14.9	13.9
median τ_{fit} (s)	4.50	3.30
median β	0.46	0.41
β_{QE}	0.42	0.38
median trajectory (τ_{fit})	747	1007
median frame rate (frames/τ_{fit})	22.7	16.5
fwhm (τ_c distribution)	0.78	0.91
fwhm (τ_{fit} distribution)	0.79	0.99
fwhm (β distribution)	0.34	0.30

Table 4. Characteristics of data obtained from the longest trajectory pPDI measurements in polystyrene and presented graphically in Figure 20

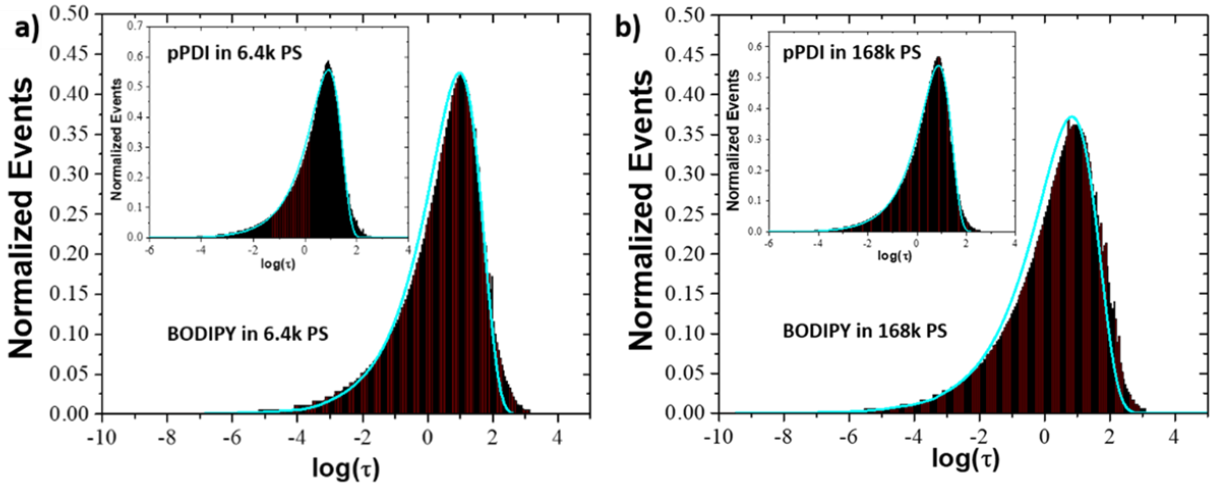

Figure 21. ILT-built distributions (red columns) of (a) 6.4 kg mol^{-1} polystyrene as measured through BODIPY268 and (inset) pPDI and compared to that predicted from the ILT transform of the ACFs$_{QE}$ (cyan lines). (b) Equivalent distributions of 168 kg mol^{-1} polystyrene.

To more fully understand pPDI and BODIPY268 single molecule reports of polystyrene dynamic heterogeneity as a function of fragility, we compare median β values measured in this study to previous measurements. Examining isobaric fragility and stretching exponents compiled by Niss *et al*. for a variety of polymers (Figure 22a), we find that measured β values as reported by pPDI probes do not follow the expected trends in mid to high molecular weight polystyrene, plateauing after the second lowest molecular weight polystyrene. We note that while the absolute value of fragility is path dependent, the general trend and thus correlation with molecular weight and stretching exponent is the same regardless of path.[104] Further, when comparing the fragility values of the molecular weights measured in the experiment of Ding *et al.* (Figure 17b) to the predicted stretching exponents of Niss *et al.*, the experimental β values obtained with pPDI do not agree with expectations.[100,104] This is consistent with the idea that pPDI averages over some dynamic heterogeneity in high fragility polystyrene. In contrast, the values obtained from BODIPY268 track closely with expectations suggested by Niss *et al.* (Figure 22a).

Given this convergence between BODIPY268 results and previous measurements together with the fact that the pPDI probes did not reveal signs of signs of variation in τ_{ex}/τ_{α} as a function of fragility (Figure 19), we performed trajectory length analysis for BODIPY268 probe measurements (Figure 22b). This analysis shows that even at relatively short trajectories, divergence between pPDI and BODIPY268 β values are evident. Moreover, distinction between BODIPY268 results in the polystyrene of these two molecular weights is evident, not only at long trajectory lengths but also at shorter trajectory lengths, in contrast to findings in pPDI and consistent with the idea that BODIPY268 is more sensitive to differences in fragility than is pPDI. In accordance with previous work, we also performed analysis of the evolution of median β using a procedure in which subsets of a given trajectory length were analyzed (Figure 23). In brief, individual molecules of a given molecular weight and median trajectory length were grouped based on their individual τ_{fit} values and trajectory lengths in terms of those individual τ_{fit} values, and

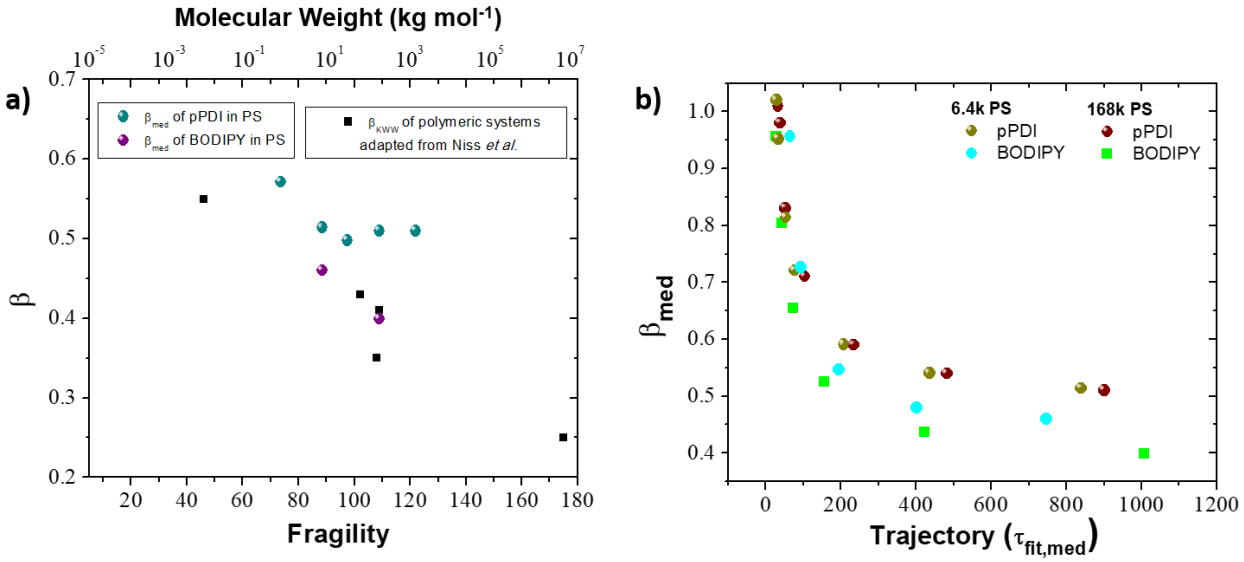

Figure 22(a) β values of various polymers as a function of isobaric fragility, adapted from Niss et al., compared to measured median β values using pPDI (purple circles) and BODIPY268 (teal circles) probes as a function of molecular weight.[104] (b) The evolution of median β values of two moderate to high molecular weights of polystyrene, using pPDI and BODIPY268.

median β of each formed subset was plotted as a function of trajectory length. In all cases, the median β value decays with increasing trajectory length, reaching a plateau at the quasi-ensemble β value. In two previous papers, we showed that analyzing this decay can be used to characterize relative τ_{ex}/τ_{α} values across variables such as temperature.[78,178]

Here, we use a related approach to characterize τ_{ex}/τ_{α} as a function of polystyrene fragility as reported by pPDI and BODIPY268, fitting the linear portion of the descent of median β as a function of trajectory length to its plateau value, with the time of plateau characterizing the timescale on which the median probe molecule has explored all the dynamic environments

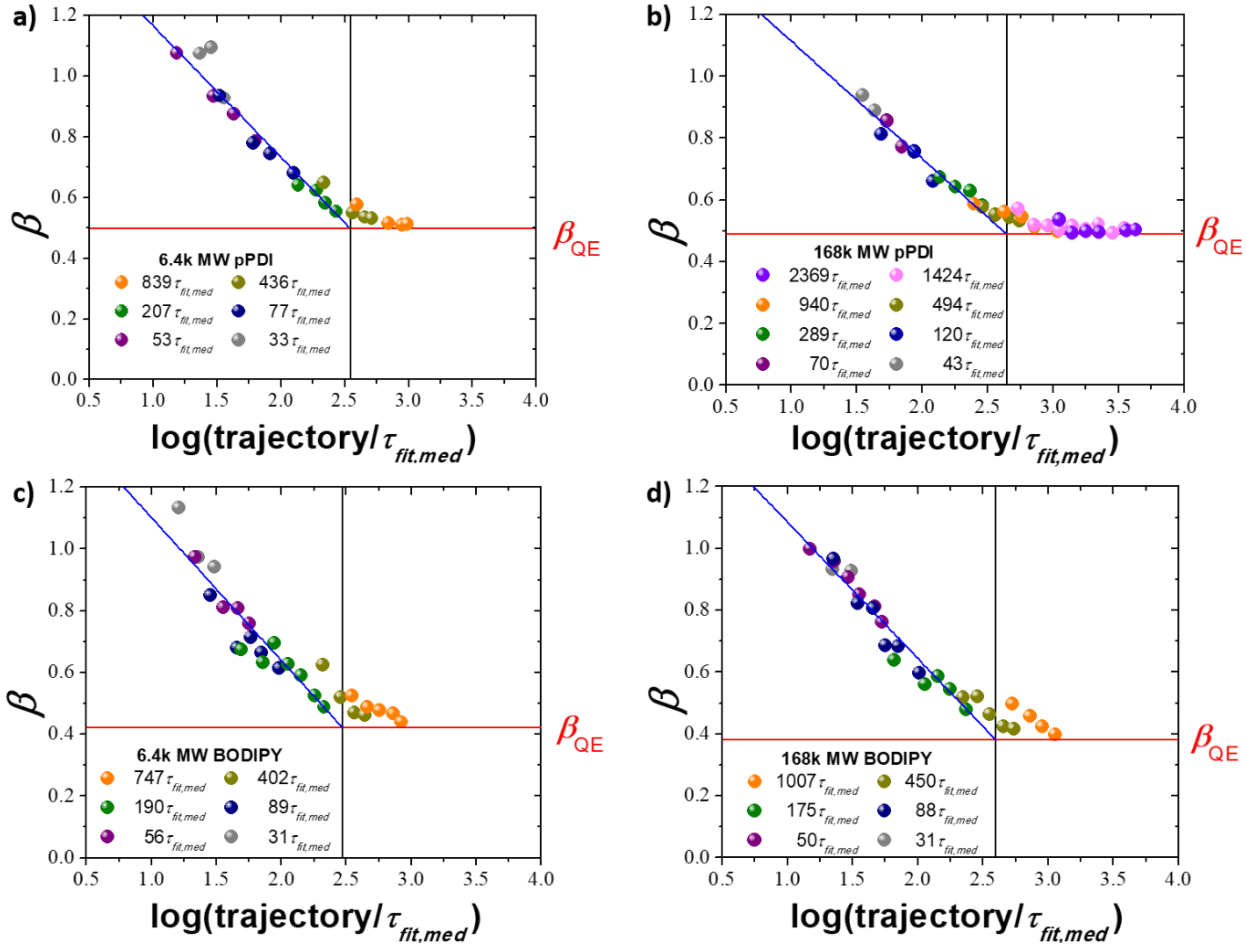

Figure 23. Median β for pPDI in (a) 6.4 kg mol^{-1} and (b) 168 kg mol^{-1} polystyrene, as well as for BODIPY in (c) 6.4 kg mol^{-1} and (d) 168 kg mol^{-1} polystyrene as a function of trajectory length for subsets of data of particular trajectory lengths.
Data shown in (b) is also presented in reference 78.

available to it. This analysis reveals that the slopes of decay are similar for all probes, with a slight increase in absolute value of slope with increasing quasi-ensemble β value for a particular probe (Table 5). Intriguingly, in all cases the time at which the single molecule median β value reaches the quasi-ensemble β value, which we term the crossover time, is quite similar in trajectory length in terms of probe rotations, with a slight shift to higher values in the higher fragility, higher molecular weight polystyrene samples (Figure 23, Table 5). We note that in the lowest molecular weight polystyrene, which was accessible with the pPDI probe but not the BODIPY268 probe, the crossover time was nearly the same as that seen in the 6.4 kg mol^{-1} polystyrene (2.52 vs. 2.54), despite the shift to a higher β_{QE} value (0.55 vs. 0.50) (Table 5). The similarity in decay rate and crossover times for median β values between the pPDI and BODIPY268 probes indicates that regardless of degree of heterogeneity reported by the probe, the probe reports no further changes after a given number of probe rotations. This indicates that difference in probe reports of dynamic heterogeneity in these systems is not due to missing dynamics on the long time side, consistent with our understanding of how probes may average over dynamic heterogeneity.[34] Additionally, the fact that for a given probe, no systematic change in crossover time occurs as a function of host fragility indicates that while fragility and β are correlated and both likely intrinsic reporters of dynamic heterogeneity, timescales associated with dynamic exchange do not show strong clear correlation with either quantity.

probe	pPDI			BODIPY		
polystyrene (kg mol^{-1})	slope	crossover time	β_{QE}	slope	crossover time	β_{QE}
0.6	-0.42 ± 0.02	2.54 ± 0.03	0.55	-	-	-
6.4	-0.41 ± 0.03	2.59 ± 0.04	0.50	-0.44 ± 0.04	2.52 ± 0.06	0.42
168.0	-0.38 ± 0.03	2.64 ± 0.05	0.49	-0.43 ± 0.02	2.63 ± 0.04	0.38

Table 5. Characteristics of decay of median β as a function of trajectory length as shown graphically in Figure 23 and discussed in the main text.

4.3 Conclusion

The dynamics of polystyrene of varied molecular weight was investigated via single molecule rotational measurements. Previous reports had shown that the fragility of polystyrene increases with molecular weight, and other studies had suggested a correlation between fragility and degree of dynamic heterogeneity, as reported by the stretching exponent, β. The current measurements revealed single molecule reports of stretching exponents indeed decrease with increasing polystyrene molecular weight. While the fluorescent probe pPDI reported differences in β between very low molecular weight polystyrene and polystyrene of higher molecular weight, it did not differentiate between polystyrene systems with high fragilities. The smaller fluorescent probe, BODIPY268, uncovered a wider range of stretching exponents than pPDI, reinforcing the anti-correlation between β and fragility on the single molecule level across the full range of accessible fragilities. Despite this, neither probe showed strong evidence for correlation between characteristic timescales of dynamic exchange and β or fragility, suggesting no or limited inherent correlation between timescales of exchange and quantities that characterize degree of glassy or anomalous behavior.

Chapter 5. Confinement Studies in Thin Film Polystyrene

In this chapter, results from single molecule approaches aimed at studying the surface dynamics of supported thin polystyrene films are described. In particular, experiments were performed in the temperature regime near, yet below, the film's bulk glass transition temperature. As previously reported by Paeng *et al.*, polymer films exhibit a layer with enhanced surface mobility, with the proportion of fast molecules growing with decreased thickness.[141] The purpose of the herein described studies is to simultaneously observe the enhanced surface molecules and the slower bulk population. In a first approach, the previously used perylene diamine probe pPDI is embedded in polystyrene films of varying thicknesses, while in a subsequent step, different probes expected to exhibit varying rotational relaxations are employed. While no evidence for previously described mobile surface molecules has been found from a single molecule perspective, this chapter provides useful foundational information for additional studies on the particularities of thin film polymers.

5.1 Motivation for Single Molecule Studies in Confined PS

5.1.1 Impact of Confinement on Polymers

As technologies have decreased in size over the past years, the interest in the properties of nanometer-sized materials near their glass transition temperatures has increased. In particular, polymers confined to the nanoscale exhibit different physical properties than their bulk counterparts, such as a shift in their glass transition temperature, T_g, and a change in the related molecular relaxation processes.[183] These differences in dynamics can have important impacts on the functionality of nanotechnologies: sensors typically rely on a target molecule's diffusion while batteries and other electronic devices require high mobility of charge carriers, and substantial attention must thus be given to systems that are continuously being reduced in size.[141] Polymers can be confined in various ways, including in nanospheres or nanopores, with all approaches increasing the proportion of the sample near an interface, thus altering the polymer's environment when compared to bulk samples.[113,126,184] A majority of studies aimed at understanding the observed particularities have been performed on thin polymer films, typically constrained to thicknesses below 100 nm, with a particular focus on measuring a shift in T_g with decreased film thickness.[119,124,126,135,185] However, conflicting reports exist on both the magnitude and direction of this change in the glass transition temperature. While molecular dynamics can often be inferred from T_g measurements in bulk films, the aforementioned contradicting results suggest that this may not be the case for thin polymer films. Indeed, as Starr and co-workers have remarked, different methods utilized to estimate the glass transition temperature exhibit different sensitivities to interface effects, thus often resulting in contradicting results.[115] Many studies have thus begun to shift away from pure T_g measurements and rather focus on directly measuring the dynamics of thin films.

Just as with bulk film measurements, a variety of approaches exist to study the dynamics in thin polymer films including atomic force microscopy, dielectric relaxation, and optical photobleaching approaches.[124,135,137,141] In some approaches, thin films must be in contact with a substrate while other approaches are possible on both substrate-supported and freestanding thin films. In films >100 nm, the proportion of molecules in contact with a surface is negligible, whereas confined thin films exhibit a higher and thus non-negligible proportion of molecules in contact with an interface. In freestanding films, only one interface must be considered, and is commonly the interface between the thin film and air. In supported films, *e.g.* films supported on a substrate as found in the experiments described in this thesis, two interfaces exist, namely the air-polymer interface as well as a polymer-substrate interface. These interfaces appear to influence the dynamics of molecules in proximity to it, and multiple studies have found a surface layer (*i.e.* molecules near the air-polymer interface) with enhanced mobility.[137,138,183,186,187] Concurrently, the impact of the substrate on the sample's dynamics is still debated, with several studies pointing toward reduced mobility dominated by surface-polymer interactions.[183,186]

5.1.2 Ensemble Approaches: Uncovering Thin Polystyrene Film Dynamics

A particularly interesting study recently performed by Paeng *et al.* found evidence for the existence of a surface layer with dynamics enhanced by several decades as compared to the bulk.[141] This study relied on monitoring the reorientation of probe molecules using a photobleaching approach in freestanding polystyrene films as thin as 14 nm in various mid to high-molecular weight polystyrene samples. As seen in Figure 24, these surface molecules (shown as yellow circles) appear to experience a lesser temperature dependence than the sample's bulk molecules (orange triangles and green squares), resulting in surface molecules exhibiting reorientation times up to 4 decades faster than their bulk counterparts at temperatures below the bulk T_g (~374 K).

Thus, as the temperature increases, these two populations begin to converge until they are no longer distinguishable. Other studies aimed at uncovering the surface diffusion of thin molecular glass forming films have found similar trends, with the fast surface molecules typically diffusing orders of magnitudes faster than those found in the bulk below T_g.[127,188,189]

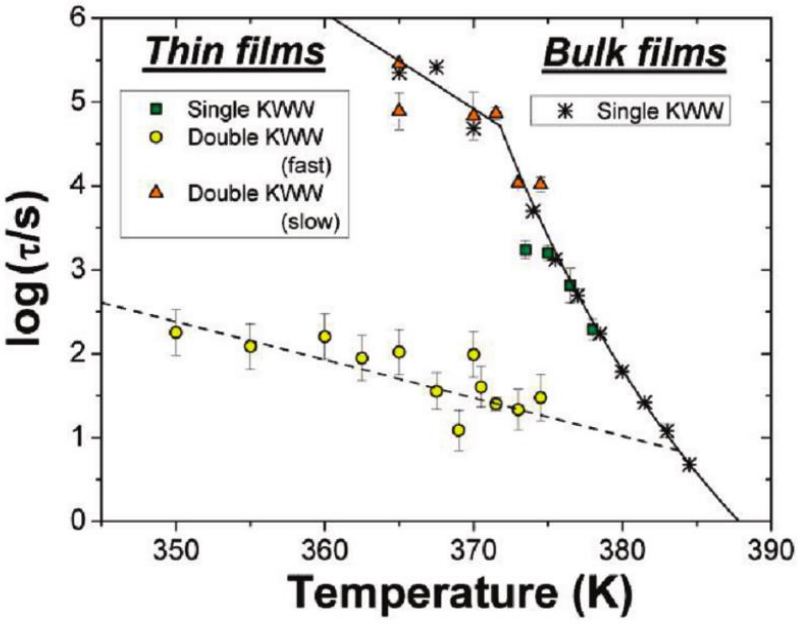

Figure 24. Reorientation times for a perylene diimide probe in free standing PS thin films. Below ~375 K, both a slow subset (solid line), as also a fast subset of surface molecules (dashed line) can be observed. The two subsets exhibit a difference in temperature dependence and converge at higher temperatures. Figure reproduced from reference 141 with permission from the publisher.

The ensemble measurements carried out by Paeng *et al*. highlight another interesting aspect of the fast surface layer. While previous T_g-based measurements have suggested that the thickness of the surface layer is molecular weight dependent, the photobleaching approach did not find evidence for this; indeed, as evidenced in Figure 25, the only factor affecting the thickness of the fast surface layer appears to be the temperature, with the surface layer becoming more prominent with increasing temperature. In other words, varying the overall film thickness does not alter the mobile layer, and only impacts the percentage of molecules exhibiting enhanced dynamics. A similar trend was found for an additional photobleaching anisotropy study of supported

polystyrene films on silicon wafers, with film thicknesses as low as 17 nm.[187] Interestingly, dielectric measurements performed by Fukao and Miyamoto found a decrease in the stretching exponent, β, and thus an increase in the degree of heterogeneity with decreasing thickness, suggesting that the heterogeneities found in the surface layer may differ from those in the bulk.[124]

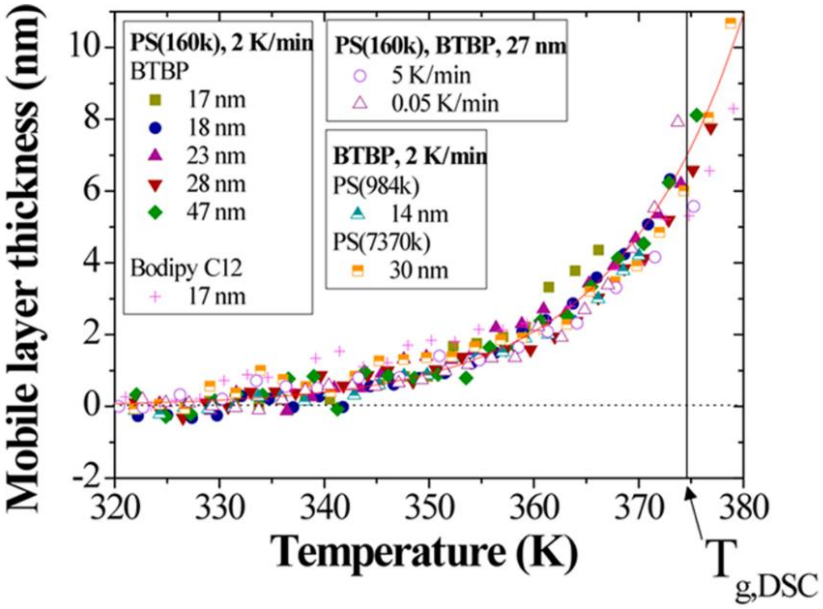

Figure 25. Temperature dependence of mobile-layer thickness.
As shown in a previous photobleaching approach by Paeng *et al*., the percentage of mobile surface molecules increases as the temperature increases, with no influence of cooling rate, probe choice or molecular weight being observed. Figure reproduced from reference 141 with permission from the publisher.

5.2.3 Single Molecule Diffusion Studies in Polymer Thin Films

The studies described above no doubt shed light onto the enhanced mobility of surface molecules in thin films, yet nonetheless remain ensemble approaches that are not capable of providing a full picture of the dynamic heterogeneity potentially involved in these processes. Indeed, as pointed out in a recent study by Oba and Vacha, most (sub)ensemble approaches to studying the surface molecules are either limited by their resolution, thus failing to fully differentiate the surface and bulk molecules, or – as in atomic force microscopy – are only capable

of accessing the surface layer and thus do not probe all mobile molecules.[183] In light of these limitations, several single molecule studies have recently been conducted, aiming at providing additional insight into the surface dynamics of thin films. Flier *et al*. conducted two studies in thin low-molecular weight polystyrene films (M_w = 3000 g mol^{-1}) using a perylene diimide (PDI) probe.[58,91] The authors measured probe diffusion in supported films ranging from 25 nm – 250 nm and found enhanced mobility for thinner samples. Additionally, one of these studies suggests the existence of two populations with discrete dynamics, one mobile and one immobile. In accordance with the previous reports by Paeng *et al.*, the authors suggest that the population of mobile molecules grows with increasing temperature. Most importantly, this study also indicates the presence of heterogeneous diffusion in these samples, suggesting the surface layer may experience similar dynamic heterogeneity as those known to exist in bulk films. However, these measurements were all performed at temperatures ranging from the bulk T_g to 1.1 T_g, *i.e*. at temperatures at which the two populations are expected to have similar if not identical dynamics (Figure 24). Thus, a clear differentiation between bulk and surface molecules appears unlikely. Interestingly, Xu *et al*. have proposed that the thickness of the substrate layer experiencing reduced diffusion – and thus the proportion of immobile molecules – is temperature dependent, suggesting the immobile layer observed by Flier *et al*. may not in fact be due to bulk dynamics, but rather interactions between the substrate and the polymer.[190] Furthermore, the PDI probe utilized for these studies was disproportionally large, thus conceivably not reporting on the full degree of heterogeneity present.

5.2.4 Single Molecule Rotational Measurements in Thin Films

Additional single molecule studies in various thin film polymers have provided supplementary insight into the anomalous surface dynamics previously observed, yet a clear single molecule approach similar to previous ensemble studies is still lacking. For one, Araoz and co-

workers utilized both an ensemble photobleaching and a single-molecule fluorescence anisotropy approach to compare the rotational dynamics of 200 nm and 25 nm films.[136] The authors embedded the Nile Red dye in films consisting of poly(methyl methacrylate), poly(ethyl methacrylate), and poly(butyl methacrylate), finding evidence for enhanced rotational mobility in the thinner films, with the results remaining consistent between single molecule and ensemble approaches. However, this study was restricted to short time scales, thus potentially missing certain heterogeneous dynamic, and did not directly compare the surface and bulk molecules present in the thin films.

In another single-molecule rotational study, Oba and Vacha relied on an astigmatic fluorescent imaging approach to study both the surface and bulk populations, using a PDI probe embedded in poly(methyl acrylate) films between 20 nm and 110 nm.[183] The authors found no difference in average rotational relaxation times between the films, yet found evidence of both a surface population characterized by fast diffusion, as well as a population of immobile molecules, thought to belong to molecules near the substrate interface. Additionally, the observed surface layer was suspected to be < 5 nm, no matter the overall film thickness, similar to claims by Paeng *et al*. However, this study was restricted to a single temperature of T_g + 13 K, a temperature at which it is again likely that the bulk and surface dynamics are indistinguishable.

The purpose of this final chapter is thus to introduce experimental single molecule approaches aimed at studying the distinct surface and bulk dynamics in thin polystyrene films at temperatures below the bulk glass transition. Previous studies in our group have uncovered similar findings as Oba and Vacha, and Flier *et al.*, yet were restricted to 100 nm polystyrene films and focused on a temperature regime above T_g.[191] By directly comparing the bulk and surface molecules' rotational dynamics, details on dynamic heterogeneity of surface molecules can be clarified. The experiments described in this chapter rely on two approaches: in a first attempt, pPDI

was utilized to measure rotational relaxations in polystyrene films of various thicknesses and at several temperatures below the bulk glass transition temperature. As all these measurements were performed below T_g, the surface and bulk relaxations are expected to be sufficiently differentiable. In a second approach, a set of large probes was utilized to attempt to identify surface molecules that may be too fast to capture. The probes were meant to report on the surface molecules slow enough to be comparable to measurements of the bulk dynamics via the smaller pPDI probe. Before these large probes were utilized for thin film measurements, their rotational dynamics were probed in bulk films and compared to results known from previous pPDI measurements.

5.2 Single Molecule Approaches in Bulk and Thin Film PS

5.2.1 Rotational Measurements with pPDI

Given the results of Paeng *et al.*, the overall population of the fast surface layer is expected to be thickness-independent and solely depend on the temperature of the sample, suggesting it will be easiest to identify fast surface molecules at temperatures at which they are most separated, *i.e.* temperatures near yet below T_g.[141] However, as the goal of this study was to observe both the surface *and* the bulk molecules, the dynamics of the two populations require clear separation. Substrate effects were not a focus of the present study, and thus only a separation between surface and bulk molecules was considered. Upon inspection of the previously published results presented in Figure 24, lower experimental temperatures assure a greater separation of rotational timescales. Thus, in an initial step, a temperature of 372.5 K, approximately 0.5 K below the bulk glass transition temperature, was chosen for rotational measurements. The fluorescent dye pPDI, previously described in Chapters 3 and 4, was embedded at low concentrations in high-molecular weight (168 g mol^{-1}) polystyrene films supported on either quartz or silicon wafers, with thicknesses varying from 25 nm to 200 nm. The ensemble studies reported by Paeng *et al*. were

used as a basis to estimate the separation between the bulk and surface dynamics, and rotational time scales were thus expected to be separated by ~2.5 decades at this temperature. At this point it should be noted that the ensemble experiments of references 141 and 187 relied on a PDI-based probe (tbPDI) structurally similar to pPDI. It is known from previous experimental work that tbPDI reports a τ_c approximately a decade slower than pPDI, with the slower probe not fully reporting on the dynamic heterogeneity of bulk polystyrene.[78,141,187] However, the separation in dynamics of the bulk and surface layer is not expected to be impacted by this difference in probe choice, and frame rates were chosen to accommodate for the rotational differences of the two probes.

An additional consideration for these measurements is the limit in dynamic range. Our typical single frame rate experiments permits capturing dynamics within circa a decade of that frame rate. This typically encompasses most dynamics found in the bulk at a single temperature, and thus differentiation between surface and bulk molecules would not be possible at a single frame rate for the temperature chosen when they are expected to differ by ~2.5 decades. To thus ensure that the full range of dynamics are captured, a variety of frame rates were chosen for each movie. This technique, from here on referred to as a frame rate sweep, is based on two assumptions. We assume that an ideal autocorrelation function (ACF) is created from an average of 20 frames per τ_{fit}: if too few frames per τ_{fit} are present, error arises from the limited points available for ACF construction; in contrast, greater frames per τ_{fit} result in shorter trajectories (in terms of probe rotations), again increasing the uncertainty of the constructed ACF. In practice this means we assume that each frame rate chosen reports best on molecules within one decade of the τ_{fit} value. Thus, movies were collected with three different frame rates separated by a factor of ten, on samples of varying thickness. Only molecules that fell within one decade of producing 20 frames per τ_{fit} were accepted during analysis of a given frame rate movie. As we assumed two populations

with vastly differing rotational dynamics to exist, the chosen frame rates were expected to produce ACFs for varying percentages of molecules, dictated both by the proportion of molecules in each layer and also by the constraints previously set. In other words, we expect the fastest frame rate to report on molecules in the fast surface layer, as the remaining bulk molecules would be rotating on timescales vastly slower than the frame rate would detect, while the slowest frame rate is expected to only accurately report on the slow bulk molecules. Hence, for the frame rate sweep approach, all data was normalized by the percentage of molecules each frame rate reported on.

The results of this frame rate sweep at 372.5 K are presented in Figure 26. Three frame rates – 0.2s, 2s, and 20s – were chosen, and movies were taken on samples with thicknesses of 25 nm, 80 nm, and >200 nm, *i.e.* bulk thickness. Two features become apparent upon inspection of

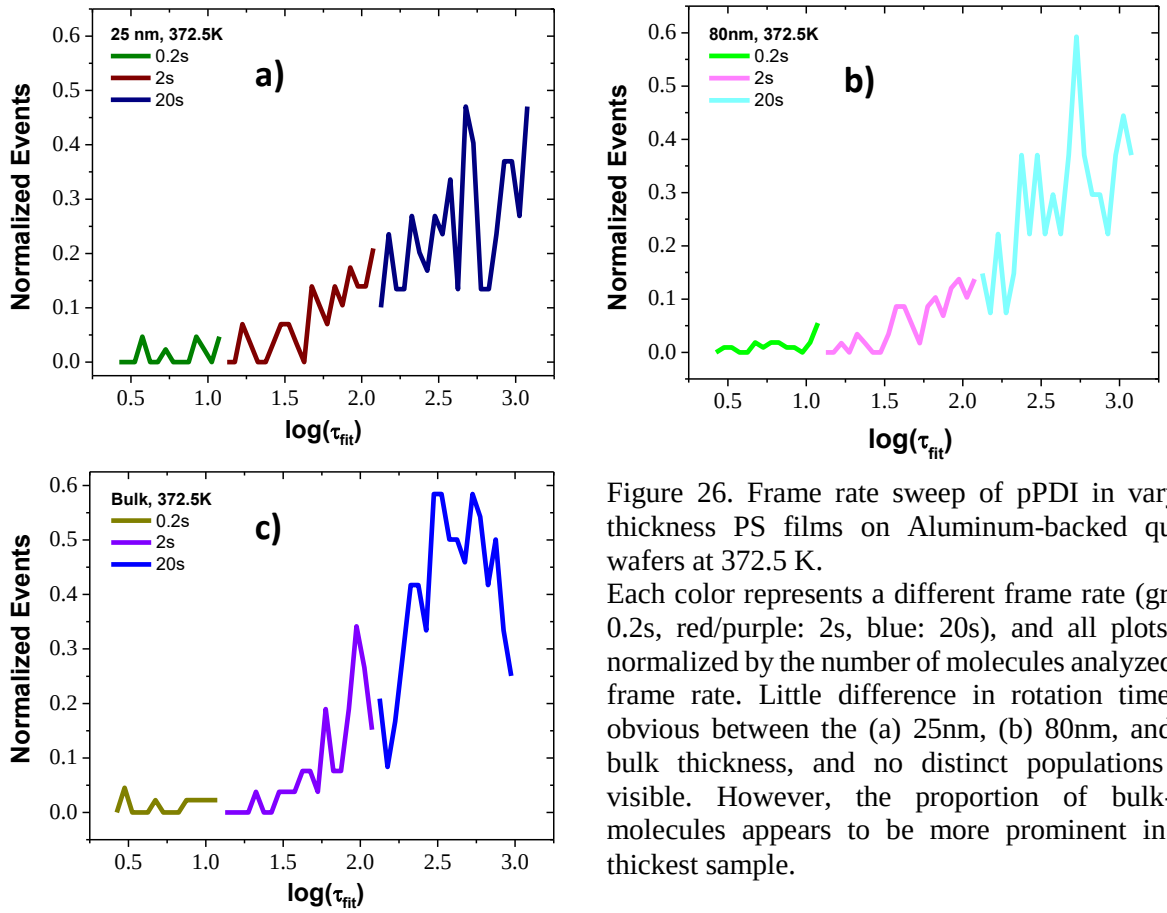

Figure 26. Frame rate sweep of pPDI in varying thickness PS films on Aluminum-backed quartz wafers at 372.5 K.
Each color represents a different frame rate (green: 0.2s, red/purple: 2s, blue: 20s), and all plots are normalized by the number of molecules analyzed per frame rate. Little difference in rotation times is obvious between the (a) 25nm, (b) 80nm, and (c) bulk thickness, and no distinct populations are visible. However, the proportion of bulk-like molecules appears to be more prominent in the thickest sample.

the results: 1) the similarity between the 25 and 80 nm samples and 2) the lack of any significant proportion of molecules captured by the fastest frame rate for all thicknesses probed. In contrast, the slowest population appears to be more prominent in the thickest sample, while virtually no molecules are captured by the fastest frame rate. Indeed, while the majority of molecules experience slow relaxation time scales in the thickest sample, the tail on the fast side is more prominent in the thinner samples, suggesting that the experimental temperature chosen may have not permitted a clear separation of bulk and surface dynamics. Hence, while the surface and bulk dynamics were expected to be differentiated by more than two decades at this temperature, these results suggest dynamics more similar for the bulk and surface molecules. However, it should also be noted that the single molecule signal to noise ratio (SNR) strongly decreases as sample thickness decreases, potentially increasing the difficulty of detecting molecules. Although we expect the proportion of fast molecules to be highest in our thinnest samples, we thus may not be able to measure their rotations due to the lower signal. While this reduced SNR in the thinnest sample is not well understood, reflection from the substrate may interfere with fluorescence as the thickness decreases, resulting in the reduced measured signal.

To increase the separation of dynamics and thus the possibility of measuring and differentiating bulk and surface molecules, additional measurements were performed at lower temperatures. To reduce the signal degradation observed in thinner samples, subsequent measurements were performed in slightly thicker films. The results of a frame rate sweep at 371.8 K on a 35 nm film can be seen in Figure 27 (a): as previously, the majority of molecules are found to exhibit relatively slow rotations, similar to those measured previously in bulk polystyrene films. Interestingly, a small population also appears to have faster rotational timescales that were not clearly observed at any thickness at 372.5 K. The existence of this enhanced fast tail may indicate

detection of a mobile surface layer. Additional measurements were performed on a thicker sample (140 nm) at 371.5 K, *i.e.* 0.3 K below the thin film frame rate sweep to confirm the existence of this population. For these measurements, shown in Figure 27 (b), the constraints set by the frame rate sweep were lifted, and all molecules fit at a given frame rate were analyzed. Nonetheless, the results shown in Figure 27 (b) remained normalized by the percentage of molecules fit to adjust for population differences. At this increased thickness, no indication of a mobile surface layer was observed, possibly due to the fact that the proportion of surface molecules is too small compared to the bulk at 140 nm. Indeed, upon close inspection, all frame rates used at this temperature and thickness appear to capture at least a segment of the same population, further suggesting that the molecules measured all belong to the bulk. On one hand, this could indirectly indicate that the previously measured fast rotations do indeed belong to a fast surface layer, which in turn is obscured in thicker samples. Alternatively however, as the fastest frame rate utilized in these

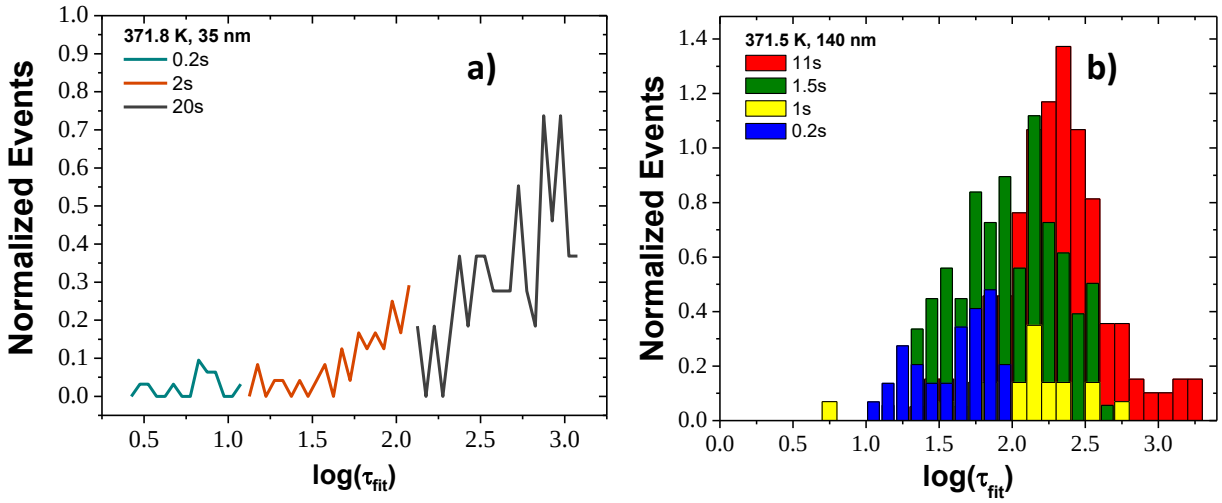

Figure 27. (a) Frame rate sweep at 371.8 K on a 35 nm thin film. (b) Various frame rates to test for populations at 371.5 K on a 140 nm film.
A small increase in events centered at $\log(\tau_{fit}) \approx 0.85$ could be a possible indication of a fast population in the 35 nm film (a). At a similar temperature of 371.5 K, yet a significantly thicker sample of 140 nm and shown in (b), several frame rates were used to potentially capture a wide range of rotations, yet no differentiation between populations can be seen. Indeed, the fastest frame rate (blue) utilized captures some of the same molecules that the slower frame rates also report on.

thicker measurements suggest no presence of a fast subset of molecules at all, this could also indicate that the previously measured "fast" molecules do not actually represent the surface layer, but rather are due to experimental noise and/or belong to the bulk population. Indeed, the measurements in the 35 nm film revealing a fast population of molecules could not be reproduced, in part due to the previously noted SNR issues. In addition, measurements in 50 nm and 100 nm films at 372 K did not show any particularly fast rotations (Figure 28). In fact, the 100 nm sample showed a higher population of molecules with fast rotational timescales than the thinner 50 nm sample, contradicting the expectation that the surface layer is more dominant in thin samples, and further supporting the conclusion that any "fast" molecules observed are solely due to experimental noise. Consequently, the frame rate sweep results suggesting a "mobile" population must be viewed quite critically.

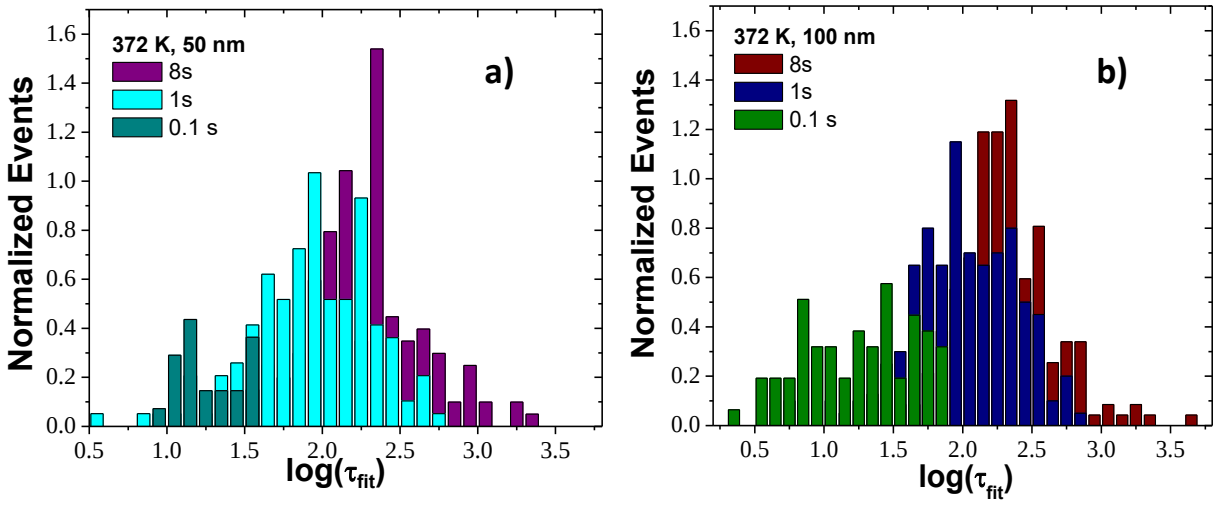

Figure 28. Single molecule measurements at 372 K in (a) 50 nm and (b) 100 nm films.
The same frame rates were used to measure probe rotations in both samples, and no difference in the spread of τ_{fit} can be observed, indicating the lack of fast surface dynamics being measured. In fact, a higher proportion of fast molecules is measured in the thicker sample, indicating the experimental approach does not permit measurement of a fast surface layer.

Several other temperature and thickness combinations were investigated to elucidate the potential existence of a fast surface layer observed in the PS thin films. In particular, two additional approaches to further separate the dynamics at 370 K are portrayed in Table 6. No particularly fast molecules could be measured at this relatively low temperature. In fact, measurements performed on both 70 nm thick and bulk films utilizing the same frame rates for image acquisition appeared to report on the exact same population of molecules. Median results in the 200 nm bulk sample are actually slightly *faster* than those measured in the 70 nm film, contradicting the existence of any detected fast surface molecules and in turn suggesting the influence of effects between the substrate and the polystyrene film.

frame rate at 370 K	**11s**	**1s**	**0.2s**
thickness		70 nm	
median τ_c (s)	1061	302	74
median τ_{fit} (s)	620	193	48
median β	0.67	0.73	0.75
% molecules fit	95	88	61
thickness		>200 nm	
median τ_c (s)	841	273	62
median τ_{fit} (s)	494	154	42
median β	0.68	0.71	0.73
% molecules fit	89	86	59

Table 6. Detailed results of thickness-dependent measurements of 70 nm and bulk films.

The lack of any distinct fast population of molecules identified in almost all measurements could be due to several limitations: for one, the proportion of fast molecules is expected to decrease with decreasing temperature, and it is thus possible that any surface layer is not significant enough

to be clearly identified through single molecule techniques at the lower temperatures chosen. Similarly, if the overall surface population is indeed thickness-independent, a 70 nm sample thickness may have resulted in the bulk overshadowing any fast surface population. However, thinner samples do not typically produce the desired SNR required for single molecule measurements, and measurements on thinner samples are not presented here as they did not result in successful data acquisition. Finally, one additional consideration must be discussed: it is possible that the fast molecules are significantly faster than expected, and all previously presented measurements simply captured dynamics of the bulk molecules. In this case, the imaging parameters chosen do not cover the dynamic range necessary, thus motivating the final set of studies described.

5.2.2 Rotational Measurements via Perylene-based Nanostructures

The concurrent measurement of surface and bulk dynamics in thin polymer films via a single molecule probe presents several challenges. First, the dynamics of the two populations must be well separated to be experimentally distinguishable. As previously indicated, this in turn likely requires a temperature sufficiently below the glass transition temperature of the bulk. On the other hand, each population must contain a sufficient proportion of molecules to be detectable. However, it is believed that the population of fast molecules found in the surface is strongly temperature dependent, with lower experimental temperatures resulting in a decrease of this population. Additionally, as the bulk population shows a significantly stronger temperature dependence than the surface layer, a decrease in temperature also drastically increases required experimental times. Hence, it is challenging to identify conditions with a large surface population, a bulk population that rotates on experimentally accessible timescales, and sufficiently discrete rotational timescales

of the two populations. Unfortunately, these conditions were not accessible in our experimental setup with a single probe.

An alternative approach to measuring the dynamics of the two populations through single molecule techniques was thus considered. Rather than attempting to characterize two populations with vastly differing relaxation times with a single probe, these dynamics can also be identified through the use of two probes of sufficiently different sizes, and thus different rotational timescales. In general, the rotations of probe molecules are expected to scale with size (and thus molecular weight), although probe-host interactions must also be considered. This relationship is given by the Debye-Stokes-Einstein equation,

$$\tau \propto \frac{\eta r_s^3}{k_B T},$$

with η corresponding to the viscosity of the host, r_s the hydrodynamic radius of the probe, and k_B the Boltzmann constant. A larger probe is expected to report on the rotations of the fast surface

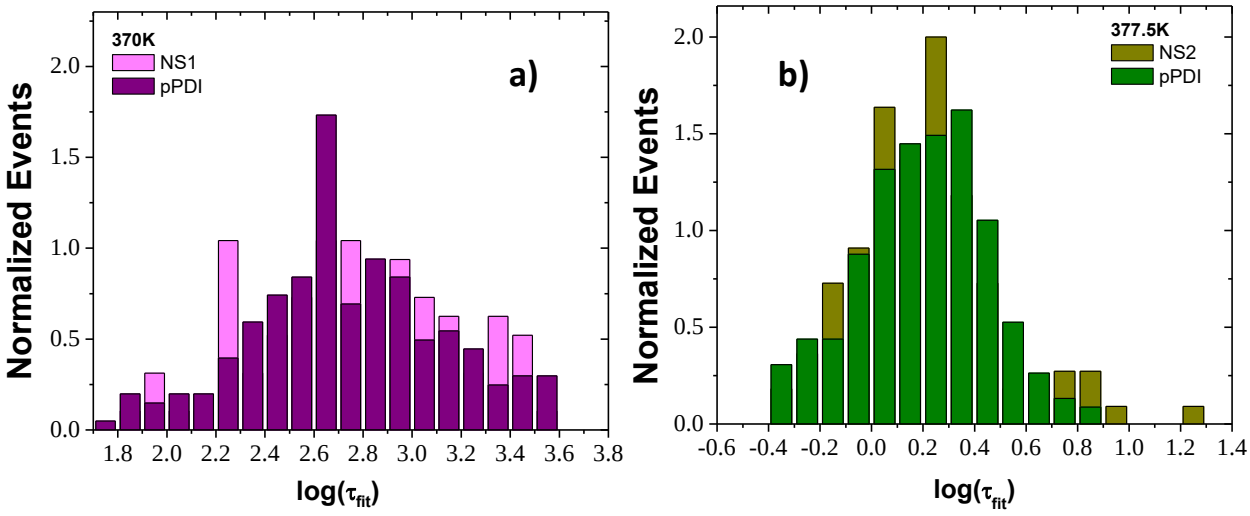

Figure 29. Rotational measurements of (a) nanostructure 1, and (b) nanostructure 2, as compared to pPDI in bulk PS.
The measurements were taken at two temperatures both above (a) and below (b) T_g. In both cases the distribution of rotational time scales of the nanostructures is almost identical to that of the smaller probe pPDI.

layer, yet on significantly slower time scales than the small probe pPDI would. Hence, it is expected that at a specified temperature, a large probe will report on the surface layer at an adequately chosen frame rate while the faster pPDI will mirror the rotations of the bulk.

Prior to embedding larger probes into thin films, the rotational dynamics of these probes in bulk films were measured to serve as a reference for subsequent surface layer measurements. Additionally, in order to limit differences in probe-host interactions, three different PDI-based nanostructures were chosen. An in-depth description of these probes is given in Reference 146. The nanostructures consist of differing numbers of PDI groups and are subsequently referred to as NS1, NS2, and NS3. These nanostructures have molecular weights approximately three (NS1), six (NS2), and nine (NS3) times larger than pPDI, and are thus estimated to exhibit rotational

0.2 s frame rate	**NS3**	**pPDI**
temperature (K)	377.5	
median τ_c (s)	5.00	5.11
median τ_{fit} (s)	3.26	3.38
median β	0.60	0.71
trajectory/$\tau_{fit,med}$	115	99
temperature	379	
median τ_c (s)	2.16	2.72
median τ_{fit} (s)	1.37	1.35
median β	0.61	0.55
trajectory/$\tau_{fit,med}$	575	492

Table 7. Detailed results of single molecule measurements of the nanostructure 3 in bulk polystyrene, and compared to results obtained with pPDI. Measurements were taken at two temperatures above T_g.

timescales ~30-700 times slower than the smaller probe. Anisotropy measurements of these probes, as well as of pPDI, are presented in Appendix C to further support the applicability of these nanostructures as single molecule probes in polystyrene.

Bulk measurements utilizing the nanostructure probes are presented in Figure 29 and Table 7, and contrasted to results obtained with pPDI. Measurements were taken at temperatures both above and below the glass transition temperature of bulk polystyrene. Initially, movies at the same temperature were taken at different frame rates in anticipation of slower probe rotation of the nanostructures as compared to pPDI. However, subsequent movies were taken at the same frame rates for a given temperature: as seen in Figure 29, the distributions of rotational time scales for the large nanostructures and pPDI are nearly identical. These identical distributions appear at temperatures both below and above T_g and are independent of the size of the nanostructure, though we note that these measurements were performed on ~ 1/10 the number of molecules usually analyzed in our single molecule measurements.

These near-identical rotational distributions are not well understood, yet factors such as symmetry of the probe and low thermal stability (thus potentially resulting in the degradation of the nanostructures into smaller PDI probes) could be possible explanations. Unfortunately, these results also preclude use of these nanostructrures for the discrete yet simultaneous measurement of bulk and surface dynamics in polymer thin films, and additional larger probes must be explored for successful surface measurements.

5.3 Summary and Outlook

The results presented in this chapter describe several approaches aimed at measuring the dynamics of mobile surface layers in polymer thin films. At temperatures below the glass transition temperature, this mobile layer is expected to exhibit rotational relaxations several decades faster

than the molecules found in the bulk of the sample. However, while previously published single molecule studies above the bulk glass transition temperature have suggested such a mobile surface layer, the current study has not found evidence for such a population below T_g.

Future optical single molecule studies aimed at understanding the particular dynamics of thin films must thus pay particular attention to two factors. 1) The difference in the temperature-dependence of rotational timescales between the surface and bulk population leads to a limited temperature range accessible in the herein described experiments: too high of a temperature may preclude differentiation of the populations, while too low of a temperature may lead to rotational timescales that are not experimentally accessible. 2) An appropriate sample thickness must be chosen as these studies require a significant proportion of surface molecules so that they may be detected even in the presence of a greater number of molecules exhibiting bulk dynamics; however, optical interference effects begin to arise in supported films < 40 nm, limiting the range of confined systems accessible in such studies. As no evidence for a mobile surface layer was found through the use of a single probe, the results presented here suggest single molecule approaches in thin films that rely on multiple probes with significant differences in rotational times. Such an approach may permit a single frame rate direct comparison between the surface and bulk dynamics of thin polymer films.

Chapter 6. Concluding Remarks

This thesis has highlighted the need for single molecule approaches to further elucidate the heterogeneous dynamics found near polystyrene's glass transition temperature: in Chapter 3, we presented single molecule studies showing temperature-independence of exchange time in the regime of 1.00 – 1.02 T_g, in part contradicting previous (sub)ensemble results. In Chapter 4, we provided single-molecule evidence for the correlation of the stretching exponent with molecular weight, even in the absence of any dependence on the system's exchange time. Finally, in Chapter 5 we presented various approaches to studying enhanced surface dynamics thought to be present in confined polymer systems though these studies did not present clear evidence for such a mobile surface layer.

While the studies discussed here present a single molecule perspective into the glassy dynamics of polystyrene, each study presents opportunities for additional investigation. For one, the single molecule studies presented cover a relatively narrow temperature range of T_g to T_g + 10 K. At high temperatures, optical limitations emerge as molecular rotations become too fast to cover. However, technological advances are already leading to higher (temporal) resolutions, and many optical limitations may soon be overcome. Similarly, the data presented in this thesis is purely rotational, yet many studies have found evidence of dynamic heterogeneities via translational diffusion studies. Interestingly, ensemble studies suggest decoupling of translational and rotational motion in glassy systems, another particularity of supercooled systems not encountered in typical liquids.[27] Indeed, current work in our group is investigating if this decoupling holds on a single molecule level. Lastly, as discussed in detail in the introduction and is especially apparent in Chapter 4, the choice of probe can severely influence single molecule

results due to the probe averaging over heterogeneous regions. Most of our work has relied on using small probes with high quantum yields, yet another approach to avoiding averaging and distinguishing changing dynamics from probe motility driven dynamics is tethering a probe to the host molecule, as is already done in some ensemble approaches and during imaging polymerization dynamics.[141,187,192] Thus, rather than the probe experiencing various (spatial) heterogeneities, a tethered probe is expected to purely report on the heterogeneities the host molecule is experiencing. However, even here care must be taken as a tethered probe could perturb the system of interest, and issues arising from photobleaching and low quantum yields can persist.[54]

The here presented work spans little more than five years, yet the questions and in part contradicting theories revolving around glassy systems have been studied for over a century. Indeed, over two decades ago, the Nobel-Prize physicist Philip Anderson remarked that "[t]he deepest and most interesting unsolved problem in solid state theory is probably the theory of the nature of glass and the glass transition."[193] The fact that the particularities found in glass formers near their T_g is still absent from most introductory chemistry and physics textbooks has not helped shed light onto this problem either. While much progress has been made in the glassy field since Anderson's quote, new questions have arisen with the appearance of new methodology, such as single-molecule microscopy. This thesis has aimed to provide a small glimpse into some of the questions (and provide some answers) still remaining in the field, with a focus on the dynamics found in glassy polystyrene near its glass transition temperature. Nonetheless, the research in this field is far from finished, and constantly evolving techniques permit a deeper investigation of the "most interesting unsolved problem in solid state theory."

References

1. Tammann, G. *Aggregatzustände*. (Leopold Ross, 1922).
2. Simon, F. Über den Zustand der unterkühlten Flüssigkeiten und Gläser. *Zeitschrift für Anorg. und Allg. Chemie* **203**, 219–227 (1931).
3. Angell, C. A. Formation of glasses from liquids and biopolymers. *Science (80-.).* **267**, 1924–35 (1995).
4. Rieger, J. The glass transition temperature of polystyrene. *J. Therm. Anal.* **46**, 965–972 (1996).
5. Rudin, A. & Choi, P. *Mechanical Properties of Polymer Solids and Liquids*. *The Elements of Polymer Science & Engineering* (2012). doi:10.1016/b978-0-12-382178-2.00004-3
6. Debenedetti, P. G. & Stillinger Frank, H. Supercooled liquids and the glass transition. *Nature* **410**, 259–267 (2001).
7. Jaeckle, J. Models of the glass transition. *Reports Prog. Phys.* **49**, 171–231 (1986).
8. Böhmer, R., Ngai, K. L., Angell, C. A. & Plazek, D. J. Nonexponential relaxations in strong and fragile glass formers. *J. Chem. Phys.* **99**, 4201–4209 (1993).
9. Ediger, M. D., Angell, C. A. & Nagel, S. R. Supercooled Liquids and Glasses. *J. Phys. Chem.* **100**, 13200–13212 (1996).
10. Angell, C. A. Strong and fragile liquids. in *Relaxations in Complex Systems* (eds. Ngai, K. L. & Wright, G. B.) 3–11 (Naval Research Laboratory, 1985).
11. Adam, G. & Gibbs, J. H. On the temperature dependence of cooperative relaxation properties in glass-forming liquids. *J. Chem. Phys.* **43**, 139–146 (1965).
12. Dyre, J. C., Hechsher, T. & Niss, K. A brief critique of the Adam-Gibbs entropy model. *J. Non. Cryst. Solids* **355**, 624–627 (2009).
13. Goldstein, M. Viscous liquids and the glass transition: A potential energy barrier picture. *J. Chem. Phys.* **51**, 3728–3739 (1969).
14. Berthier, L. & Biroli, G. Theoretical perspective on the glass transition and amorphous materials. *Rev. Mod. Phys.* **83**, 587–645 (2011).
15. Kirkpatrick, T. R., Thirumalai, D. & Wolynes, P. G. Scaling concepts for the dynamics of viscous liquids near an ideal glassy state. *Phys. Rev. A* **40**, 1045–1054 (1989).
16. Wisitsorasak, A. & Wolynes, P. G. Dynamical heterogeneity of the glassy state. *J. Phys. Chem. B* **118**, (2014).
17. Hocky, G. M. Connections between structure and dynamics in model supercooled liquids. **2014**, (2014).
18. Angell, C. A. Relaxation in liquids, polymers and plastic crystals - strong/fragile patterns and problems. *J. Non. Cryst. Solids* **133**, 13–31 (1991).

19. Xia, X. & Wolynes, P. G. Fragilities of liquids predicted from the random first order transition theory of glasses. *Proc. Natl. Acad. Sci. U. S. A.* **97**, 2990–2994 (2000).

20. Huang, D. & McKenna, G. B. New insights into the fragility dilemma in liquids. *J. Chem. Phys.* **114**, 5621–5630 (2001).

21. Deres, A. *et al.* The origin of heterogeneity of polymer dynamics near the glass temperature as probed by defocused imaging. *Macromolecules* **44**, 9703–9709 (2011).

22. Qin, Q. & McKenna, G. B. Correlation between dynamic fragility and glass transition temperature for different classes of glass forming liquids. *J. Non. Cryst. Solids* **352**, 2977–2985 (2006).

23. Sokolov, A. P., Novikov, V. N. & Ding, Y. Why many polymers are so fragile. *J. Phys. Condens. Matter* **19**, (2007).

24. Williams, M. L., Landel, R. F. & Ferry, J. D. The Temperature Dependence of Relaxation Mechanisms in Amorphous Polymers and Other Glass-forming Liquids. *J. Am. Chem. Soc.* **77**, 3701–3707 (1955).

25. Dudowicz, J., Douglas, J. F. & Freed, K. F. The meaning of the 'universal' WLF parameters of glass-forming polymer liquids. *J. Chem. Phys.* **142**, (2015).

26. Elmatad, Y. S., Chandler, D. & Garrahan, J. P. Corresponding States of Structural Glass Formers The variation with respect to temperature T of transport properties of 58 fragile structural glass-forming liquids (67 data sets in total) are analyzed and shown to exhibit a remarkable degree of universa. *Glass* **2**, 5563–5567 (2009).

27. Tarjus, G. & Kivelson, D. Breakdown of the Stokes-Einstein relation in supercooled liquids. *J. Chem. Phys.* **103**, 3071–3073 (1995).

28. Richert, R. Heterogeneous dynamics in liquids: fluctuations in space and time. *J. Phys. Condens. Matter* **14**, R703–R738 (2002).

29. Ediger, M. D. Spatially Heterogeneous Dynamics in Supercooled Liquids. *Annu. Rev. Phys. Chem.* **51**, 99–128 (2000).

30. Cicerone, M. T., Blackburn, F. R. & Ediger, M. D. Anomalous Diffusion of Probe Molecules in Polystyrene: Evidence for Spatially Heterogeneous Segmental Dynamics. *Macromolecules* **28**, 8224–8232 (1995).

31. Kaufman, L. J. Heterogeneity in single-molecule observables in the study of supercooled liquids. *Annu. Rev. Phys. Chem.* **64**, 177–200 (2013).

32. Giovambattista, N., Buldyrev, S. V., Starr, F. W. & Stanley, H. E. Connection between Adam-Gibbs Theory and Spatially Heterogeneous Dynamics. *Phys. Rev. Lett.* **90**, 4 (2003).

33. Stillinger, F. H. & Debenedetti, P. G. Glass Transition Thermodynamics and Kinetics. *Annu. Rev. Condens. Matter Phys.* **4**, 263–285 (2013).

34. Paeng, K. & Kaufman, L. J. Single molecule rotational probing of supercooled liquids. *Chem. Soc. Rev.* **43**, 977–89 (2014).

35. Sussman, D. M., Schoenholz, S. S., Cubuk, E. D. & Liu, A. J. Disconnecting structure and dynamics in glassy thin films. *Proc. Natl. Acad. Sci.* **114**, 10601–10605 (2017).

36. Kob, W., Donati, C., Plimpton, S., Poole, P. & Glotzer, S. Dynamical Heterogeneities in a Supercooled Lennard-Jones Liquid. *Phys. Rev. Lett.* **79**, 2827–2830 (1997).

37. Richert, R., Duvvuri, K. & Duong, L. T. Dynamics of glass-forming liquids. VII. Dielectric relaxation of supercooled tris-naphthylbenzene, squalane, and decahydroisoquinoline. *J. Chem. Phys.* **118**, 1828–1836 (2003).

38. Tracht, U. *et al.* Length Scale of Dynamic Heterogeneities at the Glass Transition Determined by Multidimensional Nuclear Magnetic Resonance. *Phys. Rev. Lett.* **81**, 2727–2730 (1998).

39. Kim, K. & Saito, S. Multiple length and time scales of dynamic heterogeneities in model glass-forming liquids: A systematic analysis of multi-point and multi-time correlations. *J. Chem. Phys.* **138**, 12A506 (2013).

40. Wang, C. Y. & Ediger, M. D. Lifetime of spatially heterogeneous dynamic domains in polystyrene melts. *J. Chem. Phys.* **112**, 6933–6937 (2000).

41. Léonard, S. & Berthier, L. Lifetime of dynamic heterogeneity in strong and fragile kinetically constrained spin models. *J. Phys. Condens. Matter* S3571–S3577 (2005). doi:10.1088/0953-8984/17/45/050

42. Alegría, A., Colmenero, J., Mari, P. & Campbell, I. Dielectric investigation of the temperature dependence of the nonexponentiality of the dynamics of polymer melts. *Phys. Rev. E* **59**, 6888–6895 (1999).

43. Cicerone, M. T., Blackburn, F. R. & Ediger, M. D. How do molecules move near Tg? Molecular rotation of six probes in o-terphenyl across 14 decades in time. *J. Chem. Phys.* **102**, 471 (1995).

44. Schiener, B., Bohmer, R., Loidl, A. & Chamberlin, R. V. Nonresonant Spectral Hole Burning in the Slow Dielectric Response of Supercooled Liquids. *Science (80-.).* **274**, 752–754 (1996).

45. Swallen, S. F., Bonvallet, P., McMahon, R. J. & Ediger, M. Self-diffusion of tris-naphthylbenzene near the glass transition temperature. *Phys. Rev. Lett.* **90**, 015901 (2003).

46. Böhmer, R., Hinze, G., Diezemann, G., Geil, B. & Sillescu, H. Dynamic heterogeneity in supercooled ortho-terphenyl studied by multidimensional deuteron NMR. *Europhys. Lett.* **36**, 55–60 (1996).

47. Kariyo, S. *et al.* From Simple Liquid to Polymer Melt. Glassy and Polymer Dynamics Studied by Fast Field Cycling NMR Relaxometry: Low and High Molecular Weight Limit. *Macromolecules* **000**, 5313–5321 (2008).

48. Schiener, B., Chamberlin, R. V, Diezemann, G. & Böhmer, R. Nonresonant dielectric hole burning spectroscopy of supercooled liquids. *J Chem Phys* **107**, 7746–7761 (1997).

49. Cicerone, M. T. & Ediger, M. D. Relaxation of spatially heterogeneous dynamic domains

in supercooled ortho-terphenyl. *J. Chem. Phys.* **103**, 5684–5692 (1995).

50. Schmidt-Rohr, K. & Spiess, H. W. Chain Diffusion between Crystalline and Amorphous Regions in Polyethylene Detected by 2D Exchange 13C NMR. *Macromolecules* **24**, 5288–5293 (1991).

51. Moerner, W. E. & Kador, L. Optical detection and spectroscopy of single molecules in a solid. *Phys. Rev. Lett.* **62**, 2535–2538 (1989).

52. Orrit, M. & Bernard, J. Single pentacene molecules detected by fluorescence excitation in a p-terphenyl crystal. *Phys. Rev. Lett.* **65**, 2716–2719 (1990).

53. Betzig, E. Single Molecules Observed By Near-Field Scanning Optical Microscopy (Vol 262, Pg 1422, 1993). *Science (80-.).* **263**, 159 (1994).

54. Moerner, W. E., Shechtman, Y. & Wang, Q. Single-molecule spectroscopy and imaging over the decades. *Faraday Discuss.* **184**, 9–36 (2015).

55. Schob, A., Cichos, F., Schuster, J. & Von Borczyskowski, C. Reorientation and translation of individual dye molecules in a polymer matrix. *Eur. Polym. J.* **40**, 1019–1026 (2004).

56. Braeken, E. *et al.* Single molecule probing of the local segmental relaxation dynamics in polymer above the glass transition temperature. *J. Am. Chem. Soc.* **131**, 12201–12210 (2009).

57. Adhikari, S., Selmke, M. & Cichos, F. Temperature dependent single molecule rotational dynamics in PMA. *Phys. Chem. Chem. Phys.* **13**, 1849–1856 (2011).

58. Flier, B. M. I. *et al.* Single molecule fluorescence microscopy investigations on heterogeneity of translational diffusion in thin polymer films. *Phys. Chem. Chem. Phys.* **13**, 1770–1775 (2011).

59. Uji-I, H. *et al.* Visualizing spatial and temporal heterogeneity of single molecule rotational diffusion in a glassy polymer by defocused wide-field imaging. *Polymer (Guildf).* **47**, 2511–2518 (2006).

60. Mackowiak, S. A., Herman, T. K. & Kaufman, L. J. Spatial and temporal heterogeneity in supercooled glycerol: Evidence from wide field single molecule imaging. *J. Chem. Phys.* **131**, 244513 (2009).

61. Adhikari, A. N., Capurso, N. A. & Bingemann, D. Heterogeneous dynamics and dynamic heterogeneities at the glass transition probed with single molecule spectroscopy. *J. Chem. Phys.* **127**, 114508 (2007).

62. Valĺe, R. A. L. *et al.* Analysis of the exponential character of single molecule rotational correlation functions for large and small fluorescence collection angles. *J. Chem. Phys.* **128**, (2008).

63. Bingemann, D., Allen, R. M. & Olesen, S. W. Single molecules reveal the dynamics of heterogeneities in a polymer at the glass transition. *J. Chem. Phys.* **134**, (2011).

64. Verma, S. D., Vanden Bout, D. a. & Berg, M. a. When is a single molecule heterogeneous? A multidimensional answer and its application to dynamics near the glass

transition. *J. Chem. Phys.* **143**, 024110 (2015).

65. Wei, C. Y. J., Lu, C. Y., Kim, Y. H. & Vanden Bout, D. A. Determining if a system is heterogeneous: The analysis of single molecule rotational correlation functions and their limitations. *J. Fluoresc.* **17**, 797–804 (2007).

66. Deschenes, L. A. & Vanden Bout, D. A. Heterogeneous dynamics and domains in supercooled o-terphenyl: A single molecule study. *J. Phys. Chem. B* **106**, 11438–11445 (2002).

67. Cicerone, M. T. & Ediger, M. D. Enhanced translation of probe molecules in supercooled o-terphenyl: Signature of spatially heterogeneous dynamics? *J. Chem. Phys.* **104**, 7210–7218 (1996).

68. Zangi, R., Mackowiak, S. A. & Kaufman, L. J. Probe particles alter dynamic heterogeneities in simple supercooled systems. *J. Chem. Phys.* **126**, 104501 (2007).

69. Paeng, K. & Kaufman, L. J. Which probes can report intrinsic dynamic heterogeneity of a glass forming liquid? *J. Chem. Phys.* **149**, 1–8 (2018).

70. Paeng, K., Park, H., Hoang, D. T. & Kaufman, L. J. Ideal probe single-molecule experiments reveal the intrinsic dynamic heterogeneity of a supercooled liquid. *Proc. Natl. Acad. Sci.* **112**, 4952–4957 (2015).

71. Zhang, H. *et al.* Examining dynamics in a polymer matrix by single molecule fluorescence probes of different sizes. *Soft Matter* **12**, 7299–7306 (2016).

72. Mackowiak, S. A., Noble, J. M. & Kaufman, L. J. Manifestations of probe presence on probe dynamics in supercooled liquids. *J. Chem. Phys.* **135**, 214503 (2011).

73. Zhang, H. *et al.* Retarded local dynamics of single fluorescent probes in polymeric glass due to interaction strengthening. *Polym. (United Kingdom)* **116**, 452–457 (2017).

74. Lu, C.-Y. & Vanden Bout, D. a. Effect of finite trajectory length on the correlation function analysis of single molecule data. *J. Chem. Phys.* **125**, 124701 (2006).

75. Stokely, K., Manz, A. S. & Kaufman, L. J. Revealing and resolving degeneracies in stretching exponents in temporally heterogeneous environments. *J. Chem. Phys.* **142**, 114504 (2015).

76. Mackowiak, S. A. & Kaufman, L. J. When the heterogeneous appears homogeneous: Discrepant measures of heterogeneity in single-molecule observables. *J. Phys. Chem. Lett.* **2**, 438–442 (2011).

77. Paeng, K., Park, H., Hoang, D. T. & Kaufman, L. J. Ideal probe single-molecule experiments reveal the intrinsic dynamic heterogeneity of a supercooled liquid. *Proc. Natl. Acad. Sci.* **112**, 4952–4957 (2015).

78. Paeng, K. & Kaufman, L. J. Single Molecule Experiments Reveal the Dynamic Heterogeneity and Exchange Time Scales of Polystyrene near the Glass Transition. *Macromolecules* **49**, 2876–2885 (2016).

79. Priestley, R. D., Ellison, C. J. & Broadbelt, L. J. Structural Relaxation of Polymer Glasses

at Surfaces , Interfaces , and In Between. *Science (80-.).* **309**, 456–460 (2005).

80. González-campos, J. B. *et al.* Relaxations in Chitin: Evidence for a Glass Transition. *J. Polym. Sci. Part B Polym. Phys.* **47**, 932 (2009).

81. Roth, C. B. & Baglay, R. R. Fundamentals of polymers and glasses. in *Fundamentals of polymers and glasses* 3–22

82. Hill, A. J. & Tant, M. R. The Structure and Properties of Glassy Polymers. 1–20 (1999). doi:10.1021/bk-1998-0710.ch001

83. Dalle-Ferrier, C. *et al.* Why many polymers are so fragile: A new perspective. *J. Chem. Phys.* **145**, (2016).

84. Alegría, A., Guerrica-Echevarría, E., Goitiandía, L., Telleria, I. & Colmenero, J. α-Relaxation in the Glass Transition Range of Amorphous Polymers. 1. Temperature Behavior across the Glass Transition. *Macromolecules* **28**, 1516–1527 (1995).

85. Shokri, A. A., Zamani, S. E. & Company, N. P. Relationship Between the a- and b-Relaxation Processes in Amorphous Polymers: Insight From Atomistic Molecular Dynamics Simulations of 1,4-Polybutadiene Melts and Blends. **45**, 627–643 (2007).

86. Blanchard, L.-P., Hesse, J. & Malhotra, S. L. Effect of Molecular Weight on Glass Transition by Differential Scanning Calorimetry. *Can. J. Chem.* **52**, 3170–3175 (1974).

87. Fox, T. G. & Flory, P. J. Second-order transition temperatures and related properties of polystyrene. I. Influence of molecular weight. *J. Appl. Phys.* **21**, 581–591 (1950).

88. Santangelo, P. G. & Roland, C. M. Molecular Weight Dependence of Fragility in Polystyrene. *Macromolecules* **31**, 4581–4585 (1998).

89. Yang, Z., Fujii, Y., Lee, F. K., Lam, C. & Tsui, O. K. C. Glass Transition Dynamics and Surface Layer Mobility in Unentangled Polystyrene Films. *Science (80-.).* **328**, 1676–1679 (2010).

90. Ehlich, D. & Sillescu, H. Tracer Diffusion at the Glass Transition. *Macromolecules* **23**, 1600–1610 (1990).

91. Flier, B. M. I. *et al.* Heterogeneous diffusion in thin polymer films as observed by high-temperature single-molecule fluorescence microscopy. *J. Am. Chem. Soc.* **134**, 480–488 (2012).

92. Veniaminov, A. V. & Sillescu, H. Polymer and dye probe diffusion in poly(methyl methacrylate) below the glass transition studied by forced Rayleigh scattering. *Macromolecules* **32**, 1828–1837 (1999).

93. Mizuno, H. & Yamamoto, R. Lifetime of dynamical heterogeneity in a highly supercooled liquid. *Phys. Rev. E - Stat. Nonlinear, Soft Matter Phys.* **82**, 030501(R) (2010).

94. Mackowiak, S. A., Leone, L. M. & Kaufman, L. J. Probe dependence of spatially heterogeneous dynamics in supercooled glycerol as revealed by single molecule microscopy. *Phys. Chem. Chem. Phys.* **13**, 1786–1799 (2011).

95. Qian, J. & Heuer, A. Exchange rates of dynamic heterogeneities in a glass-forming liquid. *Eur. Phys. J. B* **18**, 501–505 (2000).

96. Wang, C. & Ediger, M. D. How Long Do Regions of Different Dynamics Persist in Supercooled o -Terphenyl? *J. Phys. Chem. B* **103**, 4177–4184 (1999).

97. Lačević, N., Starr, F. W., Schroder, T. B. & Glotzer, S. C. Spatially heterogeneous dynamics investigated via a time-dependent four-point density correlation function. *J. Chem. Phys.* **119**, 7372–7387 (2003).

98. Kim, K. & Saito, S. Multiple time scales hidden in heterogeneous dynamics of glass-forming liquids. *Phys. Rev. E - Stat. Nonlinear, Soft Matter Phys.* **79**, 1–4 (2009).

99. Dalle-Ferrier, C. *et al.* The role of chain length in nonergodicity factor and fragility of polymers. *Macromolecules* **43**, 8977–8984 (2010).

100. Ding, Y. *et al.* Influence of molecular weight on fast dynamics and fragility of polymers. *Macromolecules* **37**, 9264–9272 (2004).

101. Casalini, R., Roland, C. M. & Capaccioli, S. Effect of chain length on fragility and thermodynamic scaling of the local segmental dynamics in poly(methylmethacrylate). *J. Chem. Phys.* **126**, (2007).

102. Reinsberg, S. A., Qiu, X. H., Wilhelm, M., Spiess, H. W. & Ediger, M. D. Length scale of dynamic heterogeneity in supercooled glycerol near Tg. *J. Chem. Phys.* **114**, 7299–7302 (2001).

103. Wyart, M. & Cates, M. E. Does a Growing Static Length Scale Control the Glass Transition? *Phys. Rev. Lett.* **119**, 1–5 (2017).

104. Niss, K., Dalle-Ferrier, C., Tarjus, G. & Alba-Simionesco, C. On the correlation between fragility and stretching in glass-forming liquids. *J. Phys. Condens. Matter* **19**, (2007).

105. Kozmidis-Petrović, A. F. The impact of the stretching exponent on fragility of glass-forming liquids. *J. Therm. Anal. Calorim.* **127**, 1975–1981 (2017).

106. Sokolov, A. P., Kunal, K., Robertson, C. G., Pawlus, S. & Hahn, S. F. Role of chemical structure in fragility of polymers: A qualitative picture. *Macromolecules* **41**, 7232–7238 (2008).

107. Torres, J. M., Stafford, C. M. & Vogt, B. D. Elastic modulus of amorphous polymer thin films: Relationship to the glass transition temperature. *ACS Nano* **3**, 2677–2685 (2009).

108. Keddie, J. L., Jones, R. A. L. & Cory, R. A. Size-Dependent Depression of the Glass Transition Temperature in Polymer Films Related content Topical Review. *Europhys. Lett.* **59**, (1994).

109. Christie, D., Zhang, C., Fu, J., Koel, B. & Priestley, R. D. Glass transition temperature of colloidal polystyrene dispersed in various liquids. *J. Polym. Sci. Part B Polym. Phys.* **54**, 1776–1783 (2016).

110. Kremer, F., Tress, M. & Mapesa, E. U. Glassy dynamics and glass transition in nanometric layers and films: A silver lining on the horizon. *J. Non. Cryst. Solids* **407**,

277–283 (2015).

111. Erber, M., Georgi, U., Müller, J., Eichhorn, K. J. & Voit, B. Macromolecular Nanotechnology Polystyrene with different topologies: Study of the glass transition temperature in confined geometry of thin films. *Eur. Polym. J.* **46**, 2240–2246 (2010).

112. Zhang, C., Guo, Y. & Priestley, R. D. Confined glassy properties of polymer nanoparticles. *J. Polym. Sci. Part B Polym. Phys.* **51**, 574–586 (2013).

113. Zhang, C., Guo, Y. L. & Priestley, R. D. Glass Transition Temperature of Polymer Nanoparticles under Soft and Hard Confinement. *Macromolecules* **44**, 4001–4006 (2011).

114. Glynos, E. *et al.* Vitrification of thin polymer films: From linear chain to soft colloid-like behavior. *Macromolecules* **48**, 2305–2312 (2015).

115. Zhang, W., Douglas, J. F. & Starr, F. W. Why we need to look beyond the glass transition temperature to characterize the dynamics of thin supported polymer films. *Proc. Natl. Acad. Sci.* **115**, 5641–5646 (2018).

116. Baljon, A. R. C. *et al.* Simulated glass transition in free-standing thin polystyrene Films. *J. Polym. Sci. Part B Polym. Phys.* **48**, 1160–1167 (2010).

117. Xia, W., Mishra, S. & Keten, S. Substrate vs. free surface: Competing effects on the glass transition of polymer thin films. *Polym. (United Kingdom)* **54**, (2013).

118. Glor, E. C., Angrand, G. V. & Fakhraai, Z. Exploring the broadening and the existence of two glass transitions due to competing interfacial effects in thin, supported polymer films. *J. Chem. Phys.* **146**, (2017).

119. Zhou, Y. & Milner, S. T. Short-Time Dynamics Reveals Tg Suppression in Simulated Polystyrene Thin Films. *Macromolecules* **50**, 5599–5610 (2017).

120. Forrest, J. A., Dalnoki-Veress, K. & R., D. J. Interface and chain confinement effects on the glass transition temperature of thin polymer films. *Phys. Rev. E* **56**, 570–5715 (1997).

121. Geng, K. *et al.* Conflicting Confinement Effects on the Tg, Diffusivity, and Effective Viscosity of Polymer Films: A Case Study with Poly(isobutyl methacrylate) on Silica and Possible Resolution. *Macromolecules* **50**, 609–617 (2017).

122. Tress, M. *et al.* Glassy dynamics and glass transition in nanometric thin layers of polystyrene. *Macromolecules* **43**, 9937–9944 (2010).

123. Keddie, J., Jones, R. & Cory, R. Size-Dependent Depression of the Glass Transition Temperature in Polymer Films . *Europhys. Lett.* **27**, 59–64 (1994).

124. Fukao, K. & Miyamoto, Y. Glass transitions and dynamics in thin polymer films: dielectric relaxation of thin films of polystyrene. *Phys. Rev. E* **61**, 13 (1999).

125. Priestley, R. D., Cangialosi, D. & Napolitano, S. On the equivalence between the thermodynamic and dynamic measurements of the glass transition in confined polymers. *J. Non. Cryst. Solids* **407**, 288–295 (2015).

126. Sharp, J. S., Teichroeb, J. H. & Forrest, J. A. The properties of free polymer surfaces and

their influence on the glass transition temperature of thin polystyrene films. *Eur. Phys. J. E* **15**, 473–487 (2004).

127. Zhang, Y. & Fakhraai, Z. Invariant Fast Diffusion on the Surfaces of Ultrastable and Aged Molecular Glasses. *Phys. Rev. Lett.* **118**, 1–5 (2017).

128. Swallen, S. F. *et al.* Organic glasses with exceptional thermodynamic and kinetic stability. *Science* **315**, 353–356 (2007).

129. Struik, L. C. E. Physical Aging in Plastics and Other Glassy Materials. *Polym. Eng. Sci.* **17**, (1977).

130. Paeng, K., Park, H., Hoang, D. T. & Kaufman, L. J. Ideal probe single-molecule experiments reveal the intrinsic dynamic heterogeneity of a supercooled liquid: SI. *Proc. Natl. Acad. Sci.* **112**, 4952–4957 (2015).

131. Glor, E. C. & Fakhraai, Z. Facilitation of interfacial dynamics in entangled polymer films. *J. Chem. Phys.* **141**, (2014).

132. Zhang, Y. *et al.* Long-range correlated dynamics in ultra-thin molecular glass films. *J. Chem. Phys.* **145**, 114502 (2016).

133. Mangalara, J. H., Marvin, M. D. & Simmons, D. S. Three-Layer Model for the Emergence of Ultrastable Glasses from the Surfaces of Supercooled Liquids. *J. Phys. Chem. B* **120**, (2016).

134. Vallée, R. *et al.* On the role of electromagnetic boundary conditions in single molecule fluorescence lifetime studies of dyes embedded in thin films. *Chem. Phys. Lett.* **348**, 161–167 (2001).

135. Boucher, V. M. *et al.* Tg depression and invariant segmental dynamics in polystyrene thin films. *Soft Matter* **8**, 5119–5122 (2012).

136. Araoz, B., Carattino, A., Täuber, D., von Borczyskowski, C. & Aramendia, P. F. Influence of the Glass Transition on Rotational Dynamics of Dyes in Thin Polymer Films: Single-Molecule and Ensemble Experiments. *J. Phys. Chem. A* (2014). doi:10.1021/jp500272y

137. Fakhraai, Z. & Forrest, J. A. Measuring the surface dynamics of glassy polymers. *Science* **319**, 600–605 (2008).

138. Ediger, M. D. & Forrest, J. A. Dynamics near free surfaces and the glass transition in thin polymer films: A view to the future. *Macromolecules* **47**, 471–478 (2014).

139. Chung, J. Y., Douglas, J. F. & Stafford, C. M. A wrinkling-based method for investigating glassy polymer film relaxation as a function of film thickness and temperature. *J. Chem. Phys.* **147**, (2017).

140. Biroli, G. & Bouchaud, J. P. The Random First-Order Transition Theory of Glasses: A Critical Assessment. *Struct. Glas. Supercooled Liq. Theory, Exp. Appl.* 31–113 (2012). doi:10.1002/9781118202470.ch2

141. Paeng, K., Swallen, S. F. & Ediger, M. D. Direct measurement of molecular motion in freestanding polystyrene thin films. *J. Am. Chem. Soc.* **133**, 8444–8447 (2011).

142. Schob, A., Cichos, F., Schuster, J. & von Borczyskowski, C. Reorientation and translation of individual dye molecules in a polymer matrix. *Eur. Polym. J.* **40**, 1019–1026 (2004).

143. Richert, R. Dynamics of Nanoconfined Supercooled Liquids. *Annu. Rev. Phys. Chem.* **62**, 65–84 (2011).

144. Flier, B. M. I. *et al.* Heterogeneous Diffusion in Thin Polymer Films As Observed by High-Temperature Single-Molecule Fluorescence Microscopy. *J. Am. Chem. Soc.* **134**, 480–488 (2012).

145. Mouhamad, Y., Mokarian-Tabari, P., Clarke, N., Jones, R. A. L. & Geoghegan, M. Dynamics of polymer film formation during spin coating. *J. Appl. Phys.* **116**, (2014).

146. Peurifoy, S. R. *et al.* Three-Dimensional Graphene Nanostructures. *J. Am. Chem. Soc.* **140**, 9341–9345 (2018).

147. Hoang, D., Paeng, K., Park, H., Leone, L. & Kaufman, L. J. Extraction of Rotational Correlation Times from Non-Ideal Single-Molecule Trajectories. *Anal. Chem.* **86**, 9322−9329 (2014).

148. Crocker, J. & Grier, D. Methods of Digital Video Microscopy for Colloidal Studies. *J. Colloid Interface Sci.* **179**, 298–310 (1996).

149. Hinze, G., Diezemann, G. & Basché, T. Rotational correlation functions of single molecules. *Phys. Rev. Lett.* **93**, 1–4 (2004).

150. Manz, A. S., Paeng, K. & Kaufman, L. J. Single molecule studies reveal temperature independence of lifetime of dynamic heterogeneity in polystyrene. *J. Chem. Phys.* **148**, 204508 (2018).

151. Ngai, K. L. Dynamic and thermodynamic properties of glass-forming substances. *J. Non. Cryst. Solids* **275**, 7–51 (2000).

152. Donati, C., Glotzer, S. C. & Poole, P. H. Growing spatial correlations of particle displacements in a simulated liquid on cooling toward the glass transition. *Phys. Rev. Lett.* **82**, 5064–5067 (1999).

153. Rijal, B., Delbreilh, L. & Saiter, A. Dynamic Heterogeneity and Cooperative Length Scale at Dynamic Glass Transition in Glass Forming Liquids. *Macromolecules* **48**, 8219–8231 (2015).

154. Böhmer, R., Diezemann, G., Hinze, G. & Sillescu, H. A nuclear magnetic resonance study of higher-order correlation functions in supercooled ortho-terphenyl. *J. Chem. Phys.* **108**, 890 (1998).

155. Kim, K. & Saito, S. Multi-time density correlation functions in glass-forming liquids: Probing dynamical heterogeneity and its lifetime. *J. Chem. Phys.* **133**, 044511 (2010).

156. Kim, K. & Saito, S. Hidden slow time scale of correlated motions in supercooled liquids: Multi-time correlation function approach. *J. Non. Cryst. Solids* **357**, 371–375 (2011).

157. Heuer, A. & Okun, K. Heterogeneous and homogeneous dynamics in a simulated polymer melt: Analysis of multi-time correlation functions. *J. Chem. Phys.* **106**, 6176–6186 (1997).

158. Pschorn, U. *et al.* Local and Cooperative Motions At the Glass-Transition of Polystyrene - Information From One-Dimensional and 2-Dimensional Nmr As Compared With Other Techniques. *Macromolecules* **24**, 398–402 (1991).

159. Mizuno, H. & Yamamoto, R. Lifetime of dynamical heterogeneity in a highly supercooled liquid. *Phys. Rev. E* **82**, 30501 (2010).

160. Mizuno, H. & Yamamoto, R. Dynamical heterogeneity in a highly supercooled liquid: Consistent calculations of correlation length, intensity, and lifetime. *Phys. Rev. E - Stat. Nonlinear, Soft Matter Phys.* **84**, 1–11 (2011).

161. Deres, A. *et al.* The Origin of Heterogeneity of Polymer Dynamics near the Glass Temperature As Probed by Defocused Imaging. *Macromolecules* **44**, 9703–9709 (2011).

162. Uji-i, H. *et al.* Visualizing spatial and temporal heterogeneity of single molecule rotational diffusion in a glassy polymer by defocused wide-field imaging. *Polymer (Guildf).* **47**, 2511–2518 (2006).

163. Adhikari, S., Selmke, M. & Cichos, F. Temperature dependent single molecule rotational dynamics in PMA. *Phys. Chem. Chem. Phys.* **13**, 1849–1856 (2011).

164. Wei, C.-Y. J. & Vanden Bout, D. A. Nonexponential Relaxation of Poly(cyclohexyl acrylate): Comparison of Single-Molecule and Ensemble Fluorescence Studies. *J. Phys. Chem. B* **113**, 2253–2261 (2009).

165. Flier, B. M. I. *et al.* Single molecule fluorescence microscopy investigations on heterogeneity of translational diffusion in thin polymer films. *Phys. Chem. Chem. Phys.* **13**, 1770–1775 (2011).

166. Hinze, G., Basché, T. & Vallée, R. A. L. Single molecule probing of dynamics in supercooled polymers. *Phys. Chem. Chem. Phys.* **13**, 1813 (2011).

167. Paeng, K. & Kaufman, L. J. Single Molecule Experiments Reveal the Dynamic Heterogeneity and Exchange Time Scales of Polystyrene near the Glass Transition. *Macromolecules* **49**, 2876–2885 (2016).

168. Roland, C. M. & Casalini, R. Temperature dependence of local segmental motion in polystyrene and its variation with molecular weight. *J. Chem. Phys.* **119**, 1838–1842 (2003).

169. Robertson, C. G., Santangelo, P. G. & Roland, C. M. Comparison of glass formation kinetics and segmental relaxation in polymers. *J. Non. Cryst. Solids* **275**, 153–159 (2000).

170. Thurau, C. T. & Ediger, M. D. Influence of spatially heterogeneous dynamics on physical aging of polystyrene. *J. Chem. Phys.* **116**, 9089–9099 (2002).

171. Stokely, K., Manz, A. S. & Kaufman, L. J. Revealing and resolving degeneracies in stretching exponents in temporally heterogeneous environments. *J. Chem. Phys.* **142**, 114504 (2015).

172. Léonard, S. & Berthier, L. Lifetime of dynamic heterogeneity in strong and fragile kinetically constrained spin models. *J. Phys. Condens. Matter* **17**, S3571 (2005).

173. Alegria, A., Colmenero, J. ., Mari, P. . O. . & Campbell, I. . A. Dielectric investigation of the temperature dependence of the nonexponentiality of the dynamics of polymer melts. *Phys. Rev. E* **59**, 6888–6895 (1999).

174. Fox, T. G. & Flory, P. J. Viscosity—Molecular Weight and Viscosity—Temperature Relationships for Polystyrene and Polyisobutylene [1,2]. *J. Am. Chem. Soc.* **70**, 2384–2395 (1948).

175. Fox, T. G. & Flory, P. J. Further Studies on the Melt Viscosity of Polyisobutylene. *J. Phys. Chem.* **55**, 221–234 (1951).

176. Fox, T. G. & Flory, P. J. The glass temperature and related properties of polystyrene. Influence of molecular weight. *J. Polym. Sci.* **14**, 315–319 (1954).

177. Ediger, M. D. Spatially heterogeneous dynamics in supercooled liquids. *Annu. Rev. Phys. Chem.* **51**, 99–128 (2000).

178. Manz, A. S., Paeng, K. & Kaufman, L. J. Single molecule studies reveal temperature independence of lifetime of dynamic heterogeneity in polystyrene. *J. Chem. Phys.* **148**, 204508 (2018).

179. Novikov, V. N. & Rössler, E. A. Correlation between glass transition temperature and molecular mass in non-polymeric and polymer glass formers. *Polymer (Guildf).* **54**, 6987–6991 (2013).

180. Hintermeyer, J., Herrmann, A., Kahlau, R., Goiceanu, C. & Rossler, E. A. Molecular Weight Dependence of Glassy Dynamics in Linear Polymers Revisited. *Macromolecules* **41**, 9335–9344 (2008).

181. Inoue, T., Cicerone, M. T. & Ediger, M. D. Molecular Motions and Viscoelasticity of Amorphous Polymers near Tg. *Macromolecules* **28**, 3425–3433 (1995).

182. Plazek, D. & Ngai, K. Correlation of polymer segmental chain dynamics with temperature-dependent time-scale shifts. *Macromolecules* **24**, 1222-1224 ST-Correlation of polymer segmental (1991).

183. Oba, T. & Vacha, M. Relaxation in thin polymer films mapped across the film thickness by astigmatic single-molecule imaging. *ACS Macro Lett.* **1**, 784–788 (2012).

184. Perez-de-Eulate, N. G., Di Lisio, V. & Cangialosi, D. Glass Transition and Molecular Dynamics in Polystyrene Nanospheres by Fast Scanning Calorimetry. *ACS Macro Lett.* 859–863 (2017). doi:10.1021/acsmacrolett.7b00484

185. Forrest, J. & Mattsson, J. Reductions of the glass transition temperature in thin polymer films: Probing the length scale of cooperative dynamics. *Phys. Rev. E* **61**, R53–R56 (2000).

186. Glor, E. C. & Fakhraai, Z. Facilitation of interfacial dynamics in entangled polymer films. *J. Chem. Phys.* **141**, (2014).

187. Paeng, K., Richert, R. & Ediger, M. D. Molecular mobility in supported thin films of polystyrene, poly(methyl methacrylate), and poly(2-vinyl pyridine) probed by dye

reorientation. *Soft Matter* **8**, 819–826 (2012).

188. Daley, C. R., Fakhraai, Z., Ediger, M. D. & Forrest, J. A. Comparing surface and bulk flow of a molecular glass former. *Soft Matter* **8**, 2206–2212 (2012).

189. Brian, C. W., Zhu, L. & Yu, L. Effect of bulk aging on surface diffusion of glasses. *J. Chem. Phys.* **140**, (2014).

190. Xu, J. *et al.* Probing the Utmost Distance of Polymer Dynamics Suppression by a Substrate by Investigating the Diffusion of Fluorinated Tracer-Labeled Polymer Chains. *Macromolecules* **50**, 5905–5913 (2017).

191. Leone, L. M. Single Molecule Studies of Dynamic Heterogeneities in Supercooled Liquids. (2015).

192. Qiang, Z., Shebek, K. M., Irie, M. & Wang, M. A Polymerizable Photoswitchable Fluorophore for Super-Resolution Imaging of Polymer Self-Assembly and Dynamics. *ACS Macro Lett.* **7**, 1432–1437 (2018).

193. Chang, K. The Nature of Glass Remains Anything but Clear. *New York Times* (2008).

194. Cicerone, M. T., Wagner, P. A. & Ediger, M. D. Translational Diffusion on Heterogeneous Lattices: A Model for Dynamics in Glass Forming Materials. *J. Phys. Chem. B* **101**, 8727–8734 (2002).

195. Richert, R. Spectral diffusion in liquids with fluctuating solvent responses: Dynamical heterogeneity and rate exchange. *J. Chem. Phys.* **115**, 1429–1434 (2001).

196. Bingemann, D. Analysis of 'blinking' or 'hopping' single molecule signals with a limited number of transitions. *Chem. Phys. Lett.* **433**, 234–238 (2006).

197. Lu, C.-Y. & Vanden Bout, D. A. Effect of finite trajectory length on the correlation function analysis of single molecule data. *J. Chem. Phys.* **125**, 124701 (2006).

198. Arnaoutakis, G. & Näther, D. Technical Note Quenching of Fluorescence With Temperature. 1–3 (2016).

199. Park, H., Kwon, Y. & Kaufman, L. J. Complex Photophysical Behaviors Affect Single Conjugated Molecule Optical Anisotropy Measurements. *J. Phys. Chem. C* **123**, 1960–1965 (2019).

200. Park, H., Hoang, D. T., Paeng, K., Yang, J. & Kaufman, L. J. Conformation-Dependent Photostability among and within Single Conjugated Polymers. *Nano Lett.* **15**, 7604–7609 (2015).

Appendix A. Simulated Rotational Diffusion

A.1 Evaluating Degeneracies in Rotational Diffusion Simulations

This appendix is adapted from Stokely et al.[75] As the focus of this thesis is on experimental single molecule approaches aimed at elucidating the underlying heterogeneous dynamics of supercooled liquids, simulation studies were mainly used to support experimental studies. In particular, simulated trajectories of rotations can be used to investigate how the time scale of dynamic exchange relative to underlying relaxation time scales in the system affects a probe's ability to report the distribution relaxation of time scales present, and can give important insight into experimental findings.

A.1.2 Motivation and Methods of Rotational Diffusion Simulations

In this appendix, we aim to understand the microscopic scenarios that are consistent with the measurement of a given stretched exponential decay of a single molecule probe experiencing different dynamic environments due to temporal heterogeneity. Distributions of relaxation time scales and exchange times are varied, as is trajectory length. These scenarios are investigated by simulating the orientation of a single molecule probe undergoing Brownian motion through a succession of local environments and calculating rotational correlation functions analogous to those measured in experiments. These simulations are partially described in Chapter 2; additionally, while this study also focuses on simulations dominated by rank two linear dichroisms, it goes beyond homogeneous rotational diffusion and expands to heterogeneous cases.

In particular, it is assumed that the system comprises a broad distribution of local environments. As such, the median relaxation time, τ_r, is always chosen from a log-normal distribution with median 100 steps. The full-width-at-half-maximum (FWHM) of the $\log(\tau_r)$

distribution is varied between 0.2 and 2.2. Because dynamic exchange may be a sudden process, temporal heterogeneity is initially modeled via abrupt random exchange: after a given exchange time, τ_x, the molecule is assumed to switch local environments, trading the current value of τ_r for a new value from the same distribution. An in-depth discussion of correlations between exchange times and relaxation time scales can be found in Reference 75. For the results presented in this appendix, exchange times, τ_x, are held constant throughout the simulation. Previous studies modeled similar environmental exchanges and their connection to reports of dynamic heterogeneity.[57,194,195] The herein described approach in particular assesses the importance of trajectory length in probe reports of dynamic heterogeneity. In all cases, ACFs were computed and fit until they decayed to a value of 0.02, with the resulting fit parameters averaged over simulations.

A.1.3 Modeling Degeneracies in Rotational Diffusion Simulations

To examine the manner in which the full information available from single molecule (SM) studies may be able to break degeneracies present for finite trajectories, we examine in detail systems with FWHM of $\log(\tau_r) = 1.0$ with a single exchange time – $\log(\tau_x) = 2.0$, 3.0, or 4.0 – for trajectory lengths ranging from 10 to 1000 times the median relaxation time in the system. This covers the range of trajectory lengths that have been reported in SM rotational measurements in supercooled liquids and polymer melts to date.[31] For each trajectory, the ACF is computed and fit with a stretched exponential, with the resulting distributions of parameters β and τ_{fit} then fit to normal distributions. The resulting median of the β distribution and FWHM values of the fits to the β and τ_{fit} distributions are shown in Figure 30 as a function of trajectory length.

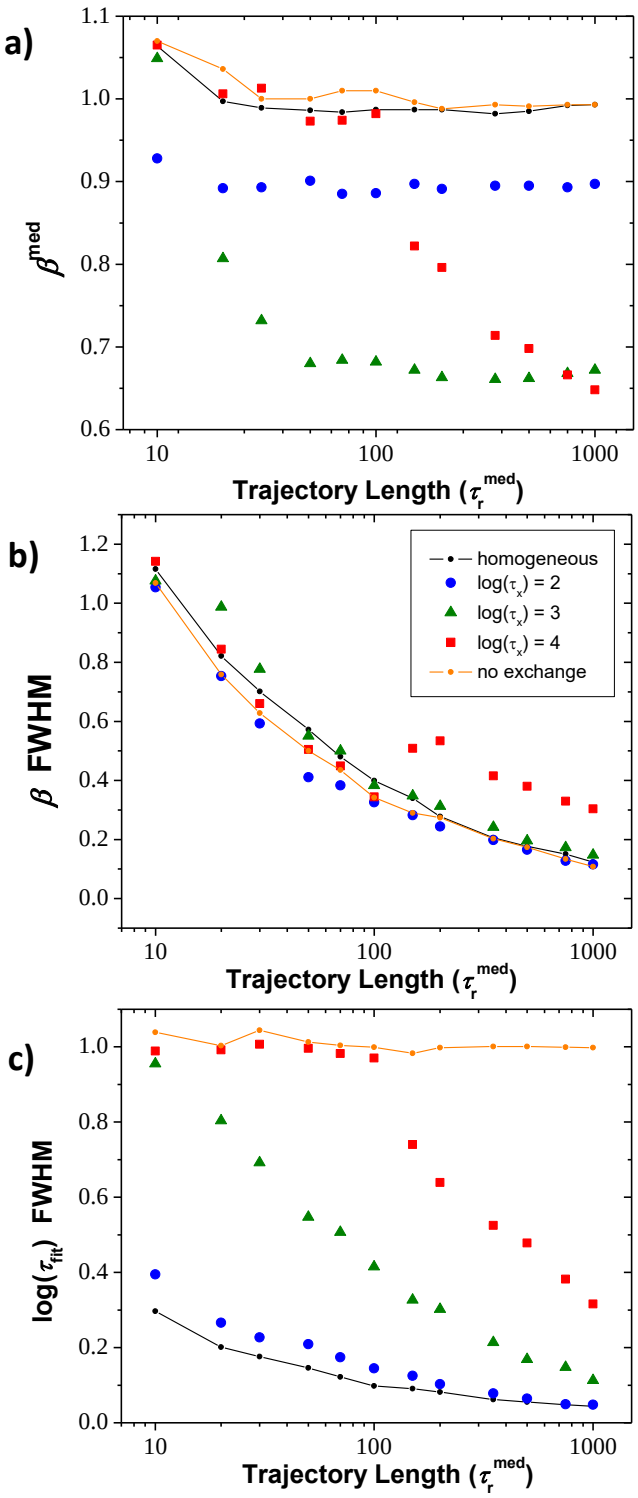

Figure 30. Various KWW parameters as a function of trajectory length in units of τ_r^{med} = 1000 steps. The FWHM of the log(τ_r) distribution is 1.0 and log(τx) =2.0 (blue circles), 3.0 (green triangles), or 4.0 (red squares). The orange line represents a system with no exchange, while the black line represents a homogeneous system (FWHM of the (τr) distribution is 0.0). (a) Median β, (b) FWHM of normal fit to β values, and (c) FWHM of normal fit to log(τfit) distribution. Data are obtained from 500 simulations for each data point.

To ascertain how effects from statistics and those from limited number of exchanges affect the data, two additional cases are considered and included on these plots: a heterogeneous system with FWHM of $\log(\tau_r) = 1.0$ and no exchange, and a homogeneous system, both with $\tau_r^{(med)} = 100$ steps. In each panel, the black line represents the homogeneous system, where any deviation from $\beta = 1$ and delta function distributions for β and τ_{fit} are due solely to poor statistics. The orange line represents the heterogeneous system without exchange, where any deviation from $\beta = 1$, delta function distribution for β, and known relaxation distribution width of 1.0 is also due to statistics. Figure 30a shows the dependence of β^{med} on trajectory length. Both the homogeneous system (black) and heterogeneous system without exchange (orange) show very limited effects even at the shortest trajectory length studied, with $\beta^{med} \sim 1$ for all trajectory lengths, demonstrating that this quantity is unaffected by statistical fluctuations associated with short trajectories. Thus, in systems with exchange and short trajectory lengths, effects due to the limited number of exchanges are expected to dominate median β. When trajectory length is shorter than the exchange time, only one environment has been sampled and $\beta^{med} \sim 1$. For many exchanges, β^{med} is independent of trajectory length, as seen for $\log(\tau_x) = 2.0$: here, 10 exchanges have occurred even at the shortest trajectory. For $\log(\tau_x) = 3.0$, β^{med} decreases from ~ 1 to a plateau after approximately 15 exchanges, showing that relatively few exchanges are necessary to accurately sample the distribution of relaxation times on the SM level. At $\log(\tau_x) = 4.0$ the reported β^{med} continues to decrease with trajectory length for the longest trajectories studied, as only 10 exchanges have taken place by this point. The values of β^{med} for the situations depicted in Figure 30a also highlight degeneracies in β^{med} values that may be seen in experimentally realistic trajectory length experiments. For a trajectory length of 100 τ_r^{med}, the long exchange case ($\tau_x = 4.0$) appears indistinguishable from both the homogeneous case and the spatially heterogeneous case. At the slightly longer, still

experimentally reasonable trajectory length of 125 τ_r, the measured β^{med} is very similar for the systems with the fastest (τ_x = 2.0) and slowest (τ_x = 4.0) exchange times. Figure 30a shows that this degeneracy can be resolved by assessing β^{med} as a function of trajectory length. This is a viable experimental approach, as longer trajectories may be achievable through lowering laser power and extending probe life to photobleaching if signal:noise is acceptable, while shorter trajectories can be obtained by truncating the longest trajectories achieved in experiment. For the case described above, where systems with fast (τ_x = 2.0) and slow (τ_x = 4.0) exchange with the same underlying distribution ($\log(\tau_{r,}^{med})$ = 2.0; FWHM ($\log(\tau_r)$ = 1.0) yield the same β^{med} ~ 0.89 at 125 τ_r^{med} , altering trajectory length by a factor of less than two in either direction would clarify the relative median relaxation and exchange times. For the case with $\tau_x > \tau_r$, a clear decay in β^{med} will be evident until the trajectory length reaches ~ $15\tau_x$ as exchanges accumulate, while no trajectory length dependence of β^{med} will be evident in the case of fast exchange. We also note that it is only in the case of exchange similar to or faster than median relaxation time, that β_{med} will not vary over the full range of experimentally obtainable trajectory lengths. Indeed, a finding of $\beta^{med} < 1$ and independent of trajectory length is a clear indication of exchange similar to or faster than $\tau_{r,}^{med}$ with the value of β^{med} then reflecting the width of the underlying τ_r distribution. In addition to evaluating β^{med} as a function of trajectory length to distinguish between possible scenarios that lead to the same β^{med} at a given trajectory length, evaluating the full distributions of obtained β and τ_{fit} values may also resolve β^{med} degeneracies. Figure 30b shows the FWHM of the β distributions for the same systems shown in Figure 30a. It is immediately apparent that scrutinizing this quantity is not particularly helpful. As can be appreciated from trends seen in all systems, including those with no heterogeneity or no exchange, statistical effects dominate this measure,

and all systems show a very similar decrease of FWHM with increasing trajectory length. On top of this effect, the effect of limited exchange is apparent for the system with $\log(\tau_x) = 4.0$, where a sudden increase in FWHM occurs after one exchange, as each single molecule has sampled the distribution of relaxation time scales differently, yielding ACFs that are variously well fit by the stretched exponential form and increasing the distribution relative to that expected statistically. This result suggests that a set of trajectories of given trajectory length with FWHM of the β distribution larger than expected due to statistical effects implies the presence of τ_x longer than τ_r and somewhat shorter than (between 1 and 1/15) the trajectory length. Unlike the β distributions, the distributions of measured relaxation time scales, τ_{fit}, provide additional information that may help distinguish between systems with identical β med values (and FWHM of β distributions). Distributions of such time scales have commonly been used to assess degree of heterogeneity in single molecule rotational experiments in supercooled liquids.[196,197] Here, we show this is an important quantity to consider in assessing the underlying relaxation time distribution, but it should not be considered in isolation. Figure 30c shows that in a system with heterogeneity but no exchange, the measured FWHM is consistent with the relaxation breadth in the system, while for a homogeneous system, where a delta function distribution is expected, poor statistics lead to a $\log(\tau_{fit})$ distribution with FWHM as large as 0.3, which decreases with increasing trajectory length. This effect is mirrored in the heterogeneous system with fast exchange, where a delta function in relaxation times - representing an average of those felt by each single molecule - is also expected. For systems with longer exchange, where systems with zero to many exchanges are represented in the trajectory lengths assessed, the spread in τ_{fit} values is large, and expected to transition from the case of no exchange (orange) to the case of a single relaxation time (black), another manifestation of motional narrowing. As this limit is approached at long trajectory lengths, the measured τ_{fit}

distribution is again dominated by statistics. As with the FWHM of the β distribution, given known trajectory length, a wider distribution of τ_{fit} than expected from statistics points to heterogeneity and, if it changes with trajectory length, can be used in determining exchange times.

Taking the information from all panels of Figure 30 together, it is apparent that either considering β^{med} as a function of trajectory length or simultaneously considering β_{med} and the FWHM of the τ_{fit} distribution at a given trajectory length can resolve degeneracies for systems with identical β^{med} at a given trajectory length. For the example described above, a system with $\log(\tau_r^{med}) = 2.0$, FWHM of $\log(\tau_r) = 1.0$, and $\tau_x = 2.0$ or 4.0, each system has $\beta^{med} \sim 0.89$ at the experimentally reasonable trajectory length of 125 τ_r. However, β^{med} is constant as a function of trajectory length for the fast exchange case and rapidly changing with trajectory length for the slow exchange case. Additionally, these systems yield radically different widths of the measured τ_{fit} distributions, with only the system with slow exchange having a τ_{fit} FWHM significantly greater than that which would be expected from statistical fluctuations associated with short trajectories.

Hence, it is necessary to use the full information available from typical single molecule experiments as this allows discrimination between various scenarios that yield identical stretching exponents. Investigating either how median stretching exponent changes with trajectory length or the value of the median stretching exponent and the breadth of the relaxation time distribution at a particular trajectory length allow resolution of such degeneracies and identification of the relative timescales of relaxation and exchange.

A.2 Detailed Instructions on Running Rotational Linear Dichroism Simulations

The following code is based on references 75 and 76, and the instructions are expanded from communications with Dr. Kevin Stokely. All instructions and simulations are written for a Linux interface.

A.2.1 Rotational Diffusion

As a first step in running simulations of temporally heterogeneous rotational diffusion, trajectories listing the *x*,*y*,z positions of a point on the surface of a unit sphere as a function of time are computed. The code for running this simulation is contained in the file `rotation_.c` and can be compiled by running

```
gcc rotation_.c -lm -o rotate
```

The parameters of the simulation (e.g. number of runs, FWHM of the exchange time) are set by calling the program with flags. For example, running

flag	default	description
-r	1	number of run
-s	0	index of first run
-h	0	prints header at top of output file
-p	0	outputs separate file of τ values
-t	10000	trajectory length
-tm	2.0	median log τ_r
-tf	1.0	fwhm log(τ_r)
-xm	2.0	median log(τ_x)
-xf	0.0	fwhm log(τ_x)

Table 8. Flags for setting parameters for running heterogeneous rotational diffusion.

```
rotate -r 500 -t 100000 -tf 2.0 -xm 3.0
```

will create 500 runs, each 10^5 steps long, with a FWHM of the $\log(\tau_r)$ distribution of 2.0 and a median exchange time given by $\log(\tau_x)$ of 3.0. The exact description of the flags are given in Table 8. All τ values are in terms of the rank-2 rotational correlation functions, i.e. setting $\log(\tau_r)$ to 2.0 will guarantee that the exponential rank-2 RCF decays to 1/e after 100 steps.

A.2.2 Linear Dichroism

The resulting trajectories may then be turned into a (noisy) linear dichroism signal. This is done by calculating the parallel and orthogonal intensities of the trajectories from the x-, y-, and z components of the dipole orientation. To perform this, the file linear `dichroism_.c` must first be compiled with

```
gcc linear dichroism_.c -lm -o dichroism
```

The resulting executable file (named `dichroism`) is then looped to create a specific number of linear dichroisms (LDs) with the following code:

```
#!/bin/bash

# max number
max_n=499
fileName="rot"

for n in `seq 0 $max_n`; do      ./dichroism "$fileName"."$n".dat
; done
```

The above code would compute the LD for runs 0-499 (i.e. the previously set 500 molecules), beginning with the file rot.0.dat.LD, containing the computed dichroism signal. The details of this procedure are given in comments in the source file, and parameters such as noise intensity, etc. may be changed by editing the corresponding variables in the source code.

A.2.3 Correlation Functions

The files `frame_.c`, `frame_.h`, `frame_corr_.h`, and `frame_rcor_.h` contain code for calculating autocorrelation functions from either of the above trajectory formats.

To calculate the ACF of a single variable (as output from the Linear Dichroism program above), one needs to make sure the file `frame_.h` has the value of FORMAT as DAT, and the value of ANALYSIS has CORR.

The program is compiled with

```
c99 frame_.c -lm -w -o frame,
```

making sure all `frame_.h`, `frame_corr_.h`, and `frame_rcor_.h` files are also in the present directory. To then loop and run correlation functions on all the LD signals previously calculated, the following code is run:

```
#!/bin/bash

# max number
max_n=499
fileName="rot"

for n in `seq 0 $max_n`; do
    ./frame -f "$fileName"."$n".dat.LD -tc 2 -nc 300 -n 400000 -
chop 30000 -q
mv "$fileName"."$n".dat.LD.corr.avg
"$fileName"."$n".corr.30k.LD.avg

     ./frame -f "$fileName"."$n".dat.LD -tc 2 -nc 300 -n 400000
-chop 90000 -q
mv "$fileName"."$n".dat.LD.corr.avg
"$fileName"."$n".corr.90k.LD.avg

done
```

The above code would run trajectories that are 30 000 and 90 000 trajectories long (so for the previously run files, this would be 300 traj/τ_r and 900 traj/τ_r as we had previously run rotational diffusion with a median log(τ) of 2, or a median τ of 100). The ACFs are calculated at base-2 exponential time points, up to time 2^{Tc}, then linearly in increments of 2^{Tc} out to time $N \cdot 2^{Tc}$, ensuring equal sampling of a signal expected to decay exponentially. These parameters are set with the flags `-tc` and `-nc`, with T_c having to be less than 32. Additionally, the program will compute ACFs using N initial frames (set with the flag `-n`), equally spaced throughout the trajectory. Lastly, the program chops trajectories to a specific length with the flag `-chop`, thus determining the trajectory length. Table 9 gives more information on possible flag meanings.

The output file begins with a number of header lines, each beginning with a # character, specifying the above set parameters used for the analysis. This header can be turned off with the `-h` flag. The additional columns of the output file are time, value, and number of points used.

flag	argument needed?	description
-f	yes	input file
-tc	yes	T_c
-nc	yes	N_c
-n	yes	N, i.e. number of initial frames
-chop	yes	trajectory length to chop at
-h	no	do not print output file head
-q	no	do not print to screen

Table 9. Possible flags used when calculating correlation functions from heterogeneous rotational diffusion simulations.

A.2.4 ACF Fitting

The resulting ACFs are lastly fit to stretched exponentials in Mathematica to give τ_{fit}, τ_c and β, using the following code:

```
Off[NonlinearModelFit::eit]

kfitfunction[indata_, forceamp_, yfitend_] :=



 Block[{fitend, tauguess, fit, amp, tau, beta, t},

  fitend =

   Min[Position[indata[[All, 2]], _?(# < yfitend &)],

    Length[indata]];

  tauguess =

   indata[[Max[1, Min[Position[indata[[All, 2]], _?(# < 1/E

&)]]], 1]];

  If[forceamp == 0,

   fit = NonlinearModelFit[

     indata[[1 ;; fitend]], {amp*Exp[-(t/tau)^beta], 0.3 < amp <

2,

      0 < tau,
```

```
      0.2 < beta < 2}, {{tau, tauguess}, {beta, .9}, {amp, 1}},
t],
   fit = NonlinearModelFit[
      indata[[1 ;; fitend]], {Exp[-(t/tau)^beta], 0 < tau,
       0.2 < beta < 2}, {{tau, tauguess}, {beta, .9}}, t];
   ];
  Return[{fit, fit["BestFitParameters"], fit["RSquared"]}];
  ]
```

Appendix B. Absorption and Fluorescence Data of BODIPY268

The fluorescent probe BODIPY268, utilized in the molecular-weight dependent studies, initially appeared as a good choice to gain insight into fast dynamics of the variously-sized polystyrene hosts due to the probe's relatively small size. Additionally, this probe had already been successfully used in several single molecule rotational studies of the small molecule glass former *o*-terphenyl.[69,77] However, as addressed in Chapter 4, the signal:noise of the probe was far inferior to that of the probe pPDI, and high temperatures appeared to worsen the signal. UV-Vis absorption and photoluminescence measurements were taken of BODIPY268 dissolved in toluene in quartz cuvettes on a Perkin Elmer Lambda 950 (Owen Group, Columbia University). To test the impact of heating on both the absorption and emission of the dye, one sample was heated at ~373 K in an oven for 2 hours prior to mimic imaging conditions. Higher temperatures would surpass the boiling

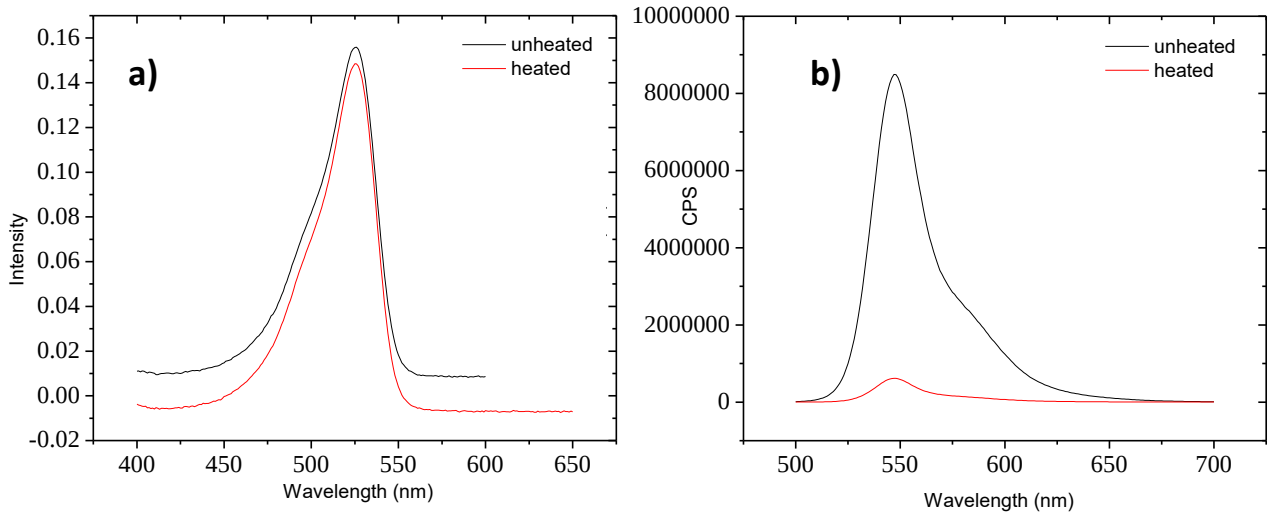

Figure 31. (a) Absorption and (b) emission spectra of BODIPY in toluene.
While the absorption does not change upon heating to ~100°C, the emission clearly decreases, in part explaining the low SNR observed in single molecule measurements with BODIPY. While no in-depth analysis was performed, this decrease could result, in part, result from the probe disintegrating at high temperatures.

point of the solvent. As is evidenced in Figure 31, no change in absorption is observed upon heating, however a drastic decrease in emission is observed when comparing the unheated and heated sample, possibly leading to low singal:noise in measurements at high temperatures via the fluorescent probe BODIPY.

The exact mechanism of this decrease in emission is not understood. One possibility is a degradation of the probe at higher temperatures, however the lack of change in the absorption spectrum of the heated sample does not support this claim. It is thus much more likely that temperature-dependent quenching effects arise at high temperatures, as have also been observed in the fluorescent dye Rhodamine-B.[198] Luckily, while the decrease in emission resulted in more difficult data acquisition, it did not completely prohibit rotational single molecule measurements via BODIPY268.

Appendix C. Anisotropy Measurements

As the experimental approach to our single molecule measurements relies on measuring the rotations and thus linear dichroism of our probes, one requirement – other than high quantum yield and high photostability – for our fluorescent probes is a high degree of anisotropy. Polarization modulation depth (M) measurements can be used to report on the transition dipole alignment of probes.[199,200] To investigate the anisotropy of potential probes used in Chapter 5, the modulation depth was measured by monitoring the intensity of probe emission as a function of polarization angle.

As described by Park *et al.* in references 199 and 200, the modulation depth is typically defined as the difference between the maximum and minimum intensities of the emitted light (I_{max} and I_{min}, respectively) as a function of polarization, namely:

$$M = \frac{I_{max} - I_{min}}{I_{max} + I_{min}} = \frac{A}{I_{ave}},$$

where A is the amplitude of a sinusoidal modulation, and I_{ave} is the mean intensity of the modulated signals. Furthermore, the modulation depth is obtained by fitting the emission intensity as a function of polarization angle to

$$I_{em} = C[1 + M\cos\{2(\varphi - \varphi_0)\}],$$

with I_{em} corresponding to the emission intensity, φ the polarization angle of the excitation light, φ_0 a reference polarization angle corresponding to the maximum intensity angle, and C a proportionality constant. The closer to unity the M value is, the higher the degree of anisotropy. Measurements above 1 typically arise from background and can be viewed as close to unity.[200]

For the M measurements presented here, samples are prepared as for all single molecule measurements, and films were at least 200 nm thick. All measurements were taken at room temperature on the same setup as described in Materials and Methods except the Wollaston prism was removed and a linear polarizer was added before the objective, which was rotated at 10^{o}/s.

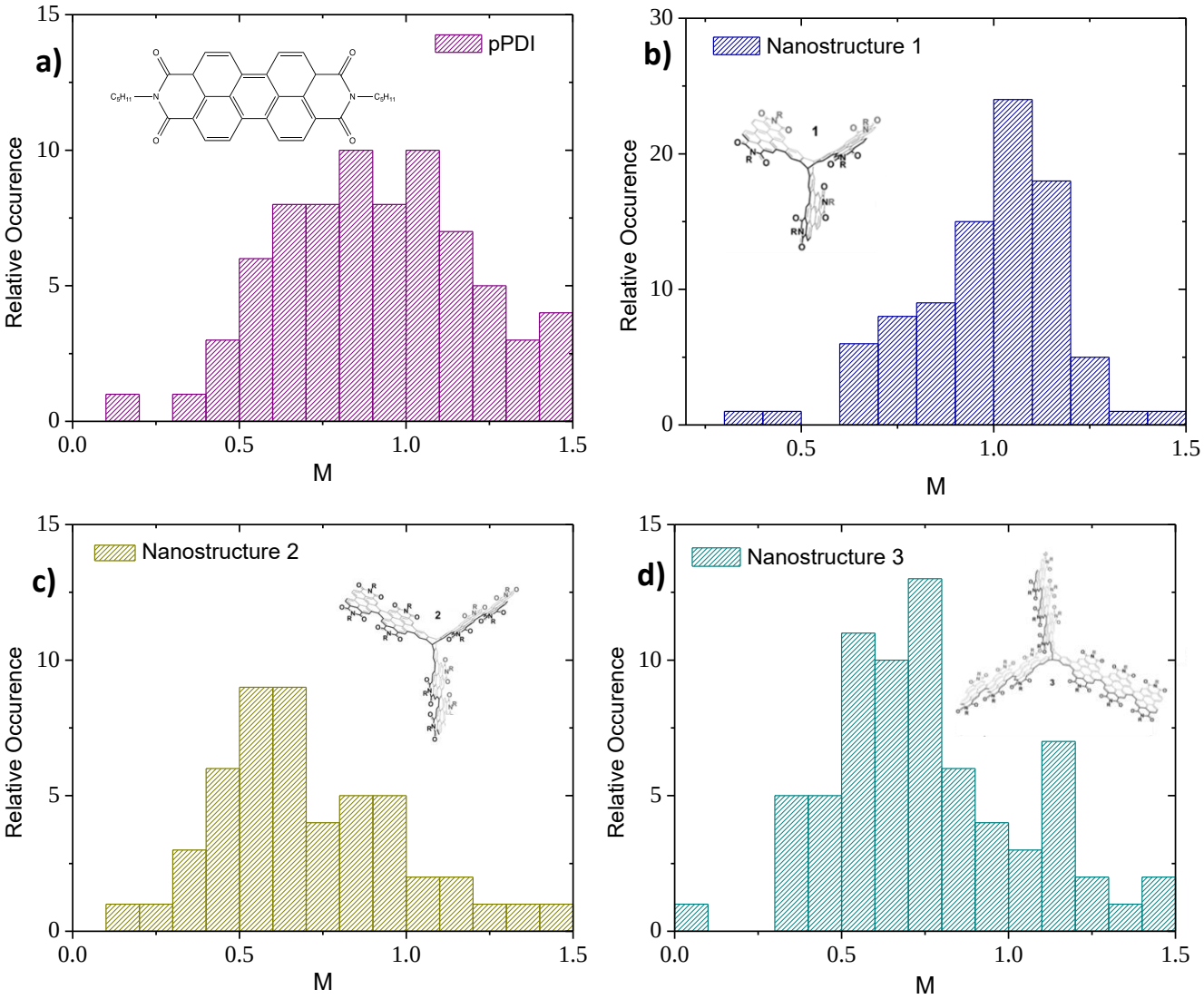

Figure 32. Histograms of modulation depth measurements of (a) pPDI and (b) nanostructures 1, (c) 2 and (d) 3 embedded in polystyrene.
All median M values are far above 0, indicating that all probes are sufficiently anisotropic for single molecule rotational measurements. However, pPDI and nanostructure 1 show median values near 1, indicating these to be the best suited fluorescent dyes for the rotational measurements in this thesis.

The power before the objective was approximately 30 mW. Excitation modulation depth values of dye molecules were obtained with a home-written Python program that fit the modulation depth data, and at least 50 molecules were analyzed per dye.

As seen in Figure 32, the modulation depth of pPDI centers around 1.0, matching the high degree of anisotropy expected from its non-symmetric structure. Surprisingly, the modulation depths of the smallest PDI-based nanostructure from Reference 146 also center around 1, while the larger nanostructures center at lower values (median ~0.7), indicating a lower degree of anisotropy of the nanostructures 2 and 3, yet still a polarization anisotropy in an acceptable range for linear dichroism measurements. In addition to changes in M, we also note that nanostructures 2 and 3 have lower emission intensities than either pPDI or the smaller nanostructure (the latter difference also appearing in spectroscopic data of reference 146), perhaps due to their less rigid structures that may enhance internal conversion rate, increasing the probability of non-radiative decay. Nonetheless, published spectroscopic data (all nanostructures show similar absorption maxima as pPDI) combined with anisotropy measurements, support the applicability of these large structures in rotational anisotropy single molecule approaches.